Polymeric Nanoparticles for the Modification of Polyurethane Coatings

Dissertation

zur Erlangerung des akademischen Grades eines Doktors der
Naturwissenschaften (Dr. rer. nat.) in Fach Chemie der Fakultät für Biologie,
Chemie und Geowissenschaften der Universität Bayreuth

vorgelegt von

Sandrine Tea

geboren in Paris/Frankreich

Bayreuth, 2011

Die vorliegende Arbeit wurde in der Zeit von November 2006 bis Januar 2011 in Bayreuth am Lehrstuhl Makromolekulare Chemie II unter Betreuung von Herrn Prof. Dr. Axel H. E. Müller angefertigt.

Vollständiger Abdruck der von der Fakultät für Biologie, Chemie un Geowissenschaften der Universität Bayreuth zur Erlangerung des akademischen Grades eines Doktors der Naturwissenschaften genehmigten Dissertation.

Dissertation eingereicht am:	16.02.2011
Zulassung durch die Promotionskommission:	23.02.2011
Wissenschaftliches Kolloquium:	15.06.2011

Amtierender Dekan: Prof. Dr. Clemens Stephan

Prüfungsausschuß:

Prof. Dr. Axel. H. E. Müller (Erstgutachter)

Prof. Dr. Stephan Förster (Zweitgutachter)

Prof. Dr.-Ing. Volker Altstädt

Prof. Dr. Carlo Unverzagt (Vorsitz)

À ma famille,

,,Es ist nicht genug, zu wissen, man muss auch anwenden; es ist nicht genug, zu wollen, man muss auch tun.''

Goethe

Table of Contents

Chapter 1

Introduction

Organic coatings or paints on a substrate give aesthetic desired appearance such as gloss and color, but also provide protection against environmental influences like mechanical or chemical damages, corrosion or radiation.

Discovered in 1937 by Otto Bayer[1], polyurethane (PU or PUR) raw materials (polyols and polyisocyanates) corresponded, in 2005, to 1 million tons of the world production of coatings in industrial applications which totaled 13 million tons. In the original equipment manufacturer (OEM) automotive coatings branch, the two-component PUR coating systems almost completely replaced the traditional alkyd resins especially in large vehicles production (planes, buses…) where baking of the coating is not always possible. Indeed, the quality of the PU films dried under mild conditions matches the performances of the baked coatings which makes PU the ideal system for such application. PU provide demanded high gloss, color retention, scratch, corrosion resistance and the presence of cross-links leads to tensile strength, good abrasion and mar resistance as well as acid, alkali and solvent resistance. However, the constant increase in demands for improved technical performances has motivated research in both industrial and academic organizations in building new PU materials with innovative properties.

The ability to control architecture and dimensions structures on a molecular scale is a key parameter in the design of new materials. The combination of organic or inorganic components in coatings has a relatively long history but with the emergence of nanotechnologies, material structures can now be controlled on a nanometer scale and more sophisticated nanocomposites with higher value-added products have arisen.

The wide applicability of PU coatings is due to their versatility in selection of monomeric materials. Recently, plastic coatings have also become a further domain for PU among wood furnishing, corrosion protection or textile coating. The chemistry involved in the synthesis of PU is centered on the isocyanate reactions.

To understand what the challenges are in creating new nanocomposite materials, some of the basics about PU chemistry and its use as coatings in the automobile industry will be reviewed in this introduction.

1.1 General remarks about polyurethane coatings

1.1.1 Urethane chemistry

The polyurethane chemistry is centered on the reactivity of isocyanate groups with compounds carrying labile hydrogen atoms like hydroxyl or amine functions. The reactions of isocyanates can be divided into two categories: (1) reactions on reactive hydrogen to give addition products, for example the reaction between an isocyanate and an alcohol that leads to the formation of the so-called urethane function, and (2) polymerization of isocyanates, i.e., self-addition reactions analog to the formation of dimers (uretdiones) or trimers (isocyanurates). An overview of basic isocyanate reactions is given in Scheme 1.

Aromatic isocyanates are more reactive than aliphatic ones with decreasing reactivity from primary through secondary to tertiary isocyanate groups unless steric or catalytic influences result in reversal reactivity. Primary and secondary alcohols will react easily at 50-100 °C while tertiary alcohols and phenols will be slower. The reaction of primary and secondary aliphatic amines or primary aromatic amines with isocyanates at 0-25 °C will proceed rapidly. Isocyanates are also very sensitive to water to yield amine groups. Therefore, PU paint films possess a complex polymeric structure with urethane groups but also urea, biuret or allophanate coupling groups.

The formation of an organic coating usually involves a liquid phase and generally speaking, two drying mechanisms can be identified during the formation of the coating paint film: physical and chemical drying. Physical drying is the evaporation of the medium where the coating is dissolved or dispersed. Chemical drying is the formation of the film by means of chemical reaction. Usually both mechanisms overlap during the formation of the film. However, a chemical drying which involves the polyaddition of high and/or small molecular weights starting products is the most interesting. Two important components can be identified: oligoisocyanates and coreactants, usually polyols.
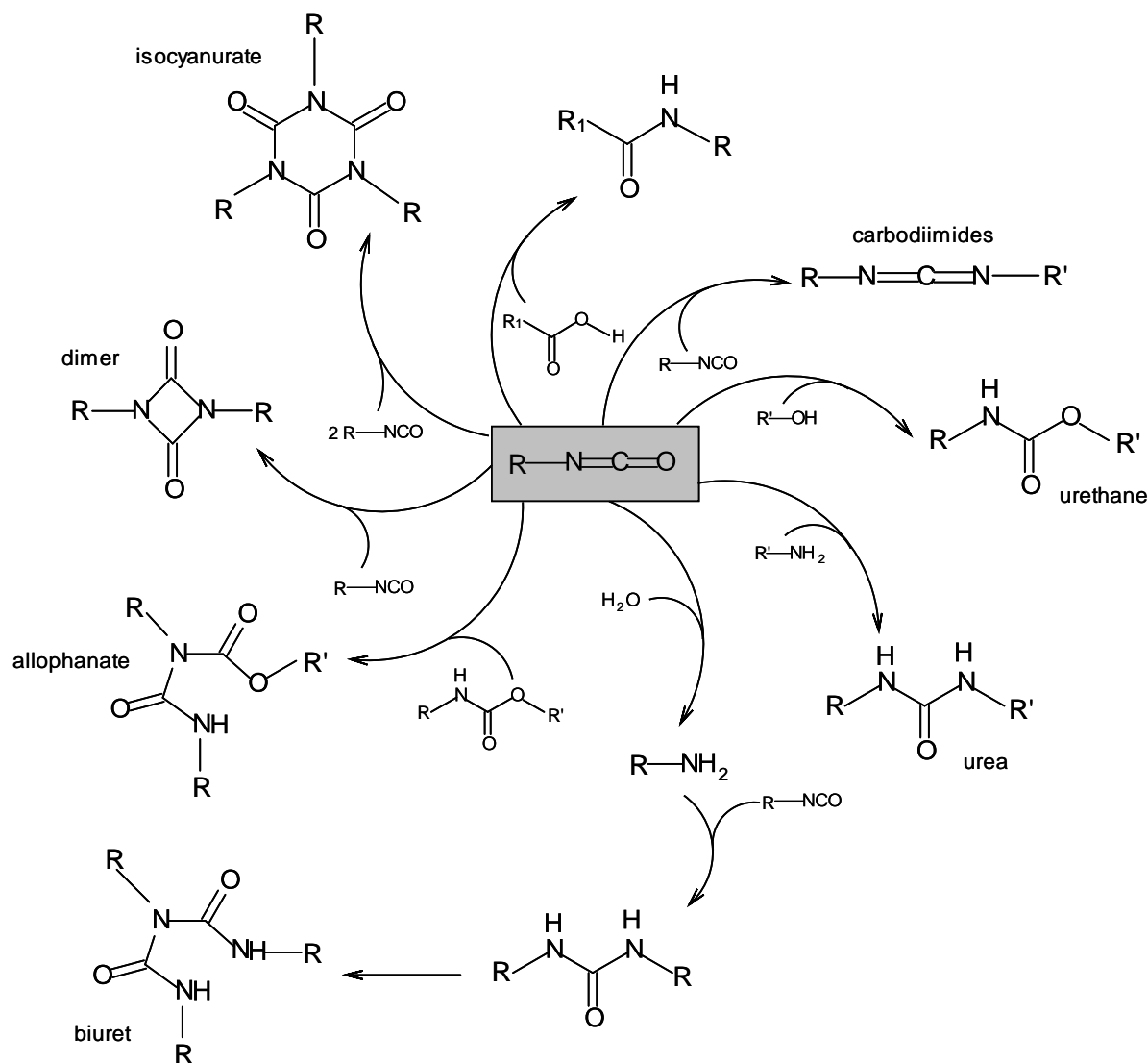
Scheme 1: Basic reactions of isocyanates with different reactants[2]

1.1.2 Isocyanates

The common PU coating formulations are based on few diisocyanates with aliphatic, cycloaliphatic or aromatic isocyanate groups. Toluene diisocyanate (TDI), hexamethylene diisocyanate (HDI), isophorone diisocyanate (IPDI), methylene diphenyl diisocynate (MDI) and 1,1-methylenebis(4-isocyanato)cyclohexane (HMDI) are those of commercial importance (see Scheme 2). Except MDI and its derivatives, all monomeric diisocyanates are classified as highly toxic substances and cannot be used into PU formulations. They have to be converted into higher molar mass products or prepolymers, physiologically benign polyisocyanates. For this, urethane chemistry is used in the production of oligomeric polysiocyanates and permits to obtain oligoisocyanates with functionalities greater than

two, necessary for spatial cross-linking. Derivatization from diisocyanates is usually performed by reaction with polyols forming isocyanate-functionalized urethanes, with water (biurets), with alcohol under catalytic influence (allophanates) or by catalytic dimerization or trimerization of diisocyanates (isocyanurates, uretdiones). The properties of the derivated prepolymers can vary as a function of molecular weight, type and functionality. For example, aromatic isocyanates are more reactive than aliphatic ones but their oxidative and ultraviolet stabilities are lower. They give more rigid PU but with limited suitability for exterior applications.
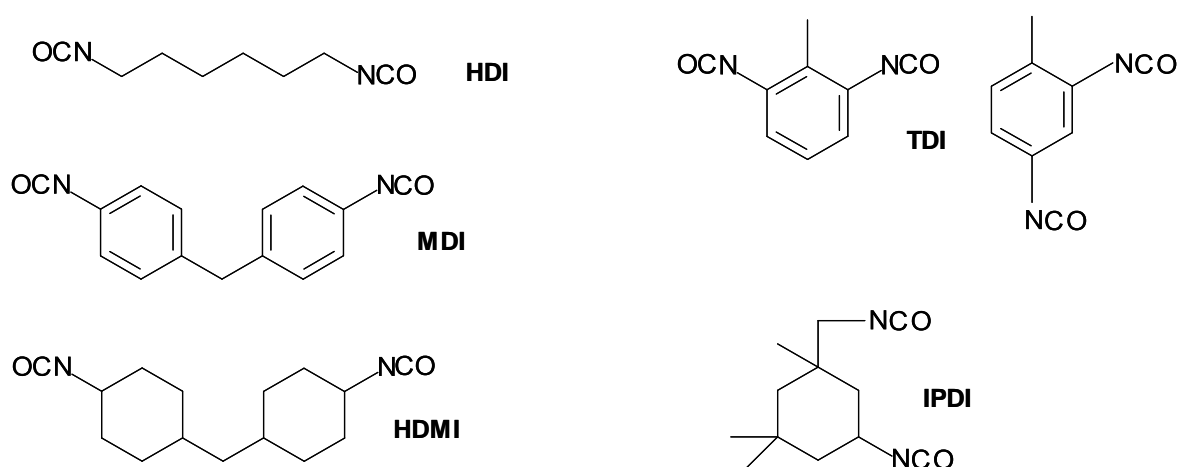
Scheme 2. Common diisocyanates used in coating formulations.

1.1.3   Polyols

Polyols (coreactants) can be polyester, polyether, polycarbonate or acrylic polymers containing hydroxyl groups (Scheme 3). The simplest are glycols like ethylene glycol, 1,4-butanediol or 1,6-hexanediol. The polyol component of the PU formulation is usually a mixture of those different polymers and includes sometimes castor oil. The choice of suitable polyols (architecture, molecular weight…) and oligoisocyanates allows us to control key characteristics of the paint film like solids content, gloss, drying, elasticity, hardness or resistance to chemicals. The ratio of isocyanate to hydroxyl functions (NCO:OH) plays therefore an important role in the design of the coating film properties. The use of low molecular weight polyols, for instance, will result in stiff and hard PU because of the high concentration of urethane groups (hard segments). High molecular weight polyols, on the other hand, will produce more flexible films due to fewer urethane groups.

Polyether polyols are obtained by a catalyzed addition of ethylene oxide or propylene oxide on small polyhydroxyl molecules such as ethylene glycol or trimethylolpropane. Polyester polyols are the result of the condensation of polyfunctional carboxylic acids (or anhydrides) with polyfunctional alcohols. Acrylic polyols are produced by free radical polymerization of 2-hydroxyethyl acrylate or methacrylate with other alkyl acrylates precursors.
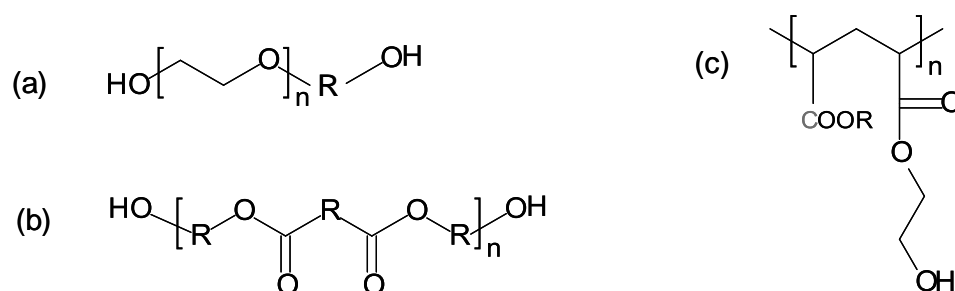
Scheme 3. Typical polyols for PU coating formulations. (a) polyether, (b) polyester, (c) acrylic polymer

1.1.4   Catalysts

The rates of the different reactions occurring during hardening of the PU coating film vary and depend on the type of oligoisocyanates and polyols used but also on the temperature, on the humidity level, on the catalyst and its nature if one is used. Most popular catalysts are tertiary amines[3] such as triethylamine (TEA), 1,4-diazabicyclo[2.2.2]octane (DABCO), organotin compounds[4] especially dibutyltin dilaurate (DBTDL) or stannous octoate (Scheme 4). The catalytic effect of organometallic compounds is due to their ability to form complexes with both isocyanates and hydroxyl groups[5,6] (Scheme 5). Tertiary amines form a complex with isocyanate groups which further react with alcohol to form urethane product[7]. In the absence of a strong catalyst, allophanate and biuret formation does not take place for aliphatic isocyanates.

DABCO
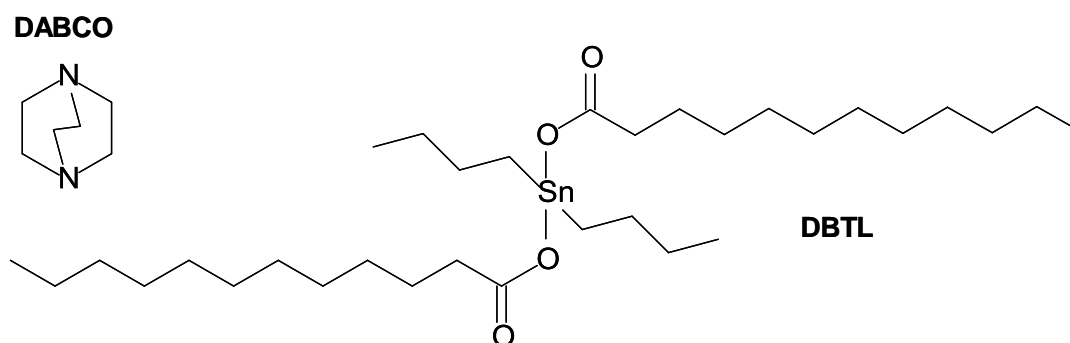
Scheme 4. Catalysts for 2K PUR formulation.
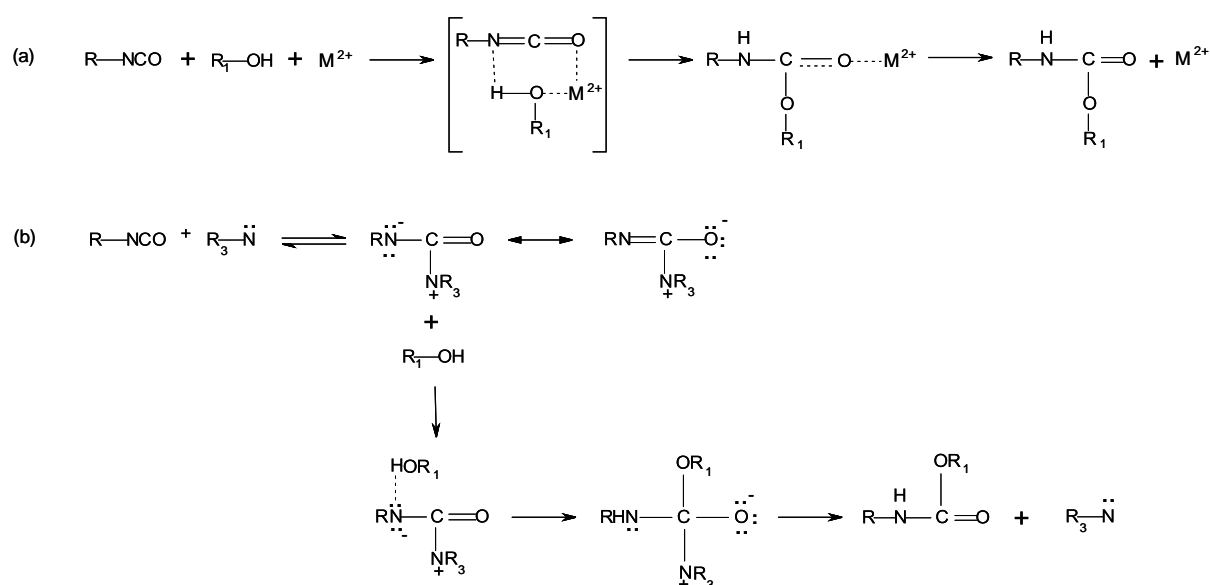
Scheme 5. Catalytic reactions with (a) an organometallic compound and (b) a tertiary amine

1.1.5   Hydrogen bonding

The high electronegativity of the nitrogen atom carried by urethane groups (or its derived functions such as allophanate, biuret or urea) induces in the N-H bond a partial positive charge on the hydrogen. This partial positive charge is therefore responsible of forming hydrogen bonding with neighbouring oxygen atoms contained in carbonyls of urethane functions themselves or of polyester and/or polyether precursors. These hydrogen bonds act as physical cross-links and strongly influence stiffness and strength of the PU matrix.

1.1.6   Aspects of one- and two-component coating technology (1K and 2K PUR)

Two types of PU formulations are available: one-component (1K) or two-component (2K) mixture. As their names indicate, the 1K PUR is a one pot formulation while the 2K PUR

keeps the two reactants (polyisocyanates and polyols) separated and brings them together only prior to application. Six different groups in the PU coating types are distinguished by the ASTM D16 standard[8] (see Table 1). Most high solids and solventless PU coatings for high performance application and corrosion protection, including automotive clearcoat paints, use the 2K format of the ASTM D16-type V.

1K PUR systems usually contain "blocked polyisocyanates" or "blocked reactants". Indeed, to be able to store the formulation in one pot at room temperature, the presence of free isocyanate groups has to be hindered. "Blocked polyisocyanates" are obtained by the addition of compounds such as phenol, butanone oxime[9] or ε-caprolactam[10], imidazoline[11], tetrahydropyrimidine, imidazole[12], pyrazole[13] that are easily eliminated or rearrange under the action of heat to generate isocyanate groups (Type III). "Blocked reactants" are activated by atmospheric moisture and then react with isocyanate groups (Type II). Other alternatives for 1K systems are formulations that form films under physical drying process exclusively (Type VI) or formulations containing polyunsaturated hydrocarbon chains which cross-link with oxygen (Type I). Another variant is the microencapsulation of the polyisocyanates[14].

In the case of a 2K system, oligoisocyanates and coreactants are kept separately and are mixed prior to application. This is by far the commercially most important system. Alkyd resins, epoxy resins, castor oil or cellulose nitrate can also be found as coreactants in such formulation in addition to polyols. The reaction between both components starts as soon as they are both brought in contact with each other and instant curing is possible (Type V). The use of "blocked reactants" in such formulation also exists especially if aliphatic amines are present in the system.

1K and 2K PUR systems can be cured over a wide range of temperatures, from room temperature to baking at ca. 200 °C. The coating film obtains its optimum properties when all solvents are evaporated and when the cross-linking reaction is complete (when both physical and chemical drying are complete). If necessary, an increase in temperature or catalysts can be employed to accelerate the process. The presence of a catalyst allows the reaction to take place faster and at lower temperatures. For aliphatic oligoisocyanates, curing in amine-containing atmosphere can also be an alternative to the introduction of a catalyst into the formulation.

Table 1. ASTM classification of different types of coatings

ASTM description	Characteristics	Curing mechanism	Polymer
Type I one-package (pre-reacted)	Unsaturated drying oil modified; no free isocyanate	Oxidation of drying oil; solvent evaporation	Alcoholysis products of drying oils reacted with isocyanate
Type II one-package (moisture cured)	Contains free isocyanate	Reaction with atmospheric moisture	Higher molecular weight diols and triols
Type III one-package (heat cured)	Blocked isocyanate	Thermal release of blocking agent and then reaction	Prepolymer forms an adduct with blocking agents
Type IV two-package (catalyst)	Isocyanate prepolymer and catalyst	Reaction of isocyanate with moisture and/or components in catalysts	Prepolymer similar to type II but catalyst could contain polyol/amine
Type V two package (polyol)	Part A: isocyanate rich Part B: polyols or amines	Reaction between Parts A and B; instant curing is possible	Relatively lower molecular weight
Type VI one-package (non-reactive lacquer)	Fully polymerized PUs dissolved in solvents	Solvent evaporation	Thermoplastic polymer with relatively high molecular weight

From the application point of view, the advantages of the 1K system are offset by numerous disadvantages including the complex formulation procedure and the need for careful drying of the pigments, for example, if they are moist. The 2K PUR system does not present such drawbacks and even has the advantage to yield blister-free paint films with high thickness but one has to pay more attention to the exact metering of the polyol and the hardener. Their pot life can be tuned by the use of different catalysts.

1.2 Thermoplastic PU coatings

Thermoplastic PU coatings can be qualified as linear copolymers made of what are described as "soft" and "hard" segments. Hard segments are composed of polar materials that can form hydrogen bonds and thus tend to aggregate into hard domains. Typically, carbonyl or amino groups are prone to such behavior. Opposite to hard segments, soft segments constitute the amorphous domains. Phase separation occurs between soft and hard segments due to their intrinsic incompatibility or thermodynamic immiscibility. Such structure was first discovered in 1966 by Cooper et al.[15] where the hard segments play the role of fillers and therefore act as physical cross-linker to inhibit the motion of soft segments[16]. Hard domains present high glass transition temperature (T_g) and provide high modulus, tensile strength and dimension stability while the soft domains with lower T_g impart elastomeric properties to the material. The degree of phase separation between

those domains is a key parameter in determining the properties of the coating. Therefore, the composition, the length of the hard and soft segments, the sequence of length distribution, the chemical nature of the units composing the polymer and its molecular weight are as many parameters that can influence hydrogen bondings and consequently phase separation and the subsequent properties of the thermoplastic PU coating.

1.3   Thermoset PU coatings

Thermoplastic PU coatings possess major drawbacks such as poor resistance against mechanical deformations and high temperature degradation. In thermoset coatings, the presence of chemical cross-linking points in thermoset coatings provides them with enhanced tensile strength, abrasion resistance and chemical resistance lacking in thermoplastic PU coatings which are essential for most industrial coatings. Cross-links are occurring by reaction of isocyanate groups as mentioned earlier. Coatings may therefore contain polyether or polyester soft segments with high functionality[17-21], isocyanates with functionality greater than two[22, 23], NCO/OH ratios greater than one[19-21, 24]. The increase in functionality increases cross-linking concentration which, in general, promotes phase mixing[25-28]. The introduction of such chemical cross-linking points reduces the mobility of the hard segments and thereby their ability to form hydrogen bonds[18, 29]. For high performance applications, a calculated amount of cross-linker is needed to adjust the properties of the PU coating. At last, the material, obtained with cross-links deliberately added or created in-situ, exhibits both phase-separated and phase-mixed structures, depending on the concentration of cross-links.

1.3.1   High solids content

For solventborne coatings, the main challenge since 1980s is to improve the solids content. For this purpose, quantities of organic solvents have been reduced leading to the so-called "high solids content" paints. Many efforts have also been made to lower the general viscosity of the formulation like the addition of reactive diluents or the reduction of the viscosity of the binder or of the polyisocyanate cross-linker[30]. In such a high solid content formulation, most common binders are hydroxy-terminated polyesters or hydroxy-functionalized acrylic resins. For polyester-urethane 2K coatings, controlling of molecular

weight and distribution, selecting the number of functional groups, using hydrogen bond acceptor solvents have been efficient ways to obtain low volatile organic compounds (VOC) paints[31]. Polyesters usually achieve higher solids content and better adhesion to metal than acrylic resins[32].

1.3.2   Acetoacetylation

The acetoacetylation of part of the hydroxyl groups contained in polyesters or acrylic polyols leads to the formation of the less polar acetoacetate groups. It allows a higher solid content at the application viscosity as well as better adhesion due to chelate effects. For the coating application their production is preferably achieved by transesterification[33-36]. The keto-enol equilibrium of these species allows the presence of two potential cross-linking sites: the active methylene group and the ketone carbonyl group. The cross-linking of the methylene groups with diisocyanates yields additional cross-links with better weathering stability and superior properties[37-40]. Furthermore, the β-ketoester groups are amphoteric and can be used to modify or cross-link polymers.

1.3.3   Introduction of specific functional groups

Imide

Chemical cross-linking of thermoset PU provides them with thermal stability or thermomechanical properties. In order to improve further such behavior, the introduction of heterocyclic structures, like imide functions, in the PU backbone has proven to be efficient. Isocyanate-capped PU prepolymers are usually reacted with acid dianhydride to produce PU containing imide groups[41-44].

Glycidyl carbamate

The introduction of glycidyl carbamate groups can provide PU with the reactivity of epoxides. These functions are generally incorporated by functional oligomers such as biuret glycidyl carbamate or isocyanurate glycidyl carbamate which are synthesized from different polyfunctional isocyanate oligomers and glycidol[45].

1.3.4   Polyurea

Within PU coatings, one can distinguish polyurea coatings in which the hydroxyl precursors are replaced by aminofunctional ones. The reaction between isocyanate and amine is significantly quicker than that occurring between isocyanate and alcohol. They are, therefore, ideal for aggressive environment where high speed curing is required (e.g. oil pipeline). However, their high reactivity implies a short pot life. The use of secondary amines instead of primary ones can, for example, increase this storage time. If the amine is bulky and sterically hindered, kinetics will be altered and the reactivity will greatly be reduced.

1.3.5   Moisture-cured PU

Moisture-cured PU contain isocyanate-terminated prepolymers and lead to highly cross-linked coatings. The diffusion and reaction of moisture produces primary amines that further react into urea groups. The drawback of such coating is their storage instability. Several side-products such as allophanate or isocyanurate are usually generated while stored. The introduction of those additional hard segments changes their volume fraction within the coating and ultimately alter adhesion or thermal properties[46-48]. However, moisture scavengers can be used to improve shelf life and pot stability. On the other hand, moisture-cured PU produce coatings with superior hardness, strength and stiffness. Since moisture is consumed, the risk of blisters or the formation of a weak boundary layer caused by water trapped under the coating is also greatly reduced.

1.3.6   UV-cured PU

UV-curable PU coatings present no or very low VOC. Their principle is based on the polymerization of unsaturated species induced by UV-radiation to lead a three-dimensional network. The main components of UV curable formulation are oligomers, reactive diluent and photoinitiator. This technique possesses many advantages: low energy requirement, fast and efficient polymerization, selective cure limited to irradiated areas and environmentally friendly with its low VOC. The major disadvantage lies in the inhibition of the reaction caused by the presence of oxygen. On the surface of the coating, oxygen

terminates the polymerization resulting in low molecular weights which leads to tacky films. To overcome such phenomenon, oxygen scavengers (tannin, carbohydrazide), high radiation intensity or high initiator concentration are applied[49]. The nature and properties of the cured film depend on the properties of the component but also on the kinetics of the photo-polymerization (rate and final conversion). The irradiation flux, sample thickness, temperature, photo-initiator concentration and reactive diluents content affect these kinetics and, therefore, the physical and mechanical properties of the final films.

1.3.7   Waterborne coatings

The constant demand in lowering VOC contents has conducted researchers to focus on waterborne coatings. They are dispersions of PU particles in continuous water phase. The particles are about 20-200 nm and have high surface energy which is responsible for the film formation after water evaporation. This technology requires new type of binder and additives to fulfill high quality requirements.

PU is usually not soluble in water and the degree of hydrophilicity is, therefore, a key parameter. The PU polymer backbone is generally modified by the introduction of hydrophilic groups (PU ionomer) or surfactant is added to obtain aqueous PU dispersion. PU ionomer exhibit pendant acid or tertiary nitrogen groups which are completely or partially neutralized or quaternized respectively, to form salts.

In all processes to prepare aqueous PU dispersion, prepolymers are formed from suitable polyols with a molar excess of polyisocyanates in the presence of an emulsifier which allows the dispersion of the polymer. The emulsifier is usually a diol with an ionic (carboxylate, sulfonate, quaternary ammonium salt) or non ionic (polyethylene oxide) group. The dispersion of the prepolymer and the molecular weight build up differ from one process to another[50-52].

Depending on the type of hydrophilic group present in the PU backbone, the dispersion can be defined as cationic, anionic and non-ionic. For each species, a minimum ionic content is required for the formation of a stable PU ionomer. Interactions between ions and their counter ions are then responsible for the formation of stable dispersion.

1.4 PU in the automotive coating industry

1.4.1 Automotive OEM coatings

The general modern automotive OEM (original equipment manufacturer) finishing process can be divided in four steps[53]:

1-Cleaning and pretreatment of the uncoated car bodies

2-Application of a cathodic electrodeposition (CED) primer

3-Application of a primer surface

4-Application of a topcoat

The application of each coating is followed by a baking cycle and each coat applied fulfills specific functions in the overall finish. The passivating pretreatment of the steel and the *CED primer* are mostly responsible for the protection against corrosion of the car. The *primer surfacer* fills remaining unevenness in the substrate and is usually sanded after baking to improve surface smoothness. Today, this coat also provides stone-chip resistance and protects the CED primer against UV transmission which could cause delamination of the coatings above it. An additional chip-stone resistant coating can be added between the CED primer and the primer surfacer on particularly vulnerable parts of the car body. The *topcoat* is, in 80 % of cases, a two-coat system comprising a *basecoat* and a *clearcoat*. It is responsible for all properties related to the appearance of the finish (gloss, brilliance, color and special effects) and is also meant to be resistant to light and weathering, to industrial and natural chemicals and to mechanical damage like scratching, stone chipping and car washes. All these requirements limit the types of binders that can be formulated for such high quality topcoats.

Most *basecoat* formulations are based on polyacrylate and polyurethane binders which enhance brilliance, adhesion, leveling, flexibility and stone chip resistance. Both solvent- and waterborne basecoat are available but waterborne systems allow, of course, a large reduction in solvent emissions.

The *clearcoat* technology uses mostly, since the 1980s, the solventborne 2K PUR system. Before this outbreak, acrylate/melamine systems referred as thermosetting acrylics (TSA) were traditionally used as clearcoats. 2K PUR have, however, superior optical properties (gloss, leveling) as well as mechanical and chemical resistance.
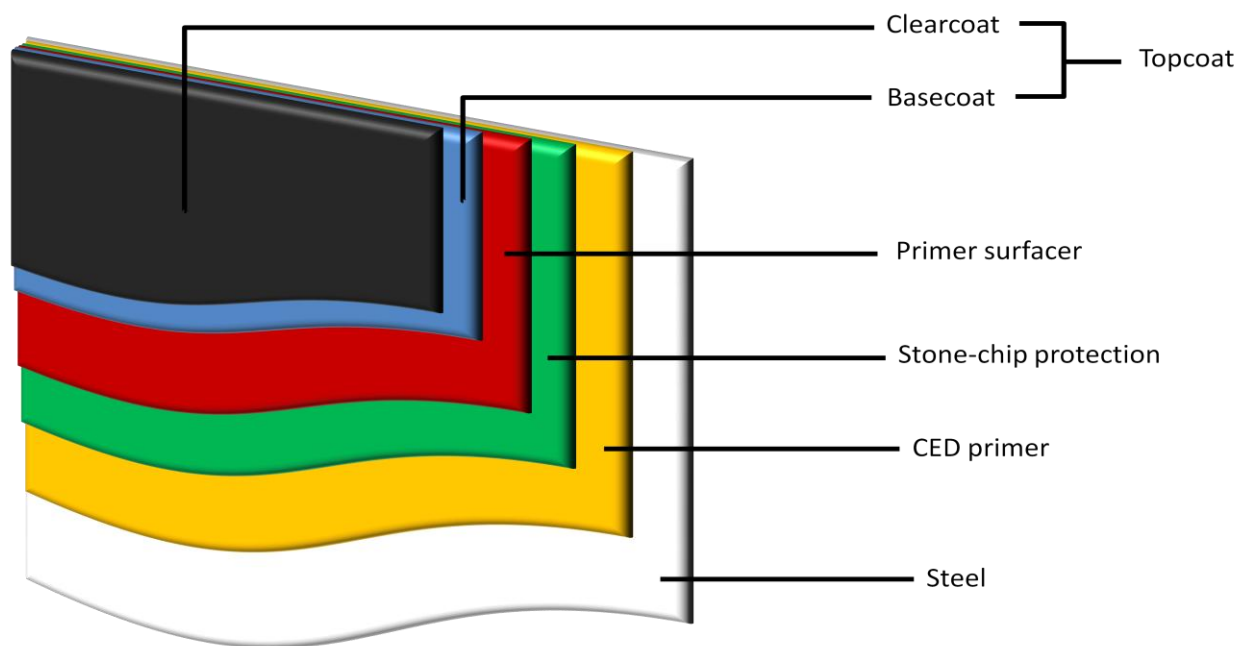
Scheme 6. Diagram of an OEM automotive finish. Chip-stone resistant coating is applied only on vulnerable areas of the car body (e.g. doors)

1.4.2   2K PUR clearcoat

2K PUR clearcoats are based on hydroxyfunctional acrylates and polyester resins which are cross-linked with aliphatic polyisocyanates such as HDI-based ("Desmodur N") or IPDI-based ("Desmodur Z"). These systems differ from conventional paints on the following aspects:

-improved chemical and etch resistance

-good mechanical properties (resist to scratch and stone chipping)

-outstanding optical properties (long-term gloss retention, brilliance)

-high solids content

-reactivity

The application of this type of paint is largely automated in the automotive OEM finishing and spraying is performed electrostatically. Flushing programs ensure that the formulation, once mixed, does not remain in the spray gun or mixer longer than the pot life.

Formulations of linear or slightly branched binders and HDI-based hardener lead to low glass transition temperature, high flexibility and excellent scratch resistance. On the other hand, polyacrylates with a higher number of hydroxyl functions or the use of an IPDI-based

hardener will results in higher glass transition temperature and hardness of the final film. The scratch resistance is lower than that of the flexible formulation but their chemical resistance is higher due to the high concentration of urethane functions and their good chemical stability.

2K PUR also has the property to reflow, for example, when heat is applied to a scratched PU coating, the scratches are observed to partially fill. This effect is promoted by the formation of hydrogen bridge bonds between urethane groups which contributes to the stability of the network. This phenomenon is usually tracked by gloss measurements or more recently by atomic force microscopy (AFM)[54].

Despite the outstanding gloss, weatherability and solvent resistance of PU coatings, the optimization of their scratch resistance and impact toughness would greatly broaden their spectrum of application. In recent years, nanotechnology has experienced significant growth in the field of materials. The area of coatings has not been spared and the combination of inorganic nanoparticles with organic building blocks, in particular, has led to innovative materials with novel properties and functions as outlined below.

1.4.3   Engineering of PU via inorganic nanofillers

A wide variety of inorganic nanomaterials, mostly clays but also silica, Fe_2O_3 or TiO_2 nanoparticles and other nanopowders are being more and more commercially available. The downscale to the nanometer size is synonym of a higher specific surface but also promoting a strong tendency towards aggregation[55]. Today, processes towards nanocomposites include dispersing nanoparticles or their creation in situ. In most cases, surface modification of the nanoparticles is necessary to achieve compatible and homogenously dispersed nanomaterials[56, 57]. The shape, average diameter and interfacial coupling with the matrix of the nanofillers determine the properties of the final material and usually confer unique features to polymers compared to micro-sized particles. This "nano-effect" relies mostly on the interfacial area between the matrix and the filler which is significantly augmented in a nanocomposite when compared to a bulk matrix. For example, in a toughened nanocomposite, such an effect promotes the transfer of stress from the matrix to the nanofiller, increasing mechanical properties of the nanocomposite. Nanoparticle shapes are essentially spherical, lamellar or rod-shaped. Lamellar nanoparticles like clays are usually

used for barrier properties[58-61] or flammability resistance[62, 63]. Rod-shaped fillers, for example, carbon nanotubes or silicon carbide (SiC) nanowires when successfully uncoiled result in high conductivity and mechanical strength[64-68]. Spherical nanoparticles exhibit a very large spectrum of possibilities: biocidal activity (Ag, Cu)[69, 70], scratch resistance (SiO_2, Al_2O_3, ZrO_2, POSS)[71-77], UV protection (TiO_2, CeO_2, ZnO)[56, 78, 79], thermal stability (Au)[80].

If the use of inorganic fillers for PU coatings modification is well documented, organic fillers such as block copolymers lack such interest. The use of rubber-based block copolymers as organic inclusions in bulk materials has proven to be an efficient way to improve impact resistance properties, toughness and/or ductility. This concept of toughness has been applied to coatings and extensive investigations of block copolymer-modified epoxy thermoset coatings have been carried out as outlined below.

1.5 Polymer toughening

Polymer toughness has attracted much attention from material researchers for some time [81, 82]. Most of this creative and resourceful attention has been directed at composites and bulk materials and very little at coatings.

When it comes to coatings, the term of toughness is typically associated with impact resistance, scratch and stone-chip resistance. There are two major differences between coatings and bulk materials:

-the presence or absence of substrate

-the thickness of the film (thin for coatings, thicker for bulk materials, composites).

Toughening a plastic material consists in altering the failure mechanism such as the formation of cracks, voids, crazes, shear bands and so on. Because of the nature of thin films, this type of approach to toughening coatings does not provide sufficient performance. Microscale damages in the coatings could already be severe enough to cause failure contrary to bulk materials. Regardless of the type of failure, coatings are rated "fail" as long as the damages are present. Thus, a "tough" coating has to pass severe deformation without displaying such damages and coating toughness can, therefore, be defined as the capability to withstand deformation rather than to resist crack propagation. It is a complex property which depends on coatings hardness, stiffness and resiliency. These properties are in turn related to the coatings structure in terms of backbone flexibility, cross-linking and

adhesion to substrate. Playing on these parameters seems to be not sufficient anymore for improving such properties and shows limitations. For example, to improve toughness, one could decrease the T_g of the coating by decreasing the degree of cross-linking but the final coating would greatly loose in chemical resistance.

In bulk materials, improved toughness is often achieved by the introduction of a rubber phase[81]. Traditionally, polymers have been modified with micro-sized inclusions but with the development of new processing techniques, fillers in the nanometer range (1 to 100 nm) could be obtained and built on. Beside the nano-effect itself, experiments have demonstrated that the particle size plays a major role in toughening as for a given volume fraction of rubber particles, the smaller the particles the higher the toughness achieved in the composite[83]. The necessary loading of nanoparticles is usually lower than for their microfillers counterparts which is an enormous advantage, industrially and economically speaking. Furthermore, many characteristic properties of the unmodified polymer like transparency, light weight or good processability are preserved after nanomodification.

1.5.1 Block copolymer-modified epoxy coatings

Epoxy thermoset coatings have been extensively modified using block copolymers as organic toughening agent. The formation of nanostructures in cured blends of epoxy resin and block copolymers has been first reported by Hillmyer et al. in 1997[84, 85]. Block copolymers with "amphiphilic" behavior were used because of their blocks differing affinity towards a potential solvent and their tendency to avoid mixing of dissimilar blocks with one another. The precursors of the thermoset act as selective solvents for the block copolymers which undergo self-organization into lamellar, cylindrical, spherical or bicontinuous structures, depending on the fraction of block copolymers incorporated into the resin[86-89]. Unusual morphologies such as raspberry- or onion-like structures were also observed in particular cases[90, 91]. The domain sizes are determined by the length of the blocks, typically on the nanometer scale. The block copolymer self-assembly occurs before the curing reaction which afterwards has the role to lock in these preformed nanostructures although it has been noticed that slight changes in morphology could occur during the curing step[85].

Another approach leading to nanostructured epoxy resins consists in inducing self-organization of completely resin miscible block copolymers upon the curing reaction[92-95].

Even if a nanostructure is already present in the resin, it still can disappear upon addition of the hardener[96] or during temperature elevation[93] for cure. Thus, before curing, the nanostructure is inexistent. During the curing step, the miscibility of the different blocks is changed resulting in phase separation and subsequently leading to a novel nanostructure. This phenomenon, so-called "reaction-induced microphase separation" (RIMS), depends on the competitive kinetics between polymerization (the curing reaction) and phase separation. The formation of nanostructures via self-assembly is, in contrast, based on equilibrium thermodynamics between the block copolymers and the thermoset precursors. Recently, Fan et al. reported the occurrence of both mechanisms within one system[97].

A third approach consists in using block copolymers, resinophilic block of which is reactive towards the resin or the hardener. The structure is therefore fixed before phase separation can occur. Chemically bound to the resin, reactive block copolymers can lead to a greater degree of toughening in epoxy systems[98].

The macromolecular topologies (branched, star-shaped, linear, di-, tri-block…) of the block copolymers also have an influence on the nanoscaled morphologies[99]. The nature of the effective polymer modifiers used to toughen epoxy thermosets can be elastomeric[93, 100, 101] as well as thermoplastic[84, 85, 102, 103] or a combination of both[90, 91, 94, 104]. The toughness attained depends strongly on the morphology adopted by the block copolymers. For example, it has been reported that vesicular inclusions improved fracture toughness significantly more than micellar morphologies[102] and that even greater improvements can be obtained when worm-like micelles are formed[105-107].

Reactive liquid rubbers constitute another category of polymer modifiers and are also used in epoxy thermosets as toughening agents. The literature reports the use of functionalized elastomers such as acrylate-based rubbers[108], carboxyl-terminated acrylonitrile-butadiene (CTBN)[109], hydroxyl- amine- or epoxy-terminated polybutadiene[110-112], diglycidyl-terminated polydimethylsiloxanes[113] or containing isocyanate functions[114]. These toughening agents form discrete rubbery particles chemically bonded to the matrix.

1.5.2   Block copolymers in PU coatings

1.5.2.1   Block copolymer-modified PU thermosets

The concept of block copolymer-modified epoxies was transfered to PU thermosets by Jaffrenou et al. in 2008[115]. The same group had reported few years earlier the use of polystyrene-*b*-polybutadiene-*b*-poly(methyl methacrylate) (SBM) block copolymer in epoxy resins [90, 91]. The PMMA block was soluble in the epoxide and the unreacted blend. During the curing reaction, PMMA remained soluble with the hardener (diamine) until complete reaction and phase separation from the other two blocks, PS and PB, occured resulting in a nanostructured epoxy thermoset. Transparency of the material was kept except when the hardener used was not miscible with the PMMA block. In PU thermoset, the resulting morphological behavior induced by the addition of SBM turned out to be very similar to that of modified epoxy.

Oligodiol precursors were based on a central bisphenol-A unit with two hydroxyl-terminated oligomers (polyethylene oxide or polypropylene oxide). Polycaprolactone triol was also used to achieve spatial cross-linking and as hardeners, XDI, IPDI or trifunctional HDI were used. In non cross-linked PU, i.e. difunctional precursors only, most systems lead to transparent materials with a maximum block copolymer loading of 10 %wt. For these systems, spherical micellar morphologies were observed within the thermoset. Non-transparent materials were obtained when the hardener showed even less affinity for one of the non miscible block and/or when the concentration of urethane groups, favorable to PB and PS miscibility, was too low (longer oligodiols). Morphologies observed in this case were a mixture of spherical micelles and onion-like particles with diameter as large as one micrometer. Flocculation of spherical micelles occurred when the PMMA block was less miscible with the oligodiols and produced opaque materials. In the case of cross-linked PU, trifunctional monomers are used which are not miscible with PMMA. Therefore, transparent materials are only obtained below a certain amount of those cross-linkers introduced into the PU. Above this limit, triblock copolymers cannot be stabilized until the end of the curing process. At higher loadings of block copolymers (>50 %wt), final PU materials appear hazy. They exhibit cylindrical structures and are getting closer to a lamellar morphology as the amount of block copolymer increases. However, transparent materials could still be

obtained when using pure block copolymers (no impurities left such as homopolymer or diblock precursor).

However, no mechanical characterization of those modified PU materials has yet been reported. One can assume similar results to those of block copolymer-modified epoxy thermoset, i.e. significant improvement in fracture toughness.

1.5.2.2 Hyperbranched polymers in PU coatings

Dendritic polymers have become one of the most exciting types of polymers in the recent past. The core of this attention is the difference in properties of these branched structures compared to their linear analogues. Dendritic polymers have lower viscosities, non-entangled globular structures and often have increased solubility in various solvents and good rheological behavior. These special features have shown a new dimension in the coatings research and development.

The chemical bonding of branched polymers with PU chains through cross-linking is especially interesting due to their high functionality. They provide multiple covalent binding sites for cross-linking reaction and therefore, increase the film's structural integrity, with excellent chemical resistance, durability and good mechanical properties while maintaining low VOC in the coating formulation. Even used in a small amount, branched structures containing hydroxyl or amino functions at the terminal unit can cross-link NCO-terminated PU prepolymers and result in manifold increased mechanical properties materials[116]. The possibility to produce specific end-groups or modify the structure of the end-groups can be used as a tool to adjust or modify the properties of the polymer with tailored cross-link densities and hydrophobicity for specific coating applications[117-120]. The increase in cost induced by those new polymers is sufficiently reasonable to justify industrial efforts concerning their studies.
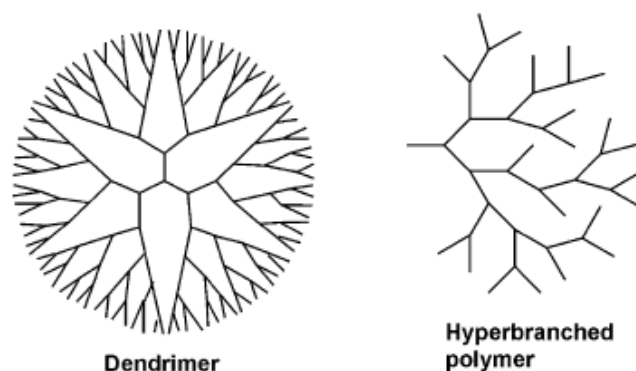
Scheme 7. Schematic description of dendritic polymers comprising dendrimers and hyperbranched polymers[121]

Dendritic polymers comprise dendrimers and hyperbranched polymers. Dendrimers are synthesized by the multiple replication of a sequence of two steps. They are, therefore, monodisperse, symmetrical, layered macromolecules and perfectly built onto a core molecule with a high degree of branching. This multistep synthesis includes protection and coupling procedures. It is tedious and time-consuming, especially regarding the low yield and the high cost it would generate in large scale preparation[122]. These factors make dendrimers less attractive for large volume coating applications.

In contrast to dendrimers, hyperbranched polymers are polydisperse, have lower degree of branching and irregular structures but possess many properties similar to dendrimers. In hyperbranched polymers, not all repeating units are fully reacted and therefore, exhibit a mixture of three different types of unit: dendritic (all groups reacted), terminal and linear units.

Their synthesis is easier and can be scaled-up to large productions at reasonable cost. The most convenient procedure to synthesize such polymers is the self-condensation of AB_x ($x \geq 2$) type monomers. The A group of one monomer is able to react with the B group of another monomer but A and B are not able to react with themselves. The reaction leads to B-terminated hyperbranched structures. The scarce commercial availability of those AB_x-type monomers and the multistep organic methodology to synthesize them led to novel alternative methods that are based on the following design considerations:

1. $AB_2 + B_x$

2. $A_2 + B_3$

3. $A_2 + B_2B^*$

4. $A_2 + CB_n$

5. $AA* + CB_2$

6. $AB + CD_n$

$A_2 + B_3$ systems are of special interest because of the commercial availability of numbers of A_2 and B_3 monomers[123-125]. However, this kind of polycondensation generally results in gelation and reaction has to be stopped before critical conversion. Flory pointed out that the polymerization of AB_x monomers, on the other hand, proceeds without gelation[126]. In an $A_2 + B_3$ system, without chemical selectivity between reaction partners, an AB_2 species will be intermediately formed and accumulated if the first condensation step between A_2 and B_3 is faster than the following propagation steps. Thus, no gelation occurs within such systems as long as reaction condition and monomer concentration are carefully controlled. Approaches 3, 5 and 6, recently developed, have in common the enhanced selectivity and reactivity of A* towards B* function. A and A* are the same functional group but have different reactivity usually due to asymmetry in the monomer structure. Important examples can be cited such as the reaction of a diisocyanate (A_2) and a dihydroxy amine (CB_2 where C is more reactive than B) monomers used as an improved method by Gao and Yan[121, 127]. This reaction produces an $A(AC)B_2$, i.e., an AB_n-type intermediate *in-situ*. Another example is the formation of hyperbranched PU-polyurea reported by Bruchmann et al.[128]. Although those methods avoid protection and deprotection, they do have some drawbacks. Some of the reactions are sensitive to different reaction conditions[129], like concentration of reagents or temperature. These demerits are balanced with longer reaction times or precise control of the temperature are applied.

Most hyperbranched polymers used in PU coating formulations are polymers containing either a large number of hydroxyl or amine functions that can react with isocyanate terminated PU prepolymers. When branched polyester polyols ("Boltron" Perstop Polyols Inc.) are introduced, the resulting polymers show unpredecented polymer architectures[130-133]. Polyamide bearing amine functions groups[134-136] are also used but due to the high reactivity of aromatic hyperbranched polyamides, linear ones are preferred such as polyethyleneimine. Low VOC-coating containing hyperbranched structures have been reported to have superior properties compared to linear polyols[137]. However, the solubility of polyester polyols can be limited and chemical modifications of the hyperbranched

structures can be necessary to control its amphiphilic balance. For example, a fraction of the –OH groups can be replaced by alkyl chains[138].

However, to the best of our knowledge, neither the use of non functionalized hyperbranched polymers nor rubber-like hyperbranched polymers in PU thermosets have been reported.

PU coatings can be modified with block copolymers but this approach usually requires a large amount of modifiers (10-50 %wt) to be effective. From this perspective, the use of hyperbranched polymer seems advantageous. They can be introduced in additive quantity (0.01 equivalent for 1.0 equivalent of PU prepolymer) and show great improvements in tensile strength, for example, without altering any other properties.

1.6   Motivation and objective of the thesis

The objective of this work is to apply the concept of "toughness", used in thermoplastic materials, to thermoset PU coatings to improve their stone-chip / impact resistance. The introduction of a rubber phase into a stiffer material has the effect to improve the impact resistance of the latter due to different mechanisms involving the elastomeric domains (cavitation of the rubber inclusions for example). As a restrictive condition, the introduction of the rubber phase has to occur without disturbing the transparency of the coating. To the best of our knowledge, the introduction of polymeric nanoparticles as PU impact modifiers has not yet been reported. Neither the use of non-functionalized hyperbranched polymers nor that of rubber hyperbranched polymers was described as PU impact modifiers in the literature.

For this purpose, novel toughening organic nanomodifiers for automotive polyurethane clearcoat based on polybutadiene (PB) are designed. To enhance miscibility with the coating and, therefore, hinder eventual aggregation of the nanomodifers, PB is copolymerized with a (meth)acrylic polymer. Different (meth)acrylates are chosen, namely, methyl methacrylate, 2-hydroxyethyl methacrylate, *n*-butyl acrylate, *n*-butyl methacrylate and *t*-butyl methacrylate.

To ensure that rubbery domains remain in the nano-size scale, all polymers are synthesized by controlled/living polymerization aiming at relatively low molecular weights and two different strategies are developed:

1. Polybutadiene based linear block copolymers are synthesized. Their ability to self-assemble into micellar aggregates in different selective solvents is studied by means of static and dynamic light scattering and transmission electron microscopy. To lock in the micellar structure and obtain stable, non fusible nanoparticles, various methods to cross-link the micellar core are undertaken. The nanoparticles, synthesized in this way, are ready to be incorporated into the coating.

2. Polybutadiene based hyperstars are synthesized. The anionic self-condensing vinyl copolymerization of divinylbenzene (DVB) and butadiene is carried out, using different DVB isomers, leading to hyperbranched PB polymers. From this hyperbranched PB, (meth)acrylate arms are grown. The hyperstar nanomodifiers,

synthesized in this way, are ready to be incorporated into the coating. Neither self-assembly nor cross-linking are required in this case.

The synthesized organic nanomodifiers are added into PU coating formulations. Appearance and transparency of the obtained "organic-modified nanocomposite coatings" are tested by gloss/haze and TEM measurements. Their stone-chip impact resistance, adhesion, hardness and chemical resistance are as well investigated.

1.7   Structure of the thesis

The following chapters describe in details

- ➤ The polymerization and characterization methods used in this work (Chapter 2)

- ➤ The synthesis and characterization of linear block copolymers based on polybutadiene (Chapter 3)

- ➤ The study of their solution behavior in different selective solvents (Chapter 3)

- ➤ The stabilization of the obtained structures by cross-linking of the polybutadiene core leading to spherical polymeric nanoparticles (Chapter 3)

- ➤ The synthesis and characterization of hyperstar polymers based on hyperbranched polybutadiene (Chapter 4)

- ➤ The use of the synthesized polymeric nanomodifiers in 2K PUR coating and the optical, mechanical and chemical coating tests (Chapter 5)

- ➤ Summary / Zusammenfassung (Chapter 6)

References

1.   Bayer, O., *Angewandte Chemie* **1947,** 59, (9), 257-272.

2.   Chattopadhyay, D. K.; Raju, K. V. S. N., *Progress in Polymer Science* **2007,** 32, (3), 352-418.

3.   Burdeniuc, J. J.; Kamzelski, A. Z., US Patent 7495131, 2006.

4.   Roy, S.; Majumdar, K. K., Indian Patent 194604, 2004.

5.   Dzierża, W., *Journal of Applied Polymer Science* **1978,** 22, (5), 1331-1342.

6.   Cooper, S. L.; Tobolsky, A. V., *Journal of Applied Polymer Science* **1967,** 11, (8), 1361-1369.

7.   Sasaki, N.; Yokoyama, T.; Tanaka, T., *Journal of Polymer Science: Polymer Chemistry Edition* **1973,** 11, (8), 1765-1779.

8.   ASTM, Standard 16-00. Technology for paint, related coatings, materials, and applications.

9.   Wicks Jr, Z. W., *Progress in Organic Coatings* **1975,** 3, (1), 73-99.

10.   Katsobashvili, V. Y.; Babkin, B. M.; Sal'nikova, G. A.; Simonova, N. I.; Eremina, T. N.; Kulikova, T. N.; Volodarskaya, Y. I.,U.S.S.R. Patent 508449, 1976.

11.   Rainer, G., Johann, O., Elmar, W., Guenter, D., Patent DE 2740253, 19790315, 1979.

12.   Nasar, A. S.; Subramani, S.; Radhakrishnan, G., *Polymer International* **1999,** 48, (7), 614-620.

13.   Mühlebach, A., *Journal of Polymer Science Part A: Polymer Chemistry* **1994,** 32, (4), 753-765.

14.   Blum, R.; Schupp, H., *Progress in Organic Coatings* **1990,** 18, (3), 275-288.

15.   Cooper, S. L.; Tobolsky, A. V., *Journal of Applied Polymer Science* **1966,** 10, (12), 1837-1844.

16.   Seymour, R. W.; Cooper, S. L., *Journal of Polymer Science: Polymer Symposia* **1974,** 46, (1), 69-81.

17.   Smith, T. L.; Magnusson, A. B., *Journal of Applied Polymer Science* **1961,** 5, (14), 218-232.

18.   Haska, S. B.; Bayramli, E.; Pekel, F.; Özkar, S., *Journal of Applied Polymer Science* **1997,** 64, (12), 2347-2354.

19.   Kothandaraman, H.; Venkatarao, K.; Thanoo, B. C., *Journal of Applied Polymer Science* **1990,** 39, (4), 943-954.

20.   Consaga, J. P.; French, D. M., *Journal of Applied Polymer Science* **1971,** 15, (12), 2941-2956.

21.   Špírková, M.; Matějka, L.; Hlavatá, D.; Meissner, B.; Pytela, J., *Journal of Applied Polymer Science* **2000,** 77, (2), 381-389.

22.   Kontou, E.; Spathis, G.; Niaounakis, M.; Kefalas, V., *Colloid and Polymer Science* **1990,** 268, (7), 636-644.

23.   Desai, S.; Thakore, I. M.; Sarawade, B. D.; Devi, S., *European Polymer Journal* **2000,** 36, (4), 711-725.

24.   Paulmer, R. D. A.; Shah, C. S.; Patni, M. J.; Pandya, M. V., *Journal of Applied Polymer Science* **1991,** 43, (10), 1953-1959.

25.   Thomas, O.; Priester, J. R. D.; Hinze, K. J.; Latham, D. D., *Journal of Polymer Science Part B: Polymer Physics* **1994,** 32, (13), 2155-2169.

26.   Dounis, D. V.; Wilkes, G. L., *Journal of Applied Polymer Science* **1997,** 65, (3), 525-537.

27.   Petrović, Z. S.; Ilavský, M.; Dušek, K.; Vidaković, M.; Javni, I.; Banjanin, B., *Journal of Applied Polymer Science* **1991,** 42, (2), 391-398.

28.   Petrović, Z. S.; Javni, I.; Bánhegy, G., *Journal of Polymer Science Part B: Polymer Physics* **1998,** 36, (2), 237-251.

29.   Chiou, B. S.; Schoen, P. E., *Journal of Applied Polymer Science* **2002,** 83, (1), 212-223.

30.   Renz, H.; Bruchmann, B., *Progress in Organic Coatings* **2001,** 43, (1-3), 32-40.

31.   Ni, H.; Daum, J. L.; Thiltgen, P. R.; Soucek, M. D.; Simonsick, W. J.; Zhong, W.; Skaja, A. D., *Progress in Organic Coatings* **2002,** 45, (1), 49-58.

32.   Hood, J. D.; Blount, W. W.; Sade, W. T., *Journal of Coatings Technology and Research* **1986,** 58, (739), 49-52.

33.   Witzeman, S. J.; Notthingam, D. W.; Rector, F. D., *Journal of Coatings Technology* **1990,** 62, 101-112.

34.   Noomen, A., *Progress in Organic Coatings* **1997,** 32, 137-142.

35.   Clemens, R. J.; Rector, F. D., *Journal of Coatings Technology* **1989,** 61, 83-91.

36.   Rector, F. D.; Blount, W. W.; Leonard, D. R., *Journal of Coatings Technology* **1989,** 61, 31-37.

37.   Narayan, R.; Raju, K. V. S. N., *Progress in Organic Coatings* **2002,** 45, (1), 59-67.

38.   Narayan, R.; Chattopadhyay, D. K.; Sreedhar, B.; Raju, K. V. S. N., *Journal of Materials Science* **2002,** 37, (22), 4911-4918.

39.   Narayan, R.; Chattopadhyay, D. K.; Sreedhar, B.; Raju, K. V. S. N.; Mallikarjuna, N. N.; Aminabhavi, T. M., *Journal of Applied Polymer Science* **2005,** 97, 1069-1081.

40.   Narayan, R.; Chattopadhyay, D. K.; Sreedhar, B.; Raju, K. V. S. N.; Mallikarjuna, N. N.; Aminabhavi, T. M., *Journal of Applied Polymer Science* **2005,** 97, 518-526.

41.   Mishra, A. K.; Chattopadhyay, D. K.; Sreedhar, B.; Raju, K. V. S. N., *Journal of Applied Polymer Science* **2006,** 102, 3158-3167.

42.   Yeganeh, H.; Shamekhi, M. A., *Polymer* **2004,** 45, (2), 359-365.

43.   Liao, D. C.; Hsieh, K. H., *Journal of Polymer Science Part A: Polymer Chemistry* **1994,** 32, 1665-1672.

44.   Lin, M. F.; Shu, Y. C.; Tsen, W. C.; Chuang, F. S., *Polymer International* **1999,** 48, 433-445.

45.   Edwards, P. A.; Striemer, G.; Webster, D. C., *Progress in Organic Coatings* **2006,** 57, (2), 128-139.

46.   Chattopadhyay, D. K.; Prasad, P. S. R.; Sreedhar, B.; Raju, K. V. S. N., *Progress in Organic Coatings* **2005,** 54, (4), 296-304.

47.   Chattopadhyay, D. K.; Sreedhar, B.; Raju, K. V. S. N., *Journal of Applied Polymer Science* **2005,** 95, 1509-1518.

48.   Chattopadhyay, D. K.; Sreedhar, B.; Raju, K. V. S. N., *Journal of Polymer Science Part B: Polymer Physics* **2006,** 44, 102-118.

49.   Studer, K.; Decker, C.; Beck, E.; Schwalm, R., *Progress in Organic Coatings* **2003,** 48, (1), 92-100.

50.   Barni, A.; Levi, M., *Journal of Applied Polymer Science* **2003,** 88, 716-723.

51.   Chinwanitcharoen, C.; Kanoh, S.; Yamada, T.; Hayashi, S.; Sugano, S., *Journal of Applied Polymer Science* **2004,** 91, 3455-3461.

52.   Yang, C. H.; Lin, S. M.; Wen, T. C., *Polymer Engineering & Science* **1995,** 35, 722-730.

53.   Meier-Westhues, U., In *Polyurethanes: coatings, adhesives and sealants*, Vincentz Network: Hannover, 2007; p 136.

54.   Pourdeyhimi, B.; Wang, X.; Lee, F.; Behnam, P., In *Imaging and Image Analysis Applications for Plastics*, William Andrew Publishing: Norwich, NY, 1999; pp 107-117.

55.   Mackay, M. E.; Tuteja, A.; Duxbury, P. M.; Hawker, C. J.; Van Horn, B.; Guan, Z.; Chen, G.; Krishnan, R. S., *Science* **2006,** 311, (5768), 1740-1743.

56.   Sabzi, M.; Mirabedini, S. M.; Zohuriaan-Mehr, J.; Atai, M., *Progress in Organic Coatings* **2009,** 65, (2), 222-228.

57.   Chen, G.; Zhou, S.; Liao, H.; Wu, L., *Journal of Composite Materials* **2005,** 39, (3), 215-231.

58.   Rahman, M. M.; Kim, H. D.; Lee, W. K., *Journal of Applied Polymer Science* **2008,** 110, (6), 3697-3705.

59.   Yeh, J.-M.; Yao, C.-T.; Hsieh, C.-F.; Lin, L.-H.; Chen, P.-L.; Wu, J.-C.; Yang, H.-C.; Wu, C.-P., *European Polymer Journal* **2008,** 44, (10), 3046-3056.

60.   Jin, H.; Wie, J. J.; Kim, S. C., *Journal of Applied Polymer Science* **2010,** 117, (4), 2090-2100.

61.   Choi, H. Y.; Bae, C. Y.; Kim, B. K., *Progress in Organic Coatings* **2010,** 68, (4), 356-362.

62.   Solarski, S.; Benali, S.; Rochery, M.; Devaux, E.; Alexandre, M.; Monteverde, F.; Dubois, P., *Journal of Applied Polymer Science* **2005,** 95, (2), 238-244.

63.   Devaux, E.; Rochery, M.; Bourbigot, S., *Fire and Materials* **2002,** 26, (4-5), 149-154.

64.   Zhao, W.; Li, M.; Peng, H. X., *Macromolecular Materials and Engineering* **2010,** 295, (9), 838-845.

65.   Song, H.-J.; Zhang, Z.-Z.; Men, X.-H., *European Polymer Journal* **2007,** 43, (10), 4092-4102.

66.   Song, H.-J.; Zhang, Z.-Z.; Men, X.-H., *European Polymer Journal* **2008,** 44, (4), 1012-1022.

67.   Rybak, A.; Warde, M.; Beyou, E.; Chaumont, P.; Bechelany, M.; Brioude, A.; Toury, B.; Cornu, D.; Miele, P.; Giffard, B.; Seyverat, L.; Guyomar, D., *Nanotechnology* **2010,** 21, (14), 145610.

68.   Guiffard, B.; Guyomar, D.; Seveyrat, L.; Chowanek, Y.; Bechelany, M.; Cornu, D.; Miele, P., *Journal of Physics D: Applied Physics* **2009,** 42, (5), 055503.

69.   Hsu, S.-h.; Tseng, H.-J.; Lin, Y.-C., *Biomaterials* **2010,** 31, (26), 6796-6808.

70.   Akram, D.; Ahmad, S.; Sharmin, E., *Macromolecular Chemistry and Physics* **2010,** 211, (4), 412-419.

71.   Bauer, F.; Flyunt, R.; Czihal, K.; Buchmeiser, M. R.; Langguth, H.; Mehnert, R., *Macromolecular Materials and Engineering* **2006,** 291, (5), 493-498.

72. Barna, E.; Bommer, B.; Kürsteiner, J.; Vital, A.; Trzebiatowski, O. v.; Koch, W.; Schmid, B.; Graule, T., *Composites Part A: Applied Science and Manufacturing* **2005,** 36, (4), 473-480.

73. Jalili, M. M.; Moradian, S.; Dastmalchian, H.; Karbasi, A., *Progress in Organic Coatings* **2007,** 59, (1), 81-87.

74. Chen, Y.; Zhou, S.; Yang, H.; Wu, L., *Journal of Applied Polymer Science* **2005,** 95, (5), 1032-1039.

75. Sung, L.-P.; Comer, J.; Forster Aaron, M.; Hu, H.; Floryancic, B.; Brickweg, L.; Fernando Raymond, H., In *Nanotechnology Applications in Coatings*, American Chemical Society: 2009; Vol. 1008, pp 232-254.

76. Sung, L.-P.; Comer, J.; Forster, A.; Hu, H.; Floryancic, B.; Brickweg, L.; Fernando, R., *Journal of Coatings Technology and Research* **2008,** 5, (4), 419-430.

77. Floryancic, B. R.; Brickweg, L. J.; Fernando, R. H., In *Smart Coatings II*, American Chemical Society: 2009; Vol. 1002, pp 220-235.

78. Zhou, S.; Wu, L.; Sun, J.; Shen, W., *Progress in Organic Coatings* **2002,** 45, (1), 33-42.

79. Zhou, S.-X.; Wu, L.-M.; Sun, J.; Shen, W.-D., *Journal of Applied Polymer Science* **2003,** 88, (1), 189-193.

80. Hsu, S. h.; Chou, C. W.; Tseng, S. M., *Macromolecular Materials and Engineering* **2004,** 289, (12), 1096-1101.

81. Bucknall, C. B., *Journal of Elastomers and Plastics* **1982,** 14, (4), 204-221.

82. Bhat, G. S., *Materials and Manufacturing Processes* **1997,** 12, (4), 745 - 747.

83. Bagheri, R.; Pearson, R. A., *Polymer* **1996,** 37, (20), 4529-4538.

84. Hillmyer, M. A., Lipic, P. M.; Hajduk, D. A.; Almdal, K.; Bates, F. S. *J. Am. Chem. Soc.* **1997,** 119, 2749-2750.

85. Lipic, P. M.; Bates, F. S.; Hillmyer, M. A., *J. Am. Chem. Soc.* **1998,** 120, 8963-8970.

86. Mijovic, J.; Shen, M.; Sy, J. W.; Mondragon, I., *Macromolecules* **2000,** 33, (14), 5235-5244.

87. Guo, Q.; Thomann, R.; Gronski, W.; Thurn-Albrecht, T., *Macromolecules* **2002,** 35, 3133-3144.

88. Kosonen, H.; Ruokolainen, J.; Nyholm, P.; Ikkala, O., *Macromolecules* **2001,** 34, 3046-3049.

89. Kosonen, H.; Ruokolainen, J.; Nyholm, P.; Ikkala, O., *Polymer* **2001,** 42, 9481-9486.

90.   Ritzenthaler, S.; Court, F.; David, L.; Girard-Reydet, E.; Leibler, L.; Pascault, J. P., *Macromolecules* **2002,** 35, 6245-6254.

91.   Ritzenhaler, S.; Court, F.; Girard-Reydet, E.; Leibler, L.; Pascault, J. P., *Macromolecules* **2003,** 36, 118-126.

92.   Larrañaga, M.; Gabilondo, N.; Kortaberria, G.; Serrano, E.; Remiro, P.; Riccardi, C. C.; Mondragon, I., *Polymer* **2005,** 46, (18), 7082-7093.

93.   Meng, F.; Zheng, S.; Zhang, W.; Li, H.; Liang, Q., *Macromolecules* **2006,** 39, 711-719.

94.   Serrano, E.; Martin, M. D.; Tercjak, A.; Pomposo, J. A.; Mecerreyes, D.; Mondragon, I., *Macromolecular Rapid Communications* **2005,** 26, (12), 982-985.

95.   Xu, Z.; Zheng, S., *Macromolecules* **2007,** 40, (7), 2548-2558.

96.   Meng, F.; Zheng, S.; Li, H.; Liang, Q.; Liu, T., *Macromolecules* **2006,** 39, (15), 5072-5080.

97.   Fan, W.; Wang, L.; Zheng, S., *Macromolecules* **2008,** 42, (1), 327-336.

98.   Serrano, E.; Tercjak, A.; Ocando, C.; Larrañaga, M.; Parellada, M. D.; Corona-Galván, S.; Mecerreyes, D.; Zafeiropoulos, N. E.; Stamm, M.; Mondragon, I., *Macromolecular Chemistry and Physics* **2007,** 208, 2281-2292.

99.   Meng, F.; Xu, Z.; Zheng, S., *Macromolecules* **2008,** 41, (4), 1411-1420.

100. Grubbs, R. B.; Dean, J. M.; Broz, M. E.; Bates, F. S., *Macromolecules* **2000,** 33, 9522-9534.

101. Dean, J. M.; Grubbs, R. B.; Saad, W.; Cook, R. F.; Bates, F. S., *Journal of Polymer Science: Part B: Polymer Physics* **2003,** 41, 2444-2456.

102. Dean, J. M.; Lipic, P. M.; Grubbs, R. B.; Cook, R. F.; Bates, F. S., *Journal of Polymer Science: Part B: Polymer Physics* **2001,** 39, 2996-3010.

103. Dean, J. M.; Verghese, N. E.; Pham, H. Q.; Bates, F. S., *Macromolecules* **2003,** 36, (25), 9267-9270.

104. Serrano, E.; Tercjak, A.; Kortaberria, G.; Pomposo, J. A.; Mecerreyes, D.; Zafeiropoulos, N. E.; Stamm, M.; Mondragon, I. A., *Macromolecules* **2006,** 39, (6), 2254-2261.

105. Wu, J.; Thio, Y. S.; Bates, F. S., *Journal of Polymer Science Part B: Polymer Physics* **2005,** 43, (15), 1950-1965.

106. Thio, Y. S.; Wu, J.; Bates, F. S., *Macromolecules* **2006,** 39, (21), 7187-7189.

107. Liu, J.; Thompson, Z. J.; Sue, H.-J.; Bates, F. S.; Hillmyer, M. A.; Dettloff, M.; Jacob, G.; Verghese, N.; Pham, H., *Macromolecules* **2010,** 43, (17), 7238-7243.

108. Kar, S.; Banthia, A. K., *Journal of Applied Polymer Science* **2004,** 92, (6), 3814-3821.

109. Thomas, R.; Durix, S.; Sinturel, C.; Omonov, T.; Goossens, S.; Groeninckx, G.; Moldenaers, P.; Thomas, S., *Polymer* **2007,** 48, (6), 1695-1710.

110. Kaynak, C.; Ozturk, A.; Tincer, T., *Polymer International* **2002,** 51, (9), 749-756.

111. Kar, S.; Banthia, A. K., *Journal of Applied Polymer Science* **2005,** 96, (6), 2446-2453.

112. Barcia, F. L.; Amaral, T. P.; Soares, B. G., *Polymer* **2003,** 44, (19), 5811-5819.

113. Kumar, R. S.; Alagar, M., *Journal of Applied Polymer Science* **2006,** 101, (1), 668-674.

114. Shih, W. C.; Ma, C. C. M.; Yang, J. C.; Chen, H. D., *Journal of Applied Polymer Science* **1999,** 73, (13), 2739-2747.

115. Jaffrennou, B.; Portal, J.; Méchin, F.; Pascault, J.-P., *European Polymer Journal* **2008,** 44, (11), 3439-3455.

116. Johansson, M.; Glauser, T.; Jansson, A.; Hult, A.; Malmström, E.; Claesson, H., *Progress in Organic Coatings* **2003,** 48, (2-4), 194-200.

117. Kim, Y. H., *Journal of Polymer Science Part A: Polymer Chemistry* **1998,** 36, 1685-1698.

118. Malmstroem, E.; Johansson, M.; Hult, A., Hyperbranched Aliphatic Polyesters. *Macromolecules* **1995,** 28, (5), 1698-1703.

119. Schmaljohann, D.; Häußler, L.; Pötschke, P.; Voit, B. I.; Loontjens, T. J. A., *Macromolecular Chemistry and Physics* **2000,** 201, 49-57.

120. Malmström, E.; Johansson, M.; Hult, A., *Macromolecular Chemistry and Physics* **1996,** 197, 3199-3207.

121. Gao, C.; Yan, D., *Prog. Polym. Sci.* **2004,** 29, (3), 183-275.

122. Peerlings, H. W. I.; Van Benthem, R. A. T. M.; Meijer, E. W., *Journal of Polymer Science Part A: Polymer Chemistry* **2001,** 39, 3112-3120.

123. Jikei, M.; Chon, S.-H.; Kakimoto, M.-A.; Kawauchi, S.; Imase, T.; Watanebe, J., *Macromolecules* **1999,** 32, (6), 2061-2064.

124. Emrick, T.; Chang, H.-T.; Fréchet, J. M. J., *Macromolecules* **1999,** 32, (19), 6380-6382.

125. Fang, J.; Kita, H.; Okamoto, K.-i., *Macromolecules* **2000,** 33, (13), 4639-4646.

126. Flory, P. J., In *Principles of polymer chemistry*, Cornell University Press: Ithaca, New York, 1953.

127. Gao, C.; Yan, D., *Macromolecules* **2003,** 36, (3), 613-620.

128. Bruchmann, B.; Schrepp, W., *e-polymers* **2003**, 014.

129. Abdelrehim, M.; Komber, H.; Langenwalter, J.; Voit, B.; Bruchmann, B., *Journal of Polymer Science Part A: Polymer Chemistry* **2004,** 42, 3062-3081.

130. Frey, H.; Haag, R., *Reviews in Molecular Biotechnology* **2002,** 90, (3-4), 257-267.

131. Sunder, A.; Frey, H.; Mülhaupt, R., *Macromol. Symp.* **2000,** 153, (1), 187-196.

132. Xinling, W.; Jianjun, C.; Ling, H.; Xiaozhen, T., *Journal of Polymer Science Part B: Polymer Physics* **2001,** 39, 2225-2230.

133. Xiaoying, S.; Xiaohui, Y.; Yunhang, L.; Xinling, W., *Journal of Polymer Science Part A: Polymer Chemistry* **2004,** 42, 2356-2364.

134. Nasar, A. S.; Jikei, M.; Kakimoto, M.-a., *European Polymer Journal* **2003,** 39, (6), 1201-1208.

135. Yang, G.; Jikei, M.; Kakimoto, M.-a., *Macromolecules* **1998,** 31, (17), 5964-5966.

136. Yang, G.; Jikei, M.; Kakimoto, M.-a., M*acromolecules* **1999,** 32, (7), 2215-2220.

137. Huybrechts, J.; Dusek, K., *Surface Coatings International* **1998,** 81, (3), 117.

138. Zhai, X.; Peleshanko, S.; Klimenko, N. S.; Genson, K. L.; Vaknin, D.; Vortman, M. Y.; Shevchenko, V. V.; Tsukruk, V. V., *Macromolecules* **2003,** 36, (9), 3101-3110.

Chapter 2

Methods

2.1   Polymerization methods

2.1.1   Anionic polymerization

Anionic polymerization has increasingly attracted attention since 1956, when Szwarc first reported the living nature of the anionic polymerization of styrene and dienes[1, 2]. Since then, living anionic polymerization has been used to prepare well-defined polymers varying in topology, composition, end functionality and microstructure. The particularity of such a living polymerization is the fact that no irreversible termination or chain transfer occur. Thus, very high molecular weight can be reached which are determined by the stoichiometry of the reaction and the monomer conversion. However, living anionic polymerization is very sensitive to moisture and therefore high vacuum techniques are required. It is applicable to a very large choice of monomers as long as the right conditions have been chosen in terms of initiator (counter-ion), solvent and eventual additives. Polar or non-polar monomers can be polymerized with the only restriction due to acidic protons (i.e. alcohols, amines or acids) as they can be abstracted by the propagating species. The use of protected monomers are usually called in. For example, protecting groups such as acetals, silyl derivatives or *tert*-butylesters are easily removable in acidic media.

The initiation step is the formation of a carbanionic adduct by the nucleophilic attack of an initiator on the vinyl bond of a monomer. This carbanion possesses an electronic structure which remains the same through further addition of monomer units during the polymerization. The anionic charge is stabilized by electronic delocalization over the monomer. The choice of the initiator depends on the reactivity of the monomer towards nucleophilic attack. The rate of initiation has to be higher than the rate of propagation to yield high initiation efficiency and a constant number of carbanionic species during

polymerization. Termination occurs principally by hydrogen transfer which is usually added after complete consumption of the monomer.
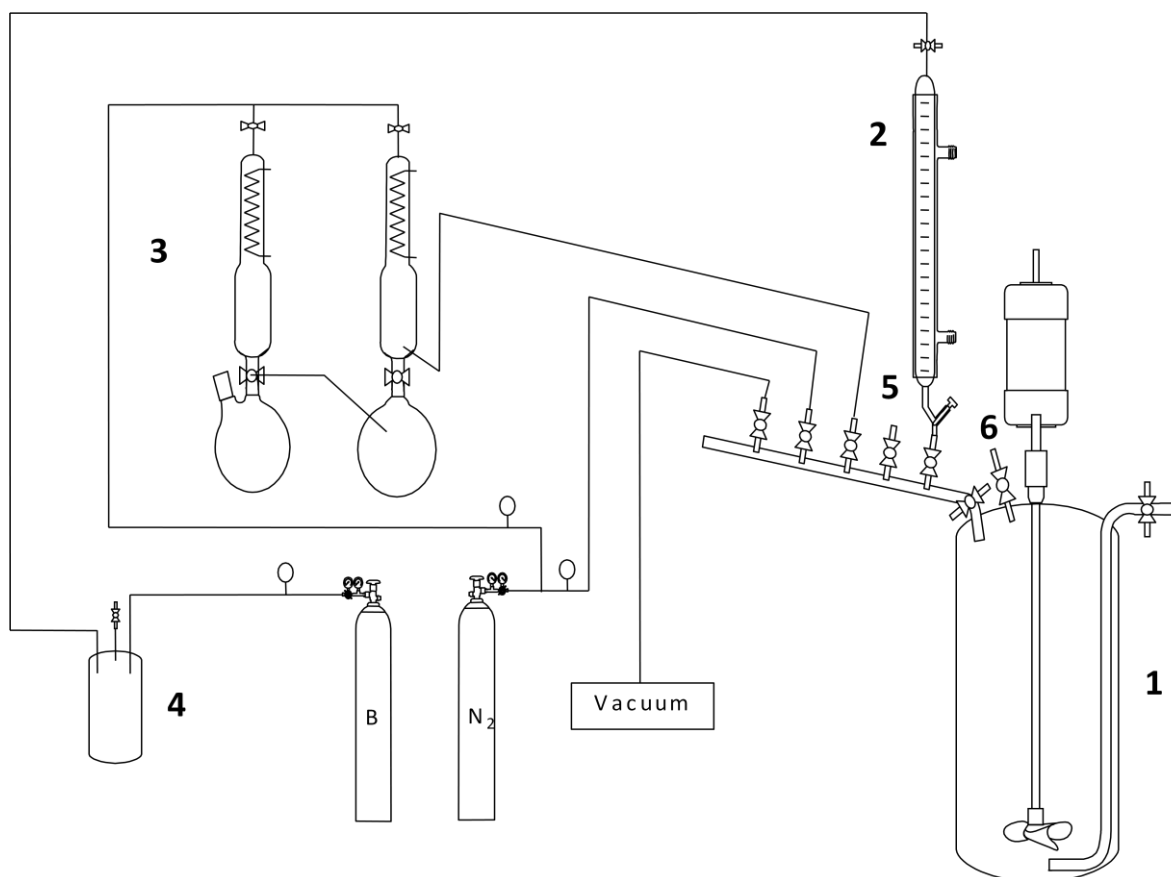
Scheme 1. Setup of anionic reactor. 1. Autoclave, 2. Burette for condensation of gaseous monomers (e.g. butadiene), 3. Solvent distillation setup, 4. Reactor for purification of butadiene, 5. Connector for monomer ampoules (e.g. methyl methacrylate), 6. Septum for injection of initiator and additives.

In the present work, the polymerization of non-polar monomers like butadiene and divinylbenzene can be initiated directly by *sec*-butyllithium. The subsequent polymerization of (meth)acrylates in polar solvent is possible if the nucleophilicity of the polybutadienyl lithium chain end is reduced by an end-capping agent such as 1,1-diphenylethylene and if the reaction is carried out at very low temperature (-78 °C). However, in a non-polar solvent, subsequent polymerization of (meth)acrylate monomers can be carried out in a controllable manner at higher temperature, without the use of an end-capping agent, if a wisely chosen Lewis base in combination with an aluminum alkyl are used as additives[3, 4]. In our case, dimethoxyethane (DME) associated with *iso*-butyl aluminum *(2,6-di-tert-butyl-4-methylphenolate)₂* (*i*BuAl(BHT)₂) are chosen as additives and allow the polymerization of methacrylate monomers to take place at room temperature while acrylates are preferably polymerized at -20 or -15 °C under these conditions.

All polymerizations are carried out in Büchi (Switzerland) vessel reactor under inert atmosphere. Except for butadiene, all monomers are purified using high vacuum techniques and freeze-thaw cycles. An alkyl aluminum agent is used to remove impurities left after freeze-thaw cycles and the appearance of a characteristic yellow colour evidences the absence of such impurities[5]. The monomer is condensed from the alkyl aluminum agent into an ampoule and is stored at liquid nitrogen temperature until use.

All solvents used were distilled over CaH_2 (3 days) and potassium (3 days) or K/Na alloy (for THF) under inert atmosphere.

2.1.2   Anionic Self-Condensing Vinyl Polymerization (ASCVCP)

In 1995, when Fréchet et al. studied the polymerization of 3-(1-chloroethyl)-ethenylbenzene under cationic conditions, highly branched and irregular dendritic structures were obtained. The detailed time-dependence investigation of the polymerization turned out to be typical of polycondensation and thus this approach to hyperbranched polymers was referred to as Self-Condensing Vinyl Polymerization (SCVP)[6]. The process involves the use of an "inimer" (initiator-monomer) which is a monomer carrying one vinyl bond and one initiating moiety. The general structure of such an inimer is designated AB*, where A stands for the vinyl bond, B is the initiating moiety and the asterisk indicates an active site. The activation of a B* group allow the polymerization to start by propagation through the double bond of a second inimer resulting in the formation of a dimer (A-b-A*-B*) which possesses two active sites (A* and B*) and one double bond. Both the initiating group B* and the newly created propagating center A* are able to react with vinyl groups of other molecules (monomers, inimers, dimers or oligomeric species) leading ultimately to highly branched structures. In the case of the reaction with a comonomer M, Self-Condensing Vinyl Copolymerization (SCVCP) will occur and lead to the creation of a third propagating site, M*. The use of a comonomer has many advantages: (i) conventional monomers are cheaper and easier to obtain than inimers, (ii) functional groups can be integrated to the branched polymer, (iii) polydispersity index can be controlled over the comonomer ratio M/AB* and lowered compared to conventional routes to hyperbranched structures, (iv) the degree of branching (DB) can be controlled. Theoretical calculations about SCVCP were reported by Müller and co-workers[7, 8] and two extreme cases of

reactions were defined. On the one hand, the inimer acts as an ordinary initiator only and the reaction resembles that of a homopolymerization of the comonomer. When the comonomer is fully consumed, those "macroinimers" (A-b-M*) undergo SCVP yielding hyperbranched species. On the other hand, when inimers will first undergo SCVP and only at high inimer conversion, add comonomer, star-shaped polymers will be obtained. Kinetics, molecular weight distribution and DB strongly depend on the comonomer/inimer ratio $\gamma = M_o/I_o$.

Applicable to cationic polymerizing systems[6, 9], SCVP has been extended to other controlled/living polymerization method like radical polymerization[10-12], group transfer polymerization[13] and anionic polymerization[14-16].
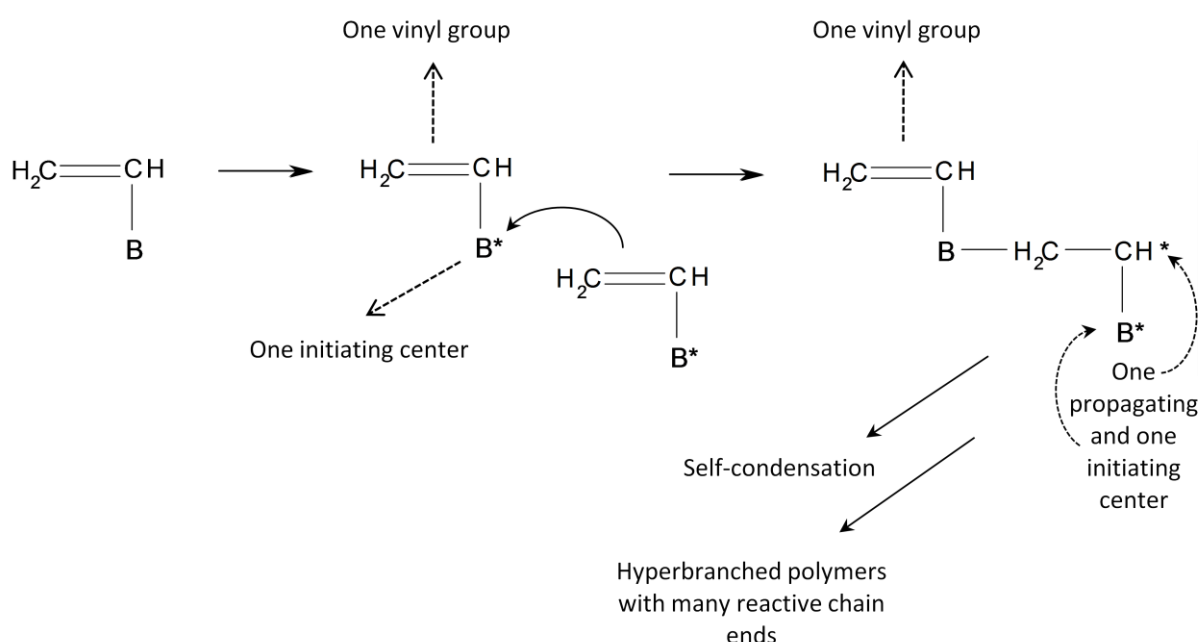
Scheme 2. Self-condensing vinyl polymerization process[6].

The so-called Anionic Self-Condensing Vinyl Polymerization (ASCVP) is therefore the extended version of SCVP to anionic polymerization and is used for the preparation of hyperbranched polymers. Up to date, it has been barely utilized because of the difficulties encountered to produce a vinyl monomer bearing an anionic initiator owing the high reactivity of carbanions and aggregation of counter-ions. Main studies have been carried out concerning the use of styrenic monomers like divinylbenzene (DVB) and 1,3-diisopropenylbenzene[14, 15] as inimers. Monomer-polymer equilibrium limited molecular weight growth. Styrene was used as a promoter comonomer and hyperbranched polymers

soluble in organic media were obtained. This one-pot process yields branched polymers with broad molecular weight distributions. Their carbanionic chain end is capable of reacting with versatile electrophilic reagents or of further polymerizing another block by anionic technique leading to desired functionality in the polymers.

2.2   Characterization methods

2.2.1   Gel Permeation Chromatography (GPC)

Conventional GPC measurements were performed on a set of 30 cm SDV-gel columns of 5 μm particles size having pore sizes of 10^5, 10^4, 10^3 and 10^2 Å with RI and UV (λ = 254 nm) detection. THF was used as eluent with a flow rate of 1 ml/min. Toluene was used as internal standard and polybutadiene or polystyrene standards were used for calibration. Win GPC software was used for data evaluation and samples were filtered using 0.2 μm PTFE filters prior to measurements.

GPC with multi-angle light scattering detector (GPC/MALS) and GPC with a viscosity detector (GPC/viscosity) were used to determine absolute molecular weight and Mark-Houwink-Sakurada parameters of the hyperbranched polymers. THF was used as eluent at a flow rate of 1 ml/min on a set of 30 cm PSS SDV gel columns of 5 μm particles size having pore sizes of 10^6, 10^5 and 10^3 Å. Agilent Technologies 1200 Series refractive index detector and Wyatt DAWN HELEOS MALS detector equipped with a 632.8 nm He-Ne laser were used for GPC/MALS. Viscotek viscosity detector Model 250 was used for GPC/viscosity measurements. Samples were filtered using 0.2 μm PTFE filters prior to measurements.

2.2.2   Refractive index increment dn/dc

A diffraction refractometer DnDC2010/620 (PSS) was used to measure refractive index increments of polymer solutions at λ = 620 nm.

2.2.3   Static Light Scattering (SLS)

SLS measurements were carried out on a Sofica goniometer with a He-Ne laser (λ = 632.8 nm) at room temperature. Micellar solutions of the polymers were prepared in the concentration range between 0.1 and 5 g/L. Prior to the measurements, sample solutions

were filtered through Millipore PTFE filters of pore size 1 µm. A Zimm plot was used to evaluate the data.

2.2.4 Dynamic Light Scattering (DLS)

DLS measurements were performed on an ALV DLS/SLS-SP 5022F compact goniometer system with an ALV 5000/E correlator and a He-Ne laser (λ = 632.8 nm). Sample solutions were filtered using Millipore Teflon filters with a pore size of 0.2, 0.45 or 1 µm. CONTIN analysis of the obtained autocorrelation functions was carried out and apparent dynamic radii, $R_{h,z}$, were calculated according to the Stokes-Einstein equation.

2.2.5 [1]H Nuclear Magnetic Resonance spectroscopy (^{1}H NMR)

^{1}H NMR spectra were obtained on a Bruker 250AC spectrometerat an operating frequency of 250 MHz or 300 MHz using various deuterated solvents (Deutero GmbH) depending on the solubility of the samples.

2.2.6 Transmission Electron Microscopy (TEM)

TEM was performed on a Zeiss CEM902 EFTEM electron microscope (CEM 902) operated at 80kV or a Zeiss EM922 OMEGA EFTEM at 200 kV. A droplet of polymer solution was placed on a carbon-coated copper grid and most of the liquid was removed using a filter paper. Staining with OsO_4 was used for the non cross-linked micellar solutions. The cross-linked samples presented a sufficient contrast attributed to the presence of sulfur or phosphor in the core depending on the cross-linking agent used.

2.2.7 Differential Scanning Calorimetry (DSC)

DSC was performed on a Perkin-Elmer PYRIS 1 apparatus under dry nitrogen atmosphere with a CCA7 liquid nitrogen cooling system. Indium was used for calibration and pans were filled with at least 8 mg of samples. The samples were heated up to 150 °C at a heating rate of 40 °C/min and then quenched to -100 °C. The cycle was repeated three times and the first run was always discarded. The glass transition temperature is evaluated at half of the C_p change.

2.2.8　Matrix-Assisted Laser Desorption Ionization - Time of Flight - Mass Spectroscopy (MALDI-ToF MS)

MALDI-ToF MS measurements were performed on a Bruker Reflex III instrument equipped with a 337 nm N2 laser in the reflectron and linear mode and 20 kV acceleration voltage. Trans-2.[3-(4-tert-Butyl phenyl)-2-methyl-2-propenylidene]manolonitrile (DCTB) was used a matrix for molecular weight determination. The cationizing agent was silver trifluoroacetate (AgTFA).

2.3　Coatings Tests

To grant approval of paint or coating, major automotive companies require specific testing protocols. In general, 2K PUR exterior automotive clearcoats must imperatively provide required gloss, distinctness of image (DOI) and durability. Additionally to appearance, performance requirements also include hardness, adhesion, chip resistance, toughness, fluid resistance, cold checking resistance, flexibility and weatherability.

Tests can be divided into two categories: optical characterization and mechanical/physical characterization

2.3.1　Optical properties

In terms of optical characterization, the appearance of coatings comprises color and gloss. PU clearcoats are transparent coatings and therefore our main interest lays in their glossiness. The best tool to evaluate the appearance of a surface, a coating is the human eye. However, the human eye is very subjective and each observer will see and appreciate what is seen differently. To minimize these differences, viewing conditions have to be defined concerning the surface, the light source and the observer. Furthermore, according to K. Lex[17], gloss can be subdivided into two groups depending on what the observer is looking at. For one group, the eye focuses on the surface itself (Figure 1a) and for the second group, it focuses on the reflected image of an object by the surface (Figure 1b).
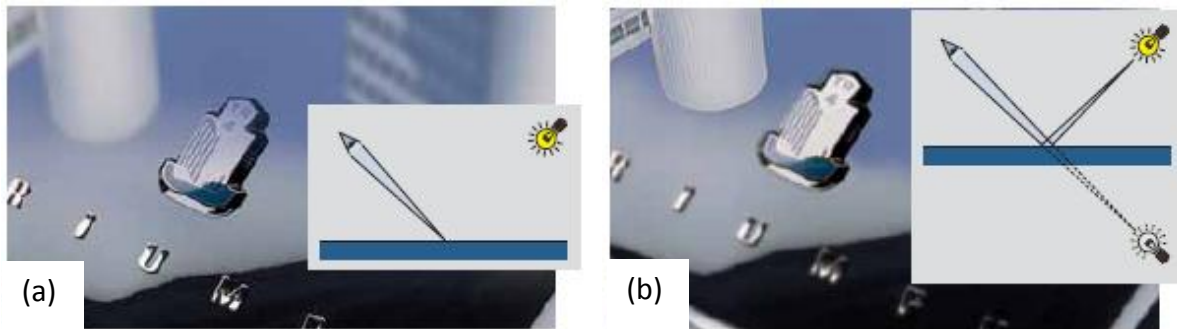
Figure 1. Pictures describing two viewing conditions: (a) focus on the surface and (b) focus on the reflected image on the surface

For each group, different information will be gathered to describe the gloss. In Scheme 3, relationships between appearance characteristics and the complexity of gloss are depicted.

When focusing on the reflected image of an object, information about how distinctly the object is reflected is obtained by the observer. The reflected light may appear brilliant or diffuse depending on the *specular gloss*. The outline of the reflected object may appear distinct or blurry depending on the *image clarity* and finally, a halo surrounding the reflected image would be an indication of *haze*. Focusing on the surface itself will provide information about its structure (size, depth, shape) contributing to *waviness* or *directionality* of the surface.

2.3.1.1 Specular gloss

The specular gloss is defined as the "ratio of flux reflected in specular direction to incident flux for a specified angle of incidence and source and receptor angular aperture"[18]. This is the most frequently measured aspect of gloss because it is the one for which an instrument is easily constructed. The design of glossmeter is based on the precise measurement of the specular component of reflected light. A light source is placed at the focal point of a collimating lens. The axis of the collimated beam is set to the desired angle of illumination. A receptor lens with an aperture in the focal plane followed by an illumination detector complete the basic optical design. In Figure 2a, the reflected light flux distribution from a semi-gloss surface is described by the grey line. Only the red portion, including the specular component, passes through the aperture and is detected. Glossmeter geometries are identified by reference to the incidence angles, typically 20°, 60° and 85° (Figure 2b). The 60° geometry is used for comparing most specimens and for determining when 20° and 85° geometries may be more applicable. The 20° geometry is advantageous

for comparing surfaces with 60° gloss values higher than 70 (very glossy surfaces) while the 85° geometry is most frequently applied for surfaces with 60° gloss values lower than 10.
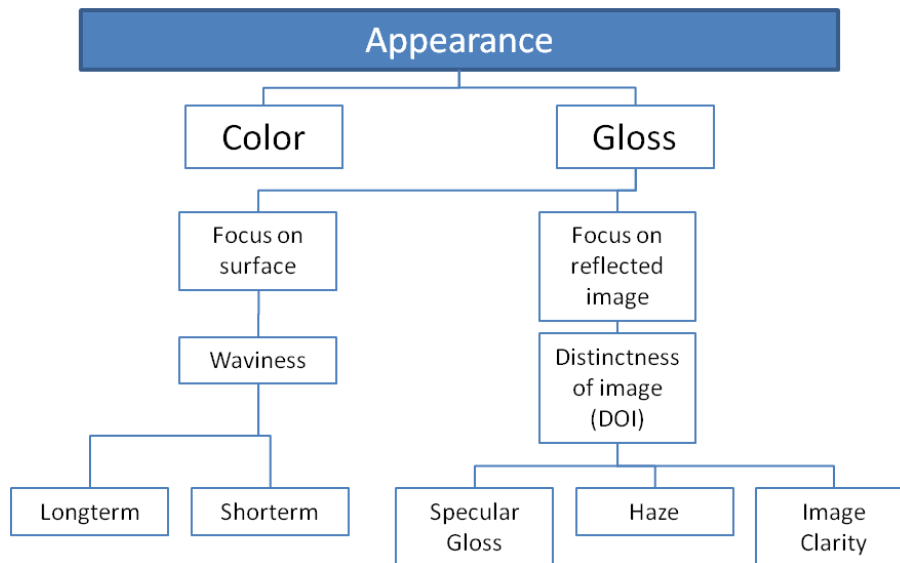
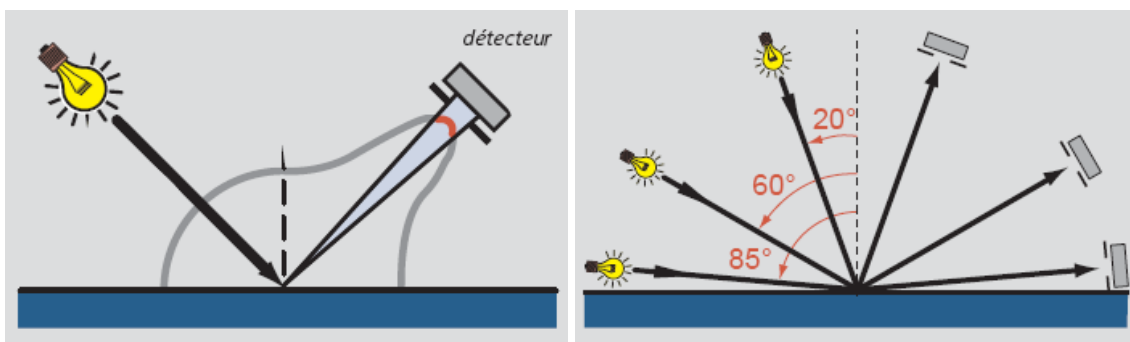**Scheme 3. Relationship of various appearance characteristics**

Figure 2. (a) Measurement of the specular gloss and (b) various glossmeters geometries (BYK Gardner)

2.3.1.2   Haze

For coating films, it is designated as "reflection haze" and defined as the "percent of reflected light scattered by a specimen having a glossy surface so that its direction deviates more than a specified angle from the direction of the specular reflection"[18]. This phenomenon is associated to high glossy surfaces and causes them to appear milky and lighter with a lost in contrast. Usually due to microscopic irregularities on the surface (degree of dispersion, flocculation of pigments or additives, incompatibility of raw material, poor application procedure), small amounts of reflected light are scattered in a direction adjacent, typically 1° to 4°, to the specular reflection (Figure 3). 20° glossmeter are usually

equipped with additional apertures for haze evaluation permitting measurements of both gloss and haze with the same instrument simultaneously.
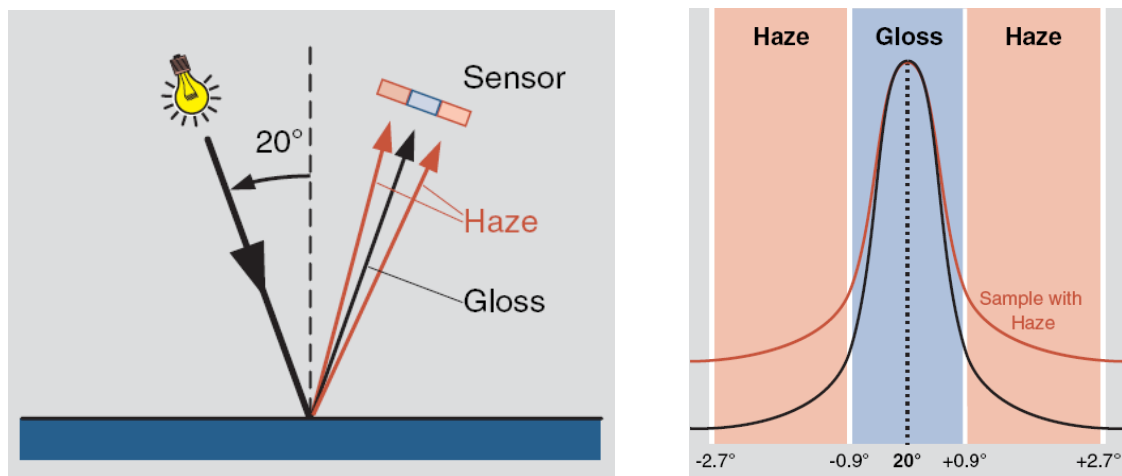

Figure 3. Schematic representation of the reflection haze phenomenon (BYK Gardner)

2.3.1.3 Image clarity

Image clarity is defined as the "aspect of gloss characterized by the sharpness of images of objects produced by reflection at a surface"[18]. It is a critical parameter for glossy surface having small amounts of waviness and is independent of change in specular gloss and haze.

2.3.1.4 Waviness

Also called "orange peel", waviness is defined as "the appearance of irregularity of a surface resembling the skin of an orange"[18]. It is the case when a surface exhibits small indentations perceived as a pattern of both highlighted and non-highlighted areas.

2.3.1.5 Directionality

Directionality is the "degree to which the appearance of a surface changes as the surface is rotated in its own plane, under fixed conditions of illumination and viewing"[18]. A surface exhibits directionality when the specular gloss is a function of the direction for which measurements are made. For example, when paint is applied with a brush in one direction, the marks of the brush will result in directionality.

Image clarity, waviness and directionality will not be of our interest and details about their measurements can be found elsewhere in the literature[19].

2.3.2   Physical/Mechanical properties

2.3.2.1   Adhesion

In general, the application of coatings on a substrate has a decorative, protective or functional purpose. It is of great importance that the coating adheres well to the substrate. Coating adhesion is, nevertheless, a complex and often poorly understood property. Few fundamental and basic concepts of adhesion and current test methods related to it will be reviewed in this section

Adhesion represents all the physico-chemical phenomena happening when two materials are putting in intimate contact with each other to resist mechanical separation. Between a surface and a coating, the adhesion can be viewed as the union of a solid and a liquid which solidifies to form a thin film. The work of adhesion, W_a, is then described by:

$$W_a = \gamma_1 + \gamma_2 - \gamma_{12}$$

γ_1 and γ_2 are the surface tension of the two phases. From the work of adhesion, one can calculate the ideal adhesive strength (maximum force per unit area):

$$\sigma^2 = (16/9(3)^{12})(W_a/Z_o)$$

where Z_o is the equilibrium separation between the two phases, usually about 5 Å.

In the following, theories describing various mechanisms of adhesion and fracture are presented. As perfect adhesion strength is never reached, deviations can be identified through the numerous proposed theories.

Wetting-contact theory (physical adsorption)

Van der Waals forces are the principal forces, providing sufficient bond strength, responsible for the adhesion of a coating/substrate system. It involves attraction between permanent dipoles and induced dipoles. This physical adsorption contributes in all adhesion mechanism[20-22] as the weakest force contribution; it is however a necessary but not sufficient condition for the establishment of coating film adhesion. One should also notice that this theory does not take into account the effects of substrates defects.

Chemical adhesion (chemical binding)

The two materials are being held together by interfacial covalent, ionic or hydrogen bonds. It can be achieved with the use of coupling agents such as silanes, titanates or the introduction of organic functionalities (isocyanates, carboxyls, hydroxyls, epoxides…). Appropriate modification of the surface's acidity or basicity of the substrate should also increase interaction between coating and substrate. Chemical adhesion greatly enhances the adhesive strength.

Mechanical adhesion (interlocking)

The coating is filling the substrate's voids and pores causing interlocking of the two materials. Roughness of the substrate is, in this case, a primordial parameter for good adhesion. However, too rough surfaces can lead to poor adhesion because of the lack of intimate contact between the coating and the substrate and therefore, the production of uncoated voids.

Electrostatic adhesion

This theory is particularly applicable to metal-polymer bonds. When they are brought into contact a charge transfer occurs resulting in the formation of an electrical double layer which requires work to be tore apart.

Diffusion theory

Exclusively valid for polymer-polymer contacts, this theory was brought by Voyutskii and proposed the coating adhesion to be due to interdiffusion of the polymer chains[23, 24]. It was supported by the fact that adhesive strength was observed to increase with polymer molecular weight and contact time but also that no clear-cut interface boundary exists. Instead, an interphase formed by the blending of polymer chains from both phases was found. Of course, interdiffusion depends on polymer-polymer compatibility and although most polymer pairs are incompatible, statistical thermodynamics have prove that interdiffusion took place as a tendency to minimize free energy at the interface[25, 26]. The

thickness of the interface could be described as a function of the Flory-Huggins interaction parameter χ and appeared to increase as the interaction parameter decreases[27].

Weak boundary layer theory

Clean substrate surfaces give strong bonds to coatings. If contaminants are present like oil, grease or rust, a layer which is cohesively weak will be formed when the coating is applied. This weak boundary layer (WBL) is usually near the interface coating/substrate (see 1, 2, 4 and 5 on Scheme 4). The fracture is, in this case, not occurring at the interface between the coating and the substrate (see 3 on Scheme 4) but in a cohesively manner (within the same material) in this layer of the material weakly bound. Some contaminants might be dissolved by the coating but not all.
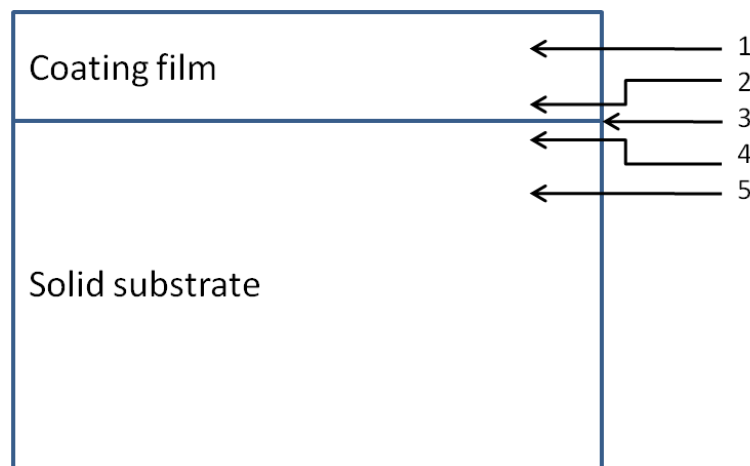
Scheme 4. Possible zones of failure according to the WBL theory .

Fracture theory

Fracture mechanics state that fracture will propagate from the weakest point, a defect. Applied to coating fracture[28, 29], these defects or voids will most likely be found at the interface between the coating and the substrate. The strength of the bond, in terms of the energy required to induce fracture, is described as a function of the defect size and the energy dissipated by irreversible processes (e.g. plastic deformation).

Each theory describes adhesion as a single phenomenon. However, it is intuitive that they all play some role in the interfacial interaction of a coating and a substrate. More realistically, adhesion is a combination of all these phenomena, a summation of all

intermolecular interactions at the interface. It is, therefore, a questionable task to study the contribution of one phenomenon independently from the others. Understanding basic adhesion is about understanding surface chemistry, surface physics, and surface architecture, coating polymer chemistry and physics, polymer rheology, coating internal stress and fracture mechanics.

Given the complexities of the adhesion process, no tests can precisely assess the actual physical strength of an adhesive bond. But it is possible to obtain an indication of relative adhesion performance.

The **tape test** or peel test is by far the most used test to assess "adhesion" of coatings since 1930s. In its simplest version, a piece of adhesive tape is pressed against the coating film and the test consists in observing how the film is peeled off when the tape is removed. The test is refined by cutting a lattice pattern in the coating film (to the substrate) before applying the adhesive tape and removing it. According to the thickness of the dried paint film, the pattern is different as spaces between the cuts vary:

- < 50 μm, eleven cuts spaced 1 mm apart are used.

- > 50 μm and < 125 μm, six cuts spaced 2 mm apart are used.

- > 125 μm, a 3.8 cm X-cut is made.

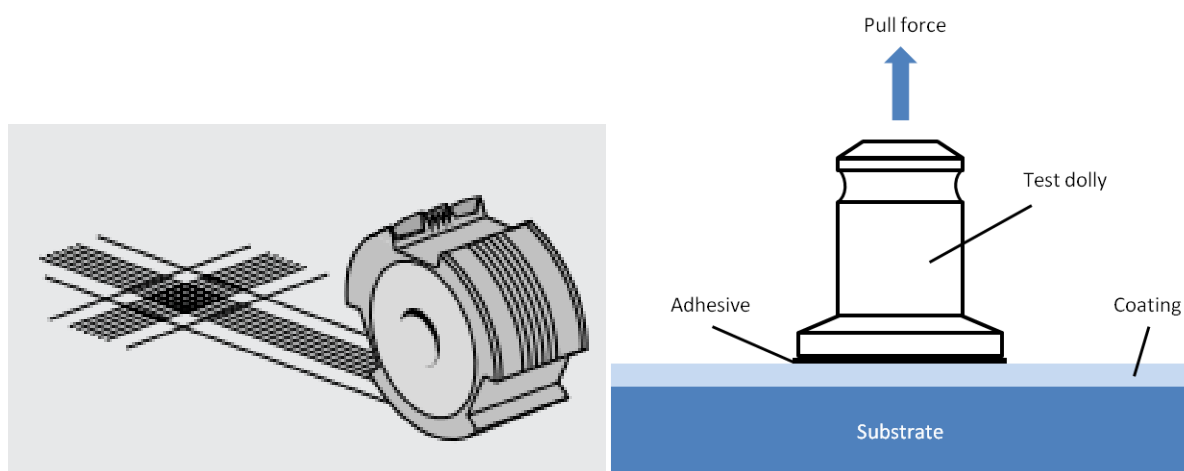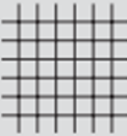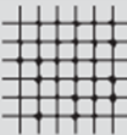Adhesion is rated according to a scale illustrated in Table 1.

Figure 4. Cutting tool for the tape test (six parallel cuts) and schematic representation of the pull-off test

Table 1. Classification of adhesion tape test results for a six parallel cuts. DIN EN ISO 2409.

Surface of cross-cut area	Classification ISO	Description
	0	none of the squares of the lattice is detached
	1	small flakes are detached at intersections (<5% of surface area affected)
	2	Small flakes are detached along edges and intersections (5-15% of surface area affected)
	3	Flakes along edges and on parts of squares (15-35% of surface area affected)
	4	Large ribbons along edges and whole squares (35-65% of surface area affected)
> 65% of the surface area	5	Worse than grade 4

The ***pull-off test*** consists in measuring the pull-off strength of coatings. Perpendicularly to the coated surface, a stud (cylinder) is applied and bonded. The normally applied force, which is required to remove the film, is measured. If failure occurs at the substrate-film interface, this force is taken as the "force of adhesion".

2.3.2.2   Abrasion resistance

Abrasion regroups the actions of scuffing, scratching, wearing down, marring and rubbing away. Abrasion resistance of an organic coating is, therefore, its ability to withstand these actions which tend to disfigure the surface appearance of the coating. It is the resistance to permanent deformation as a consequence of dynamic mechanical forces. In the case of automotive coatings, typical examples are the impact of gravel, as usually found on roads,

on the car body ("chip resistance") or the action of a brush during car-wash on the organic coating of a car body ("scratch resistance"). In both cases, damages are caused by mechanical action that removes material from the surface of the coating. Thus, abrasion resistance is not an isolated property but most likely related to other physical characteristics such as hardness, tensile strength or toughness.

One could think that the harder a material is, the better its abrasion resistance will be. This is not always the case. As an example, a steel wheel will not last long compare to a rubber tire on our concrete roads even though steel is much harder than rubber. The ability of rubber to undergo elastic deformation is associated to its good abrasion resistance. Indeed, the energy transfered to an elastic material is returned to the impacting object instead of being expended in the destruction of the impacted surface. If the deformation is not elastic, the material will yield and flow causing damages. Therefore, a soft material with low tensile strength will not be abrasion resistant. This does not mean hard materials cannot be abrasion resistant. When two materials with same tensile strength are compared, the one with the lowest modulus will be more abrasion resistant. But in fact, hard materials have usually higher tensile strength than soft ones. A hard material might be a very good abrasion resistant with adequate hardness and tensile strength but a weak material.

Mechanism of abrasion will differ according to the contact angle between abrasive particles and the tested surface. When abrasive particles are striking the surface with a normal or nearly normal incidence, the coating tends to be compressed, disfigured or cut resulting in removal of small portions of the coating. This is typically the case during chipping tests. When near the grazing incidence angle (scratching tests), the coating will tend to undercut, shear through thin layer in successive and irregular slices which will ultimately wear away.

On account of this, testing abrasion resistance is measuring a complex combination of interrelated properties. This task is however possible and allows us to correlate or predict the service performances of the coating at least in a qualitative and relative way.

Three ways are distinguished to test mar resistance:

-single scratches made with a needle or other sharp instrument

-a large number of scratches made by abrasive particles falling or impinging on the specimen (chipping tests)

-a large number of fine scratches made by an abrasive medium being rubbed against the specimen, called scuffing (scratching tests)

2.3.2.2.1   Chipping Tests

Here, damages caused by stone-chips are simulated. In our investigation, three different tests were carrying out as listed in Table 2.

Table 2. Chip resistance tests

Method	Characteristics	Required by
Multi-impact test (VDA-test)	Steel shot (D = 4-5mm), 2*500g, 2 bars, 45° or 90°, RT	Audi, Porsche, PSA, VW, Ford, Volvo
Single-impact test (Wedge impact)	3 bars, -20°C/ RT	BMW
Ball shot test	Steel bullet (D = 2 mm), 250 km/h, 90°, -20°C/ RT	Daimler Chrysler

Figure 5. VDA chipping tester, type 508, Erichsen GmbH & Co. KG (Hemer, Germany) and standard steel shots used as abrasive particles for the test.
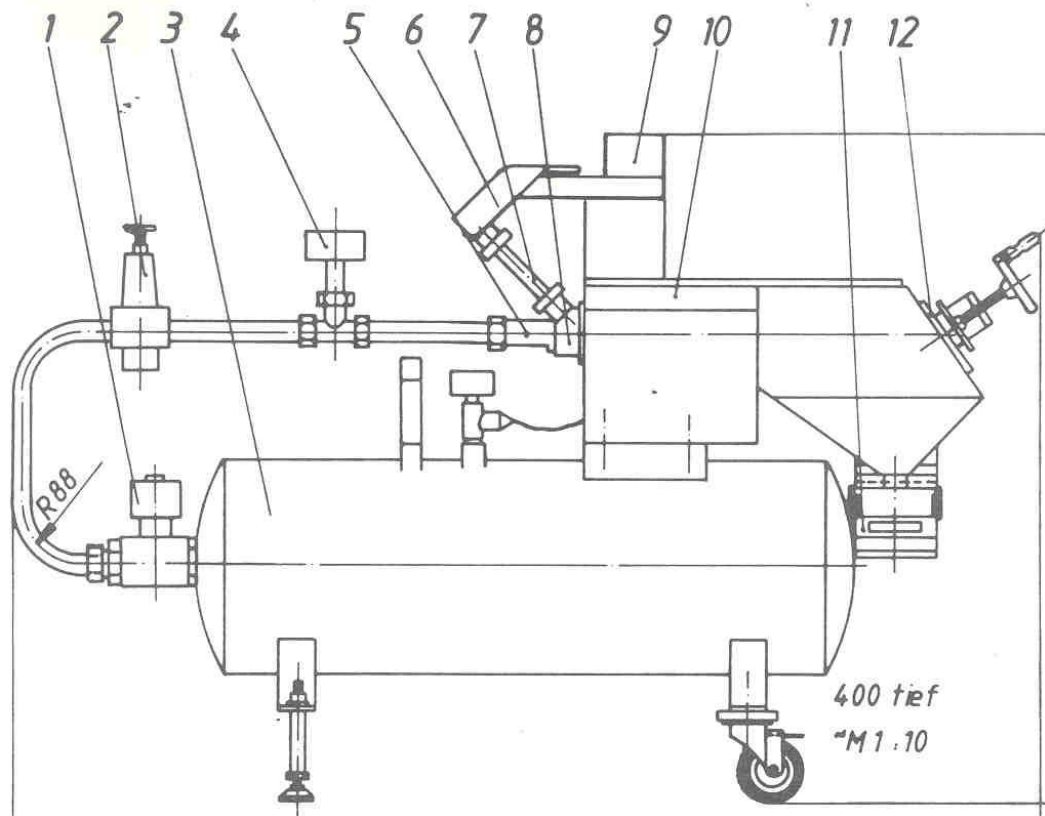
Figure 6. Schematic view of the VDA chipping tester. 1-Valve, 2-Air pressure regulator, 3-Pressure tank, 4-Manometer, 5-Nozzle, 6-Slide, 7-Acceleration tube, 8-Fastener, 9-Vibrating gravel hopper, 10-Operator's control, 11-Catchment tank, 12-Test panel.

Multi-impact test (VDA-test)

In this test, a stream of particular gravel (500 g of sharp-edged steel shot with 4-5 mm diameter size) is propelled twice, with a pressure of 2 bars, on the coated surface. The incidence angle of the stream can be regulated to 45° or 90° and is carried out at room temperature. Loose pieces of the coating are removed using an appropriate adhesive tape. The blasted panels are visually evaluated and rated in terms of affected area from 0.5 (0.2 % affected area) to 5.0 (81.3 % affected area). This test is required by most cars manufacturers

Single-impact or wedge-impact test

The principle of multi- and single-impact tests is the same except that instead of a handful of gravel, in the case of a multi-impact test, a single defined impact body is used here. The impact body is a wedge-shaped cutting edge to obtain a damage pattern on the test panel. This impact body is pushed onto the coating by a steel ball accelerated by compressed air (3 bars). Loose pieces of coatings are removed using an adhesive tape and the panel is visually evaluated and rated. The test is performed at room temperature but

can also be performed at -20 °C to simulate winter-like driving conditions. Three tests are run for each sample.
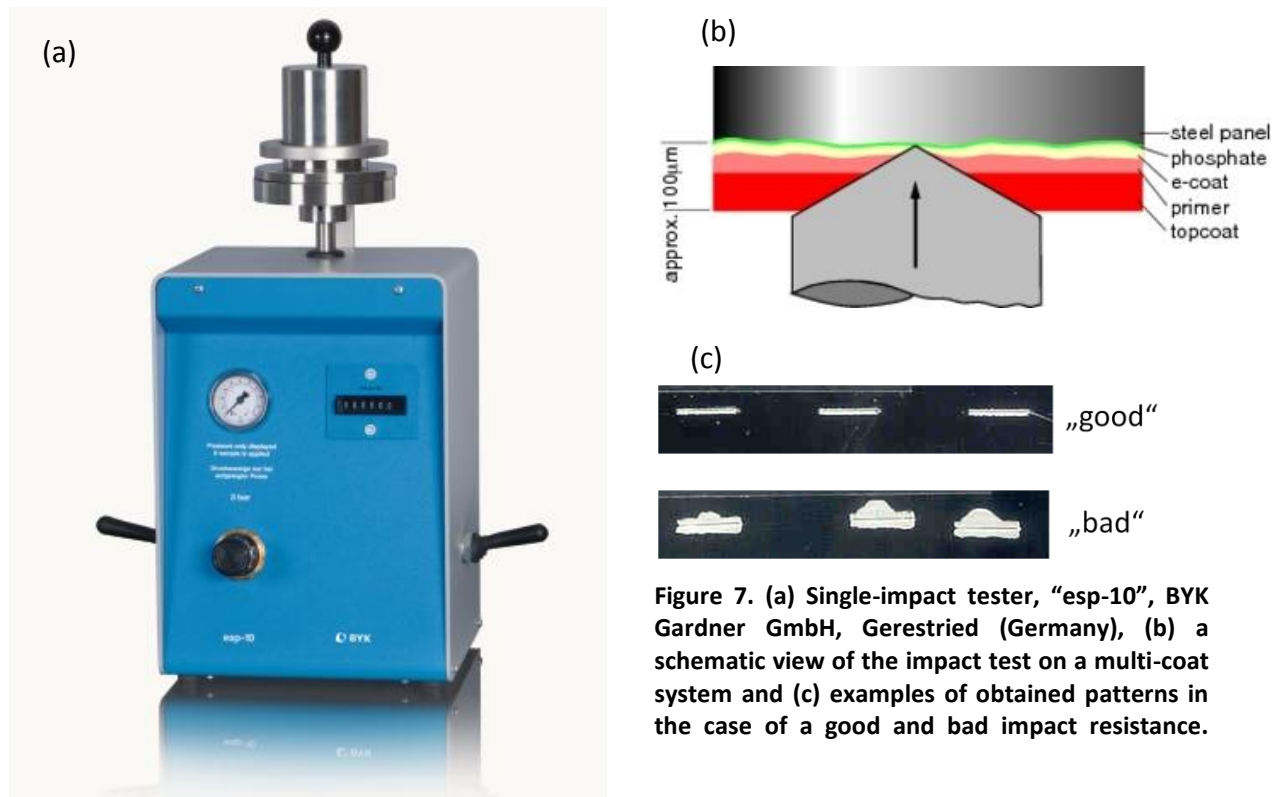

Figure 7. (a) Single-impact tester, "esp-10", BYK Gardner GmbH, Gerestried (Germany), (b) a schematic view of the impact test on a multi-coat system and (c) examples of obtained patterns in the case of a good and bad impact resistance.

Ball shot test

For this test, the single impact body used is a steel bullet of 2 mm diameter which is shot-blasted onto the panel test (incidence angle of 90°) by compressed air at a speed of 250 km/h. The test is carried out at room temperature but can also be conducted under winter-like driving conditions. Like previously, the test panel is evaluated visually and three runs are performed for each sample.
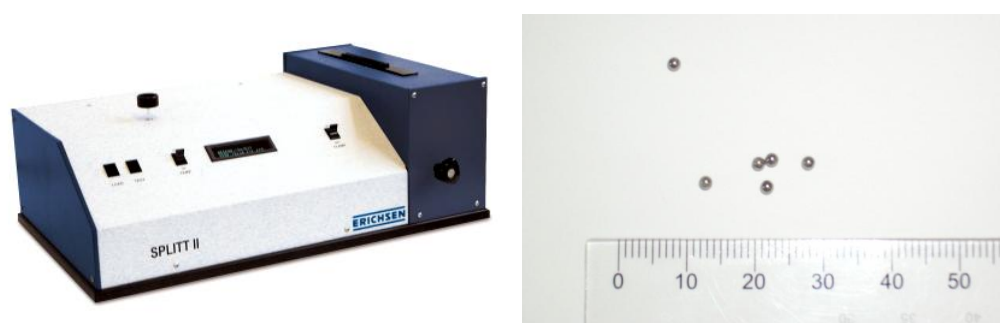

Figure 8. Chipping tester SPLITT II, type 408, Erichsen GmbH & Co. KG, Hemer (Germany) and typical steel bullets (D = 2mm)

2.3.2.2.2   Scratching tests

"Wet" scratch resistance (car-wash plant)

Here, repetitive car-washing is simulated and the scratch resistance of the coating is tested according to DIN 55668. For this, a mini car-wash plant (Amtec Kistler GmbH) equipped with a brush (d = 1000 mm, w = 400 mm) and a test table is used. The brush is made of polyethylene bristles (x-form, split ends) which have a diameter of 0.8 mm and are 440 mm long. The brush speed is about 120 revolutions per minute and spins in the opposite direction of the test table (when the test table changes direction, the brush must spin in the opposite direction). The brush depth is 100 mm. The test table moves at 5 ± 0,2 m/min. Two spray nozzles are located on both sides of the apparatus and are positioned to form a 60° angle with the test table. In this position, the spray stream contacts the brush 5 cm above the test table and the width of the spray stream covers the entire width of the brush. The wash mixture is prepared by mixing 1.5 g of quartz powder (Sikron SH 200, average particle size of 24 μm) with 1 L of tap water. The water temperature is maintained between 15 and 28 °C and the mixture is constantly stirred during the test to prevent the quartz powder to settle and thus to avoid differences in concentration. The mixture is spread with a flow rate of 2.2 L/min at a pressure of 3 bars. The OEM automotive panels are disposed on the test table and go through 10 washings (10 double strokes on the test table). After the test, the panels are rinsed with cold tap water and cleaned using a soft, non scratching paper towel and a solution of white-spirit to remove any residual of quartz powder or brush bristles. A scheme of the mini car-wash is shown in Figure 9.

The gloss (20°) is measured before and after the test on 5 different places on the panel and perpendicular to the direction of the scratches. The highest and the lowest values are deleted and the average of the 3 middle values is calculated as the gloss value after stress. The percent residual gloss is also reported. The gloss is measured again after reflow at 60 °C for 2 hours.

"Dry" scratch resistance

Steel wool (N°00 from Rakso) is attached to a hammer (800 g) as abrasive medium. The weight applied to the film is approximately 860 g, and on 10 double passes are applied on each panel as scratching cycles. The gloss (20°) is measured before and after the scratching

cycles on five different positions. The highest and the lowest values are deleted and the average of the 3 middle values is calculated as the gloss value before and after stress respectively. The percent residual gloss is also reported. The gloss is measured again after reflow 2 hours at 60 °C.
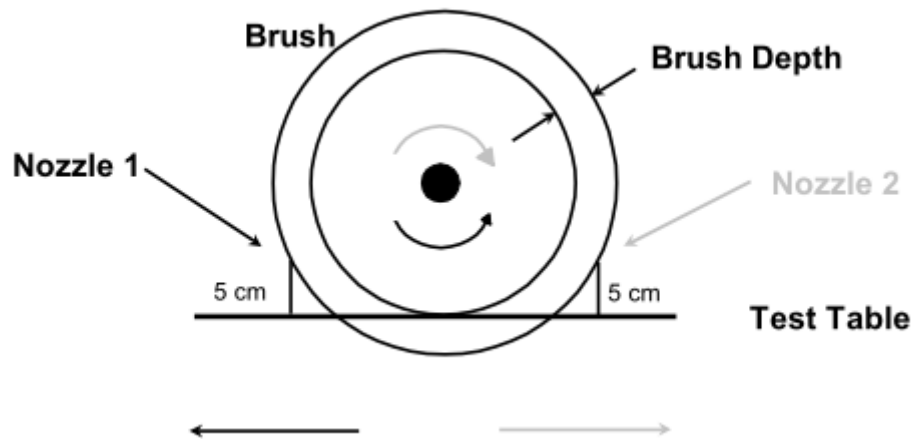

Figure 9. Schematic view of the mini car-wash plant.

The same test is performed with a piece of polishing paper (9 µ 281Q supplied from 3M) instead of steel wool and the gloss is measured at 20° like previously described.

Finally, the same test is performed using a piece of Scotch Brite ® and the gloss is measured like previously indicated but at 60°.

2.3.2.3 Hardness

As mentioned earlier, hardness is a complex property related to the elastic moduli, tensile strength etc. Many tests exist to measure the hardness of a coating. However, surveys reported that industries were often using methods to measure some form of scratching or abrasion, pendulum tests or indentation tests to evaluate hardness. For our purpose, hardness was measured as indentation hardness and pendulum hardness (also called damping or entropy hardness).

2.3.2.3.1   Indentation hardness

Here, the "microhardness" is measured by indentation hardness tests that have been very popular in the industry because of their simplicity. An indenter is used and pressed against the surface. Usually, the load is maintained constant, and the size of the indentation

is measured (depth of the indentation) with a microscope after removal of the load. The load per unit area of the impression left is taken as the measure of hardness. The obtained values are independent of the coating thickness as long as the indentation depth is less than one tenth of the sample thickness. Different geometries of indenters exist: ball (Brinell), cone (Rockwell) or pyramid (Vickers and Knoop). In our investigation, Vickers geometry (see Figure 10a) is used and results are expressed in N/mm^2.

2.3.2.3.2   König Pendulum hardness

This method uses the damping properties of organic surfaces to determine the hardness. The pendulum rests on two stainless steel balls of 5 mm diameter, 30 mm apart, and is counterpoised (to adjust the natural frequency of oscillation) by means of a weight sliding on a vertical rod attached to a cross bar. The period of oscillation on a polished glass substrate (without coating) is 1.4 s. The total weight of the pendulum is 200 g. The damping time from a 6° displacement to a 3° displacement is 250 ± 10 s. The oscillations of the König pendulum on a test surface are observed and the damping time from 6° to 3° displacement is measured. If the surface exhibits elastic properties (hard surface), the oscillations of the pendulum will not be softened as fast as for a less elastic surface (soft surface). In other terms, the harder the surface is the longer the damping time will be. Hardness is measured according to ASTM D 4366 and DIN EN ISO 1522.
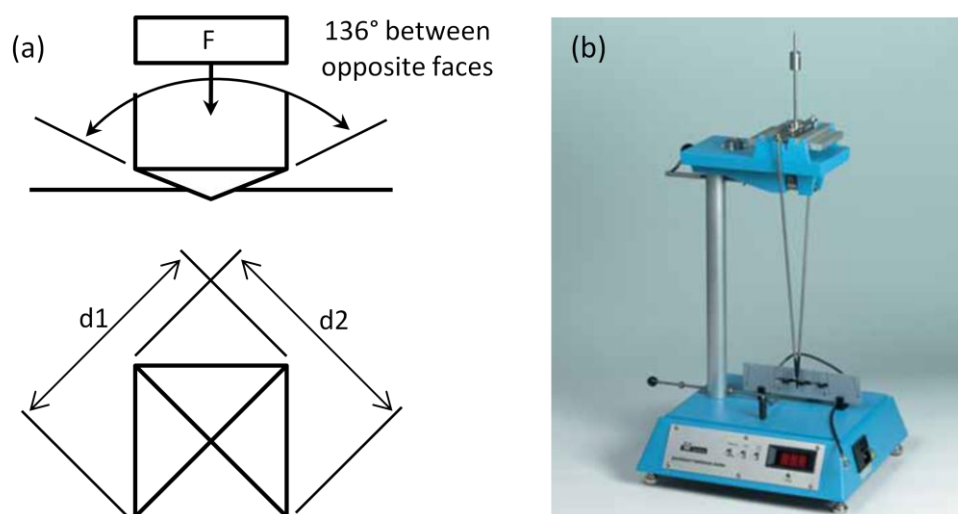

Figure 10. (a) Schematic representation of Vickers indentation, (b) König pendulum (BYK Gardner).

2.3.3   Chemical resistance

The resistance of an organic coating to chemical deterioration is an essential element of its evaluation. As automotive clearcoats, no loss of adhesion, blistering, softening, swelling or discoloration should appear when panel tests are subjected to specified fluids for specified times under specified conditions.

2.3.3.1   Chemical resistance (10 minutes stress)

Pieces of cotton wool impregnated with the following fluids are disposed on the panel and left for 10 minutes except for distilled water (1 hour):

   -Distilled water (1 hour stress)

   -FAM mixture (50% xylene, 30% isooctane, 15% di-isobutylene, 5% ethanol in volume)

   -Gasoline

   -Methoxypropyl acetate (MPA)

   -Xylene

   -Ethyl acetate

   -Acetone

After 10 minutes (or 1 hour for distilled water), the balls of cotton wool are removed and the surface is wiped with a soft cloth and assessed for each fluid according to an evaluation scale from 0 to 5 detailed in Table 3.

Table 3. Evaluation scale for chemical resistance test

Grade	Meaning	Explanation
0	No change	No damage
1	Minor change	Very slight swelling visible only by reflection in light Swelling clearly interrupted
2	Slight change	Swelling visible in light Slight scratches visible
3	Moderate change	Swelling and scratches clearly visible Softened
4	Severe change	Swelling very clearly defined Scratched through substrate
5	Film destroyed	Severe swelling Dissolution of the film

2.3.3.2   Chemical resistance - Gradient-oven method

The coatings are tested for their resistance to tree resin, pancreatin (simulated bird's excrement), distilled water, sodium hydroxide, and sulfuric acid (see Table 4)
Special OEM steel panels (420 mm * 98 mm * 1 mm) are provided especially for use in the gradient-oven and are already coated with a primer surfacer and a base-coat. The base-coat is applied in order to give a color (in our case black) which facilitates the visualization of the defects during evaluation. The coating is applied and dried on the substrate as described later in Chapter 5.

Table 4. Description of chemical tested with the gradient-oven method.

Chemical	Solution	Size of test patch	Temperature interval	Supplier
Tree resin	Supply form	Ø 5 mm	2 °C	DuPont
Pancreatin	50 %wt in deionised water	Ø 5 mm	2 °C	Merck
Demineralized water	--	Approx. 100 µL	2 °C	--
Sodium hydroxide (NaOH)	1 %wt	Approx. 25 µL	1 °C	--
Sulfuric acid (H_2SO_4)	1 %wt	Approx. 25 µL	1 °C	--

The panel can be virtually divided in segments (see Figure 11) and each segment corresponds to a temperature from 36 °C to 68 °C which is the maximum temperature a car body can reach when expose to sunlight.
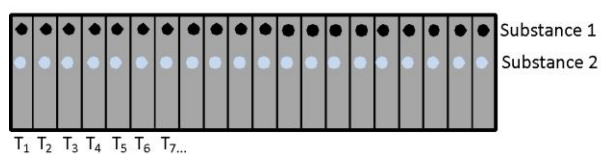

Figure 11. Schematic representation of a panel test (lines delimit temperature segments but are only drawn to facilitate visualization) and gradient –oven (BYK Gardner)

The preparation of the panel and the test are carried out at room temperature and 50 % relative atmospheric humidity. The effect of the latter cannot be eliminated completely. A

drop of each fluid is deposited on each segment (or every two segments) with an Eppendorf pipette and the time between the application and the transfer to the gradient-oven should not be longer than 10 minutes. The panel is then put into the gradient-oven which applies a temperature gradient from 35 °C to 80 °C with a temperature difference of 1 °C per segment. The panel is heated for 30 minutes and afterwards carefully cleaned using a soft cloth and white spirit to remove the tree resin and warm water to rinse off the other chemicals. The panel is assessed after storage for 1 hour and 24 hours at room temperature, 50 % relative atmospheric humidity. The result is given as the temperature at which the first damage occurs.

References

1.   Szwarc, M., *Nature* **1956,** 178, 1168.

2.   Szwarc, M.; Levy, M.; Milkovich, R., *Journal of the American Chemical Society* **1956,** 78, (11), 2656-2657.

3.   Schlaad, H.; Schmitt, B.; Müller, A. H. E.; Jungling, S.; Weiss, H., *Macromolecules* **1998,** 31, (3), 573-577.

4.   Ruckdäschel, H.; Sandler, J. K. W.; Altstädt, V.; Rettig, C.; Schmalz, H.; Abetz, V.; Müller, A. H. E., *Polymer* **2006,** 47, (8), 2772-2790.

5.   Allen, R. D.; Long, T. E.; McGrath, J. E., *Polymer Bulletin* **1986,** 15, (2), 127-134.

6.   Fréchet, J. M. J.; Henmi, M.; Gitsov, I.; Aoshima, S.; Leduc, M. R.; Grubbs, R. B., *Science* **1995,** 269, (5227), 1080-1083.

7.   Litvinenko, G. I.; Simon, P. F. W.; Müller, A. H. E., *Macromolecules* **1999,** 32, (8), 2410-2419.

8.   Litvinenko, G. I.; Simon, P. F. W.; Müller, A. H. E., *Macromolecules* **2001,** 34, (8), 2418-2426.

9.   Paulo, C.; Puskas, J. E., *Macromolecules* **2001,** 34, (4), 734-739.

10. Gaynor, S. G.; Edelman, S.; Matyjaszewski, K., *Macromolecules* **1996,** 29, (3), 1079-81.

11. Fréchet, J. M. J.; Leduc, M. R.; Weimer, M.; Grubbs, R. B.; Liu, M.; Hawker, C. J., *Polymer Preprints (American Chemical Society, Division of Polymer Chemistry)* **1997,** 38, (1), 756-757.

12. Mori, H.; Seng, D. C.; Zhang, M.; Müller, A. H. E., *Langmuir* **2002,** 18, (9), 3682-3693.

13. Simon, P. F. W.; Müller, A. H. E., *Macromolecules* **2004,** 37, (20), 7548-7558.

14. Baskaran, D., *Macromolecular Chemistry and Physics* **2001,** 202, (9), 1569-1575.

15. Baskaran, D., *Polymer* **2003,** 44, (8), 2213-2220.

16. Jia, Z.; Yan, D., *Journal of Polymer Science, Part A: Polymer Chemistry* **2005,** 43, (16), 3502-3509.

17. Lex, K., In *Pruftechnik bei Lackherstellung und* Lackverarbeitung, Vincent Verlag: Hannover, 1992; p 70.

18. ASTM, Standard E 284, Terminology of Appearance. In *Annual Book of ASTM Standards*, Philadelphia, PA, 1994.

19.   Koleske, J. V., In *Paint and Coating testing manual*, ASTM manual: Philadelphia, PA, 1995.

20.   Wu, S., *The Journal of Adhesion* **1973,** 5, (1), 39 - 55.

21.   Barbarisi, M. J., *Nature* **1967,** 215, (5099), 383-384.

22.   Boucher, E. A., *Nature* **1967,** 215, (5105), 1054-1071.

23.   Voyutskii, S. S., *The Journal of Adhesion* **1971,** 3, (1), 69-76.

24.   Anand, J. N., *The Journal of Adhesion* **1973,** 5, (3), 265 - 267.

25.   Helfand, E., *The Journal of Chemical Physics* **1975,** 63, (5), 2192-2198.

26.   Helfand, E.; Sapse, A. M., *The Journal of Chemical Physics* **1975,** 62, (4), 1327-1331.

27.   Roe, R.-J., *The Journal of Chemical Physics* **1975,** 62, (2), 490-499.

28.   Good, R. J., In *Recent Advances in Adhesion*, Gordon and Breach: New York, 1973; p 357.

29.   Williams, M. L., In *Recent Advances in Adhesion*, Gordon and Breach: New York, 1973; p 381.

Chapter 3

Synthesis of soft nanoparticles based on block copolymer self-assembly in organic solvents

3.1   Introduction

Block copolymers are a valuable class of materials and defined as macromolecules with a linear and/or radial arrangement of two or more blocks, of varying monomer composition, covalently bonded together. In most cases, these blocks are thermodynamically incompatible and therefore block copolymer molecules are driven to self-organize[1] via microphase separation where contact between similar and dissimilar parts is maximized and minimized, respectively. The morphology of these microdomains can be tuned by the composition and/or structure of the involved block copolymers. This has given rise to a rich variety of structures in the bulk[2] as well as in solution[3] and, further, the possibility of controlling their self-assembly on the nanometer scale has attracted much attention.

Polymeric nanoparticles have applications in various technological and biomedical fields[4-6]. Depending on the application and when optimally designed, they may enhance physical, chemical, or biological properties. One technique, amongst others[7], to synthesize them is the self-assembling property of block copolymers in solution resulting in micelle formation. The use of a selective solvent, i.e. a good solvent for one block but poor for the other one, in case of a diblock copolymer, is usually required. The obtained micelles consist of a collapsed core and a protective corona of soluble blocks. Two methods can be employed to obtain micelles: directly dispersing the block copolymer in a selective solvent or first, dissolving it in a common solvent for both blocks and subsequently replacing the solvent, via dialysis for example, by a seledctive solvent (solvent displacement method). The preparation method used and the solvent polarity strongly influence the formation of these aggregates which can vary in shape from spherical micelles to rods or cylinders[8, 9] to vesicles[10-16]. Studies about micellization reported in the literature deal mainly with aqueous systems[17-23] or

mixtures of aqueous and organic solvents[8, 12-15, 24-27] and fewer exclusively about organic systems[28-37].

Typically, micelles are dynamic in nature. Their size and shape can vary upon changes in temperature, concentration or solvent which can lead to partial or complete dissociation of the aggregates. This can be desired but in other applications can be a major drawback. To circumvent this problem, stabilization has been attempted by cross-linking of the micelles existing under given conditions. Several potential cross-linking sites exist in a diblock copolymer micelle: within the core domain, within the shell layer, at the core-shell interface, at the core chain end and on the surface of the micelle. Cross-linking reagents or external stimuli are use to trigger reactions of polymerizable and/or cross-linkable groups present on these locations to stabilize micellar particles. Many efforts have been undertaken to cross-link the core[11, 36, 38-41] or the shell[42, 43].

Here, we report on the synthesis soft nanoparticles with cross-linked polybutadiene (PB) core and a corona of PMMA and other acrylic polymers. For that aim, we synthesized block copolymers of poly(butadiene)-*b*-poly((meth)acrylate) via sequential anionic polymerization having at least 60 %wt of the poly(meth)acrylate block. For poly(butadiene)-*b*-poly(methyl methacrylate) (B-M) micelles consisting of a PB core and a poly(methyl methacrylate) shell were obtained in acetonitrile, which is a selective solvent for PB, but also in acetone and DMF (in some particular cases). Similar micellization occurred for poly(butadiene)-*b*-poly(*n*-butyl methacrylate) (B-*n*BMA), poly(butadiene)-*b*-poly(*n*-butyl acrylate) (B-*n*BA) and poly(butadiene)-*b*-poly(*t*-butyl methacrylate) (B-*t*BMA) in DMAc, DMF and acetone respectively. The micellar cores could be stabilized in solution using "cold vulcanization" with S_2Cl_2 [10, 11, 41, 44] or radical reaction[39, 45] with a photo-initiator to cross-link the polybutadiene core. Their solution behavior and thermal properties are investigated by means of static and dynamic light scattering (SLS, DLS), transmission electron microscopy (TEM) and differential scanning calorimetry (DSC).

3.2   Experimental part

3.2.1   Materials

Sec-butyl lithium (*sec*-BuLi) (Aldrich), triethylaluminum (Et$_3$Al) (Aldrich), *iso*-butyl aluminum *(2,6-di-tert*-butyl-4-methylphenolate)$_2$ (*i*BuAl(BHT)$_2$) (Kuraray Co. Ltd.) were used without further purification. Butadiene (Messer Griesheim) was passed through columns filled with molecular sieves (4Å) and basic aluminum oxide and stored over dibutyl magnesium. Methyl methacrylate (MMA), *n*-butyl acrylate (*n*BA), *n*-butyl methacrylate (*n*BMA) and t-butyl methacrylate (*t*BMA) (BASF) were condensed from Et$_3$Al on a vacuum line and stored at liquid nitrogen temperature until use. *2*-(trimethylsilyloxy)ethyl methacrylate (TMS-HEMA) was condensed from trioctyl aluminum (Aldrich) on a vacuum line using active vacuum and stored at liquid nitrogen temperature until use. Toluene (Merck) was distilled from CaH$_2$ and potassium. THF was distilled from CaH$_2$ and K/Na alloy. 1,2-Dimethoxyethane (DME) was purified using a certain amount of *sec*-BuLi and condensed on a vacuum line. S$_2$Cl$_2$ (Aldrich), (*2, 4, 6*-trimethylbenzoyl)diphenylphosphine oxide (Lucirin® TPO) (BASF) were used as cross-linking agents without further purification. Selective solvents used for the self-assembly into micelles were all p.a. grades.

3.2.2   Anionic synthesis of poly(butadiene)-*b*-poly(methyl methacrylate) (B-M)

Different B-M diblock copolymers with varying block length and narrow molecular weight distribution were synthesized by sequential anionic polymerization in toluene[46]. Typically, 0.63 ml (0.88 mmol) *sec*-BuLi was added to 500 ml of toluene under nitrogen atmosphere at 10 °C. 9.1 ml (0.11 mol) of butadiene was condensed from Bu$_2$Mg into an ampoule that was cooled down to -20 °C and then added to the reaction mixture. The temperature was increased up to 30 °C. Under these conditions a predominant 1,4-microstructure is obtained. After complete conversion of butadiene, the solution was cooled down to -10 °C. A mixture of 2.75 ml (26.5 mmol) of DME and 9.2 ml (5.5 mmol) of *i*BuAl(BHT)$_2$ was introduced prior to the addition of 9.57 ml (0.09 mol) of MMA to enable its subsequent polymerization in a controllable manner without the use of an end-capping agent. The solution was warmed to room temperature. After complete conversion of MMA, the reaction was terminated with methanol and the reaction mixture was stirred for an hour

with an aqueous solution of sulfuric acid (2 %wt) to remove the catalyst. The organic phase was extracted and washed with distilled water. The polymer was finally precipitated in methanol and dried under vacuum at room temperature. Each time an aliquot of the PB precursor was withdrawn for characterization, before adding the second monomer.

For the synthesis in THF, 90 ml (1.1 mol) of butadiene was initiated with 7.04 ml (0.01 mol) *sec*-BuLi and polymerized at low temperature (-10 °C) in 1 L of THF. The polybutadiene was endcapped with 5.30 ml (0.03 mol) of diphenylethylene (DPE, Aldrich) to reduce the nucleophilicity of the chain end[47] prior to the addition of 95.7 ml (0.9 mol) of MMA which was polymerized at -70 °C. The reaction was terminated with degassed methanol and the diblock copolymer was precipitated in water and dried under vacuum at room temperature.

The molecular weights and molecular weight distributions of the PB blocks were measured using GPC and PB standards. Molecular weights of the diblock copolymers were then determined from the monomer number fractions obtained by ^{1}H NMR. The samples are denoted as $B_nM_m^X$, where n and m are the degree of polymerization of each component and X is the rounded weight average molecular weight of the diblock copolymer in kg/mol.

3.2.3   Functionalization of B-M via poly(2-hydroxyethyl methacrylate) (B-M-H)

After complete conversion of MMA, an aliquot of the B-M diblock precursor was withdrawn for characterization and the protected monomer, TMS-HEMA, was subsequently added to the reaction mixture in toluene and polymerized at room temperature. The reaction was terminated with methanol and the reaction mixture was stirred for an hour with an aqueous solution of sulfuric acid (2 %wt). The organic phase was extracted and washed with distilled water. The deprotection of the monomer is assumed to take place during the extraction of the aluminum catalyst. The polymer was finally precipitated in methanol and dried under vacuum at room temperature.

In THF, after withdrawing the B-M precursor, TMS-HEMA was added at -70 °C. The reaction was terminated with degassed methanol, the polymer was precipitated into distilled water with few drops of sulfuric acid and dried under vacuum at room temperature.

The molecular weights and molecular weight distributions of the PB blocks were measured using GPC and PB standards. Molecular weights of the diblock and triblock copolymers were then determined from the monomer number fractions obtained by ^{1}H

NMR. The samples are denoted $B_nM_mH_o^X$, where n, m and o are the degree of polymerization of each component and X is the rounded weight average molecular weight of the triblock copolymer in kg/mol.

3.2.4   Anionic synthesis of Poly(butadiene)-*b*-poly(*n*-butyl methacrylate) (B-*n*BMA)

The procedure is similar to that followed for B-M block copolymer in toluene. The molecular weights and molecular weight distributions of the PB blocks were measured using GPC and PB standards. Molecular weights of the diblock copolymers were then determined from the monomer number fractions obtained by ^{1}H NMR. The samples are denoted $B_n nBMA_m^X$, where n, m are the degree of polymerization of each component and X is the rounded weight average molecular weight of the diblock copolymer in kg/mol.

3.2.5   Anionic synthesis of poly(butadiene)-*b*-poly(*n*-butyl acrylate) (B-*n*BA)

Sequential anionic polymerization of the B-*n*BA block copolymers was carried out in 500 ml of toluene using 1.26 ml (1.76 mmol) *sec*-BuLi as initiator. 18.2 ml (0.22 mol) of butadiene were polymerized first at 30 °C. After the polymerization of butadiene, an aliquot of the PB precursor was withdrawn and a mixture of 5.50 ml (0.05 mol) of DME and 24.5 ml (0.01 mol) of *i*BuAl(BHT)$_2$ was introduced. 20 ml (0.14 mol) of *n*-butyl acrylate were added drop-wisely with a syringe into the reactor at -15 °C. The reaction was terminated with methanol and the reaction mixture was stirred for an hour with an aqueous solution of sulfuric acid (2 %wt). The organic phase was extracted and washed with distilled water. The polymer was finally precipitated in methanol and dried under vacuum at room temperature. The molecular weights and molecular weight distributions of the PB blocks were measured using GPC. Molecular weights of the diblocks were then determined from the monomer number fractions obtained by ^{1}H NMR. The samples are denoted as $B_nBA_m^X$, where n, m are the degree of polymerization of each component and X is the rounded weight average molecular weight of the diblock copolymer in kg/mol.

3.2.6   Anionic synthesis of poly(butadiene)-*b*-poly(*t*-butyl methacrylate) (B-*t*BMA)

The polymerization of B-*t*BMA was carried out in 500 ml THF using 0.70 ml (1 mmol) *sec*-BuLi as initiator. Butadiene (9.1 ml, 0.11 mol) was first polymerized at -10 °C. After complete

conversion, the temperature was cooled down to -30 °C and the PB was endcapped with an excess of DPE (0.88 ml, 5 mmol). An aliquot of the precursor was withdrawn for characterization and 15 ml (0.09 mol) of tBMA was added into the reactor and polymerized at -70 °C. The reaction was terminated with degassed methanol. The polymer was precipitated into water and dried under vacuum at room temperature. Molecular weights and molecular weight distributions were measured using MALDI-ToF. The samples are denoted $B_n t BMA_m^X$, where n, m are the degree of polymerization of each component and X is the rounded weight average molecular weight of the diblock copolymer in kg/mol.

3.2.7   Self-assembly in selective organic solvents

For B-M block copolymers, acetone, N,N-dimethylformamide (DMF) and acetonitrile (ACN) were chosen as non- solvents for PB and micelles with PB core and PMMA corona were obtained. Such aggregates formed by directly dispersing the block copolymers in the selective solvent at room temperature. The solutions were stirred over night to ensure complete dissolution and equilibrium.

B-nBA and B-nBMA micelles were prepared following the same procedure in DMF and N,N-dimethylacetamide (DMAc) respectively. In both cases, micelles with a PB core were obtained.

For B-tBMA, DMAc and acetone were used as selective solvents.

Samples possessing a predominant 1,2-PB microstructure were noticed to take longer to disperse completely and annealing of the solution at 60 °C overnight was also performed for these samples.

3.2.8   Cross-linking of block copolymer micelles

Cross-linking of block copolymer micelles in selective solvents was carried out at a concentration of 1 g/L. S_2Cl_2 was added to the degassed micellar solution and the mixture was left at room temperature for 24 hours. For UV-induced radical cross-linking, photo-initiator Lucirin® TPO was added to the micellar solution and left under UV lamp for 2 hours (Hoehnle VG UVAHAND 250 GS, cut-off at 300 nm wavelength to avoid the depolymerization of the methacrylate block). All the samples were purified by dialysis after

reaction. Molar ratios of the butadiene units to the respective cross-linker were typically 1:0.5, 1:1.

### 3.2.9   Hydrolysis of P*t*BMA towards water-soluble nanoparticles

Hydrolysis of the P*t*BMA corona of the nanoparticles was carried out in dioxane. Typically, the desired amount of cross-linked nanoparticles is weighted in a round bottom flask and according to the amount of *t*BMA, a five-fold excess of water is added as aqueous HCl solution (37 %wt). In our case, for 0.5 g of nanoparticles, 0.3 g of the dilute aqueous HCl solution was needed and 2.7 ml of dioxane were added. The reaction mixture was refluxed overnight and the hydrolyzed nanoparticles precipitated into diethylether and dried under vacuum at room temperature. The hydrolyzed product was not directly soluble in water and was dialysed from THF against water for three days.

3.3   Results and discussion

3.3.1   Anionic synthesis of B-M(-H), B-*n*BA, B-*n*BMA and B-*t*BMA block copolymers

The synthesis of B-M in toluene is depicted in Scheme 1a where subscripts m and n denote degrees of polymerization for each block and x is the fraction of 1,4 units. The polymerization of PB is initiated by *sec*-BuLi and takes place at 30 °C. After complete conversion of butadiene, the mixture of DME and *i*BuAl(BHT)$_2$ is added to the reactor at 25 °C. Upon the subsequent introduction of MMA, a yellow color appears caused by the formation of the aluminum complex with the methacrylate monomer[46]. The PMMA block is polymerized at 25 °C and the reaction is terminated with degassed methanol after the yellow color has vanished.

Block copolymers $B_{109}M_{98}{}^{16}$, $B_{540}M_{452}{}^{75}$ were synthesized in THF[48] to achieve a predominant 1,2-PB microstructure and the corresponding synthesis is shown in Scheme 1b. The polymerization of PB is initiated with *sec*-BuLi at -10 °C. After complete conversion of butadiene, a three-fold excess, according to the initator, of distilled DPE is added at -30 °C and left reacted for 30 minutes. The deep red reaction media becomes colorless upon the addition of MMA at -70 °C giving a hint that all the end-capped chain ends reacted. The reaction is finally terminated with degassed methanol.
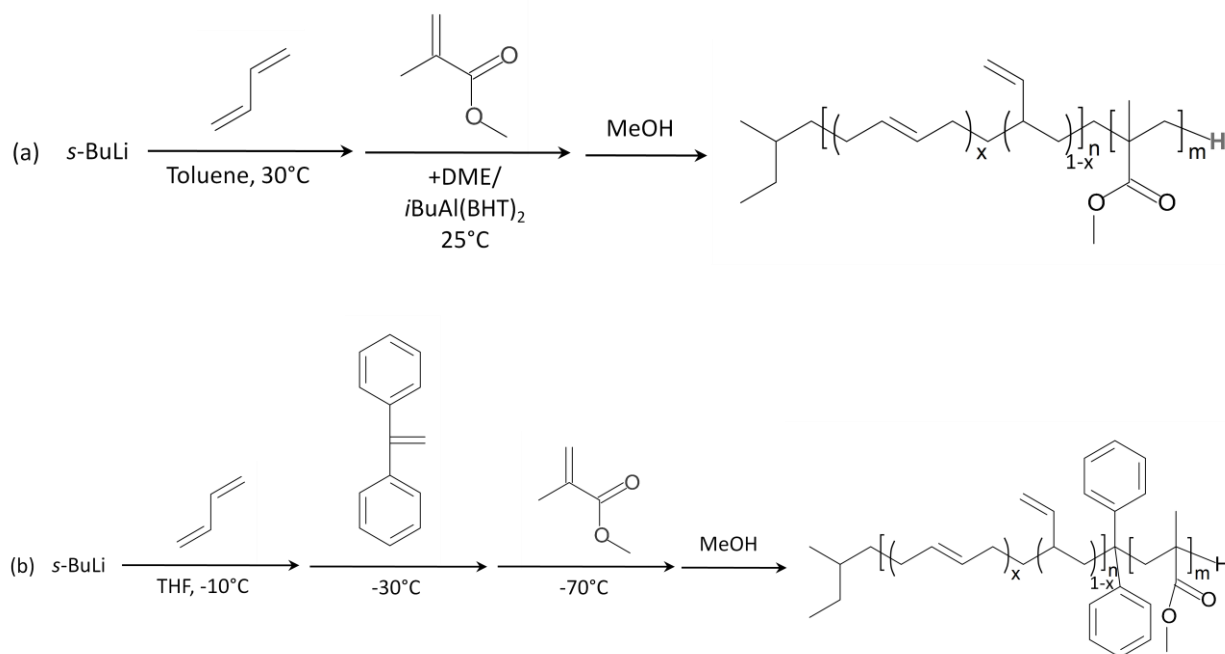
Scheme 1. Synthesis of B-M via sequential anionic polymerization in toluene and in THF. n and m denote degrees of polymerization for each block. x is the fraction of 1,4 units.
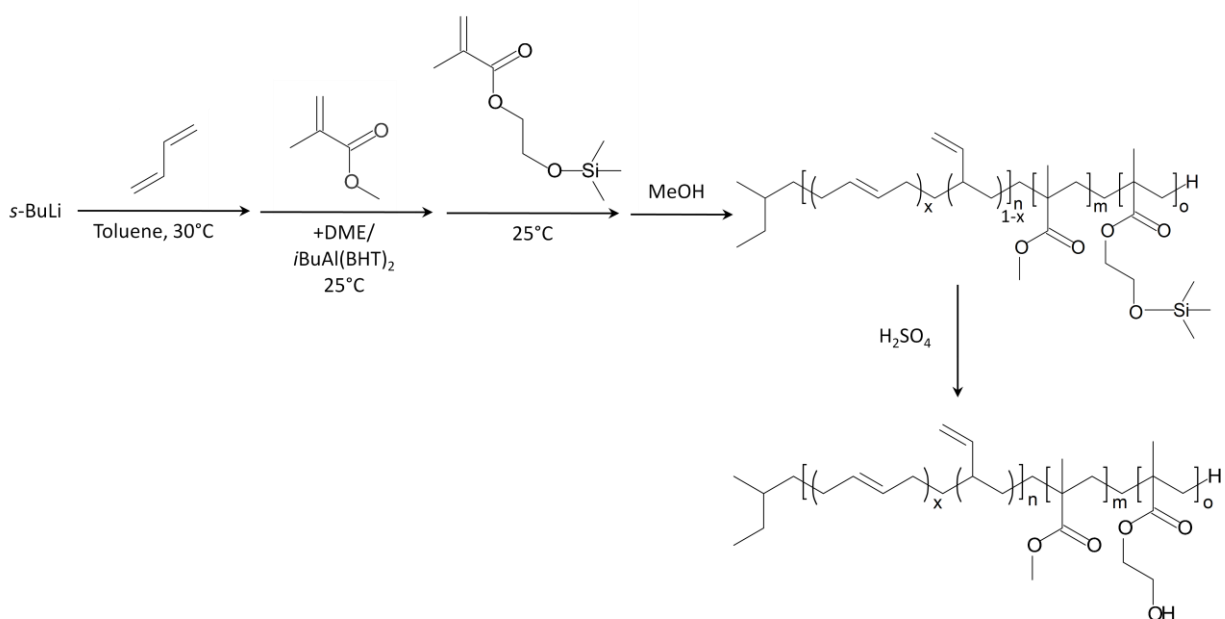
Scheme 2. Synthesis of B-M-H via sequential anionic polymerization in toluene. n, m and o denote degrees of polymerization for each block.

The synthesis of B-M-H is depicted in Scheme 2 where m, n and o denote the degrees of polymerization of each block and x is the fraction of 1,4 units. The polymerization of the B-M precursor is the same as described previously. After complete conversion of MMA, TMS-HEMA is added directly to the reactor at room temperature. The yellow color appears again

indicating the complexation of the aluminum compound with the introduced monomer. As the yellow color vanished, the reaction is terminated with degassed methanol.

The GPC traces in Figure 1a shows narrow molecular weight distribution for PB precursor, B-M diblock and B-M-H triblock copolymer (PDI < 1.06). Complete initiation of the second block can also be noticed, no PB precursor is left. Complete initiation of the PHEMA block, on the other hand, cannot be confirmed by GPC due to the low amount of TMS-HEMA introduced. However, a shift of the GPC curve towards lower elution volume can be observed. The incorporation of MMA and HEMA was confirmed by ^{1}H NMR (Figure 2). The methoxy groups of PMMA show a characteristic peak at 3.56 ppm while protons of the ethyl groups of HEMA appear at 4.0 and 3.75 ppm. The α-methyl protons peaks are also visible at 0.85 ppm and 1.02 ppm corresponding to rr and rm triads respectively. The resonance for mm triads at 1.2 ppm is almost inexsitant. The PMMA block is predominantly syndiotactic, similar to polymers obtained in THF. The stereostructure of the PB block is also determined by ^{1}H NMR and calculated according to the vinyl signals at 4.9 ppm and 5.4 ppm. 80 % of 1,4-PB microstructure was reported for these block copolymers.

Few block copolymers were synthesized in THF in order to achieve a high amount of 1,2 microstructure of the PB block as depicted earlier in Scheme 1b. GPC traces also show narrow molecular weight distributions with low polydispersity indices (PDI < 1.08) and ^{1}H NMR spectroscopy revealed at least 80 % 1,2-PB microstructure.

In Figure 1, the GPC traces for B-nBA diblock copolymer exhibit termination from the PB precursor. This termination occurred in a small amount and is attributed to impurities introduced during reaction. As the presence of PB precursor should not interfere with the micellization process we want to carry out later on, the extraction of the homopolymer was not systematically performed. The incorporation of the acrylate monomer was assessed by GPC where a clear shift towards lower elution volume is observed and ^{1}H NMR spectroscopy which let appear a signal at 4.0 ppm corresponding to -OC$\underline{H}_2$(CH$_2$)$_2$CH$_3$.
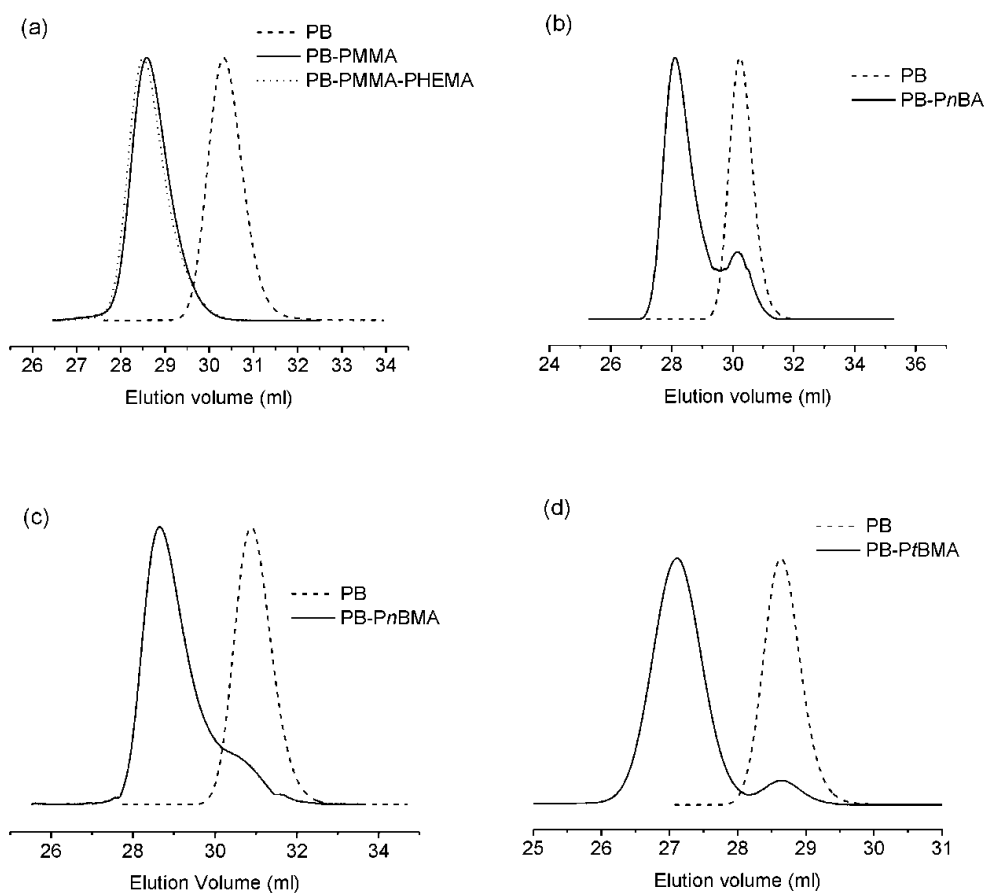
Figure 1. GPC traces (PB calibration) of (a) B-M, B-M-H, (b) B-*n*BA, (c) B-*n*BMA and (d) B-*t*BMA and their respective PB precursor.
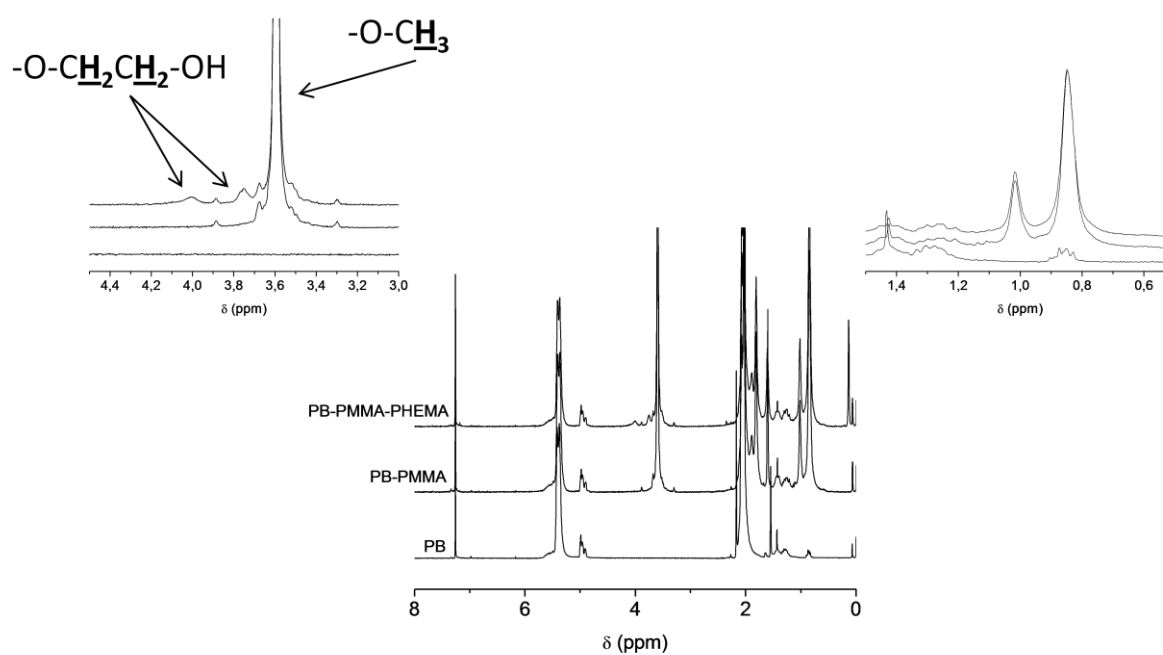

Figure 2. ^{1}H NMR (250MHz) spectra of B_{115}, $B_{115}M_{122}$[19] and $B_{115}M_{122}H_2$[19].

The same observations were made on the GPC traces for B-*n*BMA and B-*t*BMA which both exhibit a shoulder at the same elution volume than their respective PB precursor. For reasons mentioned above, the homopolymer was not removed before micellization. We assume the termination being caused by the introduction of some impurities while injecting the butyl methacrylate monomer. The incorporation of the second monomer into the block copolymer was further confirmed by ^{1}H NMR (-OC$\underline{H}_2$(CH$_2$)$_2$CH$_3$ at 3.9 ppm for P*n*BMA and - OC(C$\underline{H}_3$)$_3$ at 1.4 ppm for P*t*BMA).

Molecular characteristics of the different synthesized block copolymers are summarized in Table 1.

Table 1. Polymer Characterization of B-M, B-*n*BA, B-*n*BMA and B-*t*BMA diblock copolymers.

Sample	M_n [a] (PB) (kg/mol)	M_w/M_n [a] (PB)	%1,4 [b]	M_n [a+b] (PB-PMMA) (kg/mol)	M_w/M_n [a] (PB-PMMA)	%wt PB [b]
B$_{115}$M$_{122}$[19]	6.2	1.03	89	18.4	1.04	34
B$_{59}$M$_{63}$[10]	3.2	1.06	84	9.5	1.06	34
B$_{69}$M$_{100}$[14]	3.7	1.04	87	13.7	1.05	27
B$_{41}$M$_{152}$[17]	2.2	1.06	85	17.4	1.06	13
B$_{109}$M$_{98}$[16c]	5.9	1.03	16	15.7	1.04	38
B$_{540}$M$_{452}$[75c]	29.2	1.03	14	73.2	1.04	40
B$_{119}$*n*BA$_{79}$[18]	6.4	1.02	57	16.5	1.13	39
B$_{91}$*n*BMA$_{58}$[15]	4.8	1.04	85	13.2	1.12	37
B$_{230}$*t*BMA$_{129}$[31c]	12.6 [d]	1.01 [d]	17	30.9 [d]	1.04 [d]	40 [d]

[a] GPC, PB standards; [b] ^{1}H NMR; [c] synthesized in THF, [d] MALDI-ToF

3.3.2   Solution behavior

3.3.2.1   B-M micelles

To induce micellization, acetone, DMF and acetonitrile were chosen as good solvents for PMMA but poor solvents for PB in order to achieve micelles with a cross-linkable PB core. After direct dispersion of the block copolymers in the different selective solvents, dynamic light scattering (DLS) was used to investigate the average hydrodynamic sizes of the B-M micelles in solution. Measurements were performed at concentrations of 1 g/L and

hydrodynamic radii were measured at a 90° angle if not noted otherwise. Results are listed in Table 2. Please note that $B_{109}M_{98}{}^{16}$ and $B_{540}M_{452}{}^{75}$ were both synthesized in THF.

In acetonitrile and DMF, all samples exhibit monomodal CONTIN plots of comparable width (Figure 3a) hinting to very narrowly dispersed micelles (PDI = 0.008 for $B_{115}M_{122}{}^{19}$ in acetonitrile). Depending on the molecular weight of the sample, radii are roughly varying from 12 to 18 nm in acetonitrile and are 1 to 2 nm smaller in DMF. These aggregates do not present significant angular dependence and plots of the decay rate, Γ, versus the square of the scattering vector, q^2, show that linear fit of the data passes through the origin (Figure 3b), which confirms pure translational diffusion and the formation of spherical micellar aggregates[49]. Measurements were also performed at different concentrations varying from 0.1 to 10 g/L and no alteration of the structure's shape and size seemed to occur (Figure 3c). The hydrodynamic radii remain unchanged even at 10 g/L.

Table 2. Hydrodynamic radii of B-M micelles in different selective solvents obtained by DLS and TEM.

	%wt PMMA[a]	Acetonitrile		DMF		Acetone	
		$R_{h, z}$ (nm)	$R_{n, core\ TEM}$ (nm)	$R_{h, z}$ (nm)	$R_{n, core\ TEM}$ (nm)	$R_{h, z}$ (nm)	$R_{n, core\ TEM}$ (nm)
$B_{115}M_{122}{}^{19}$	66	17.4	aggr.	16.6	--	--	12
$B_{59}M_{63}{}^{10}$	66	12.4	aggr.	11.0 (30°, 10 g/L)	aggr.	--	17
$B_{68}M_{100}{}^{14}$	73	14.3	aggr.	12.1 (10 g/L)	aggr.	--	11
$B_{41}M_{152}{}^{17}$	87	17.3	7	--	--	--	--
$B_{109}M_{98}{}^{16b}$	61	17.5	14	14.6	10	--	11
$B_{540}M_{452}{}^{75b}$	60	68.8	42	52.6	27	32.7	16

[a] ^{1}H NMR; [b] synthesized in THF

However, $B_{41}M_{152}{}^{17}$ with 87 %wt PMMA content only forms unimers in DMF and acetone. This is possible if the soluble block of the diblock copolymer is long enough to act as a protective corona for the insoluble block in solution. On the other hand, for that same polymer, micelles are formed in acetonitrile.

$B_{555}M_{452}{}^{75}$, which possesses a higher molecular weight and 60 %wt PMMA clearly undergoes micellization in all three selective solvents with radii varying from 33 nm in acetone, 53 nm in DMF, to 69 nm in acetonitrile. With lower molecular weight but similar

composition, $B_{109}M_{98}{}^{16}$ forms well-defined micelles in DMF and acetonitrile with radii of 15 and 17 nm respectively. The size of the micellar aggregates increase from acetone to DMF to acetonitrile. When the calculated interaction parameters of PMMA (δ_{PMMA} = 11.09 (cal/cm³)$^{1/2}$) in those three solvents are compared, $\chi_{acetone-PMMA}$ = 0.14 > $\chi_{DMF-PMMA}$ = 0.10 > $\chi_{ACN-PMMA}$ = 0.06. From these results, it can be assumed that acetonitrile is a better solvent for PMMA and therefore leads to larger micelles than in DMF and acetone.
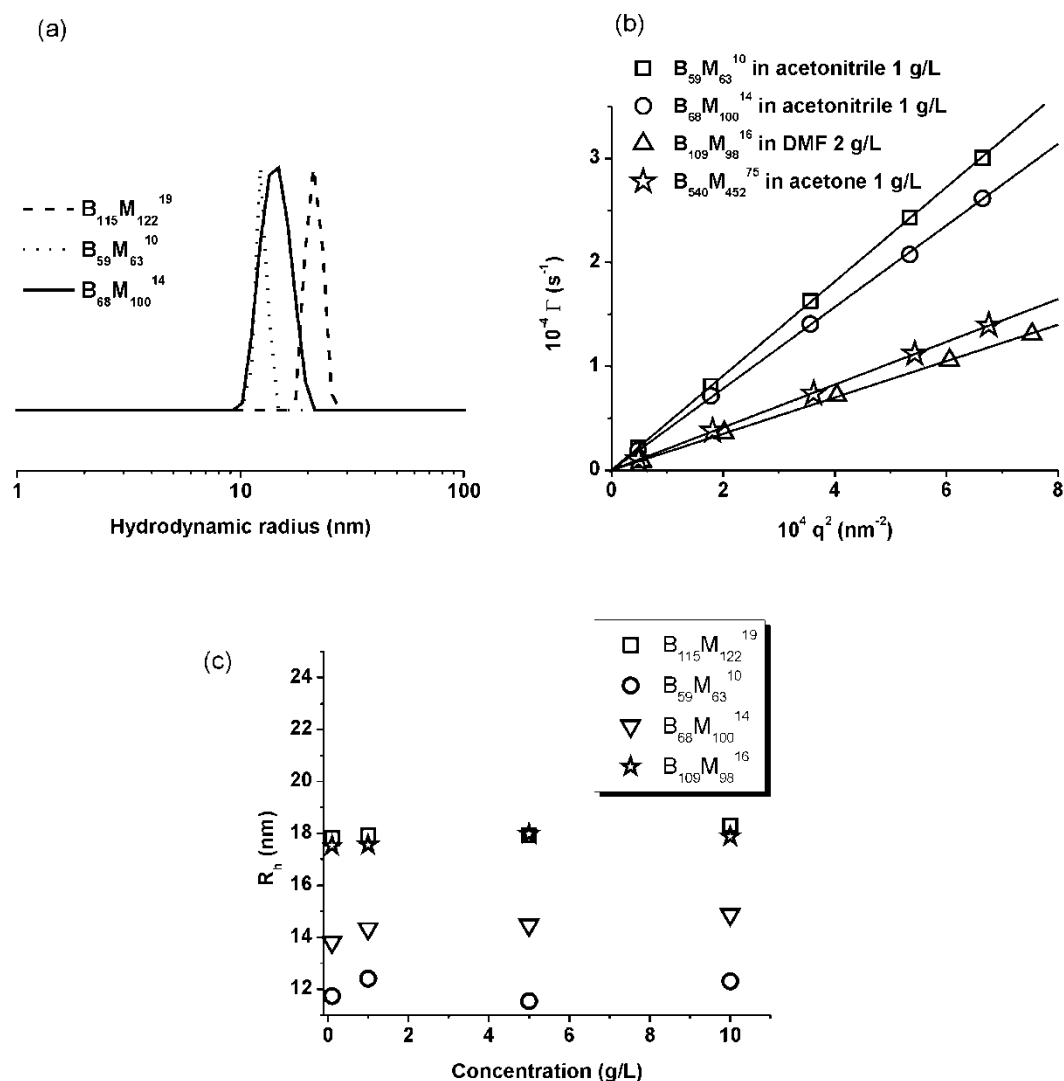
Figure 3. (a) CONTIN plots at 90° for B-M micelles in acetonitrile at 1 g/L, (b) Γ vs. q² plots for B-M micelles in different solvents, (c) concentration dependence of $R_{h,z}$ for B-M micelles in acetonitrile.

Transmission electron microscopy (TEM) images of B-M copolymer micelles deposited onto carbon-coated grids are shown in Figure 4, Figure 5 and Figure 6.
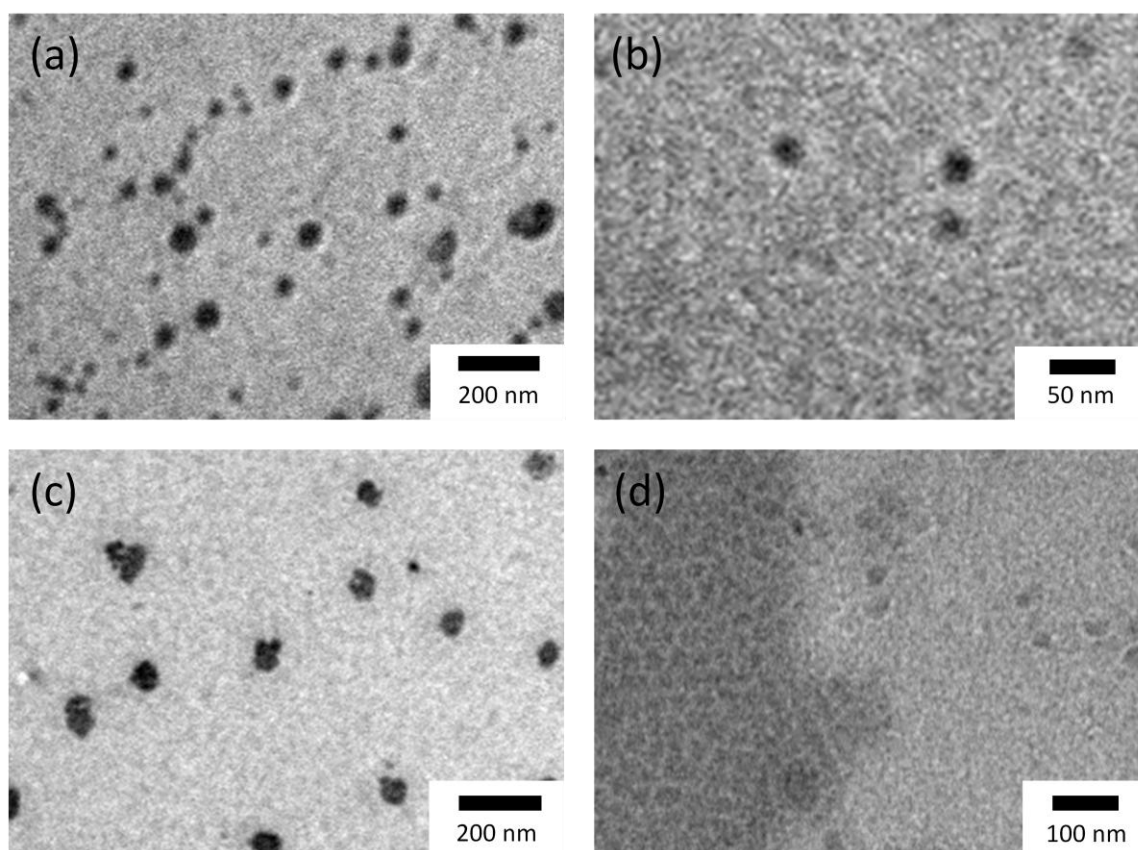
Figure 4. TEM micrographs of drop-casted micellar solution of (a) $B_{59}M_{63}$[10], (b) $B_{115}M_{122}$[19] in acetonitrile and (c) $B_{69}M_{100}$[14], (d) $B_{109}M_{98}$[16] in DMF.

From acetonitrile and DMF solution, polydisperse aggregates are observed with larger sizes compared to the DLS measurements (Figure 4). Such a discrepancy could result from the sample preparation method used, the low molecular weights we are dealing with and the dynamic nature of our system ($T_{g,PB}$ ~ -80 °C). Indeed, we drop-cast on the TEM copper carbon-coated grid a micellar solution (0.1 g/L or less) and let the solvent evaporate at room temperature. During the drying process, we assume the system to be mobile enough so that the previously well-defined micelles aggregate into larger objects. This renders the visualization of the single uncross-linked micelles relatively difficult. For $B_{109}M_{98}$[16], which possesses a higher T_g of PB due to the 1,2-microstructure present, possible rearrangement is hindered and individual micelles can be better observed (Figure 4d). Micelles with a radius of 14 nm could be measured. This radius is smaller than that obtained with DLS measurements but one has to keep in mind that on the TEM grid, the micelles are dried and present, therefore, collapsed cores. Furthermore, due to beam damage, the methacrylate corona is not visible under TEM. Thus, we measure stained core of the micelles only. Also, radii obtained by TEM are number-averaged while DLS gives us z-average values. Micelles in

acetone can be observed due to the fast evaporation of the volatile solvent, avoiding rearrangement of the structures (Figure 5).
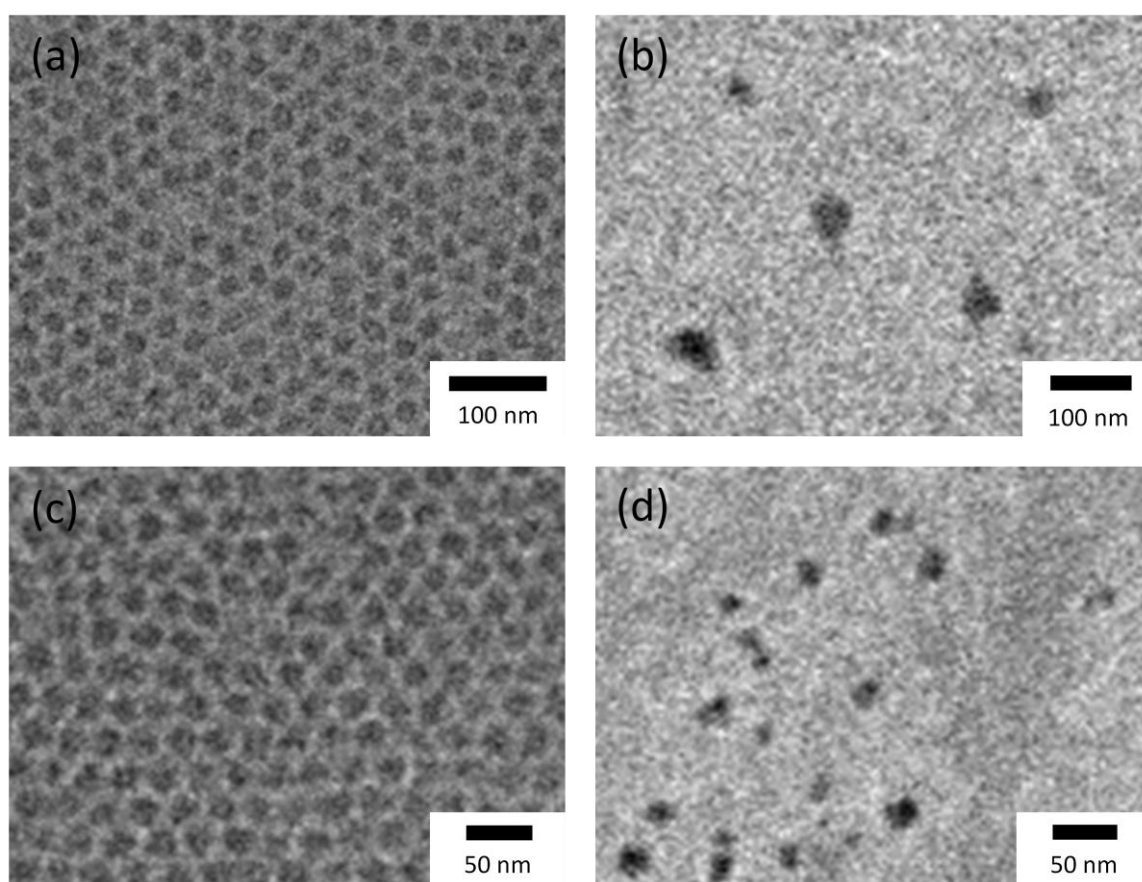

Figure 5. TEM images of micellar solution of (a) $B_{115}M_{122}$[19], (b) $B_{59}M_{63}$[10], (c) $B_{109}M_{98}$[16] and (d) $B_{41}M_{152}$[17] in acetone.

The observation of $B_{555}M_{452}$[75] single uncross-linked micelles in all three solvents is possible because of the higher molecular weight of the block copolymer and, more importantly, the higher T_g of 1,2-PB (see Figure 6). However, when not annealed, the solution of $B_{555}M_{452}$[75] in acetonitrile exhibits a mixture of spherical micelles and worm-like micelles (Figure 6a). After 12 hours at 60 °C, the worms disappear indicating that these are non-equilibrium structures (Figure 6d). The diameters of the micelles remain unchanged after annealing. This phenomenon is only observed in acetonitrile for polymers with a predominant 1,2-PB microstructure. The radii measured by TEM in acetone and DMF for $B_{555}M_{452}$[75] are 16 and 27 nm respectively. Again, TEM radii are smaller than DLS radii, 33 and 53 nm respectively (see Figure 7), for the same reasons mentioned above.
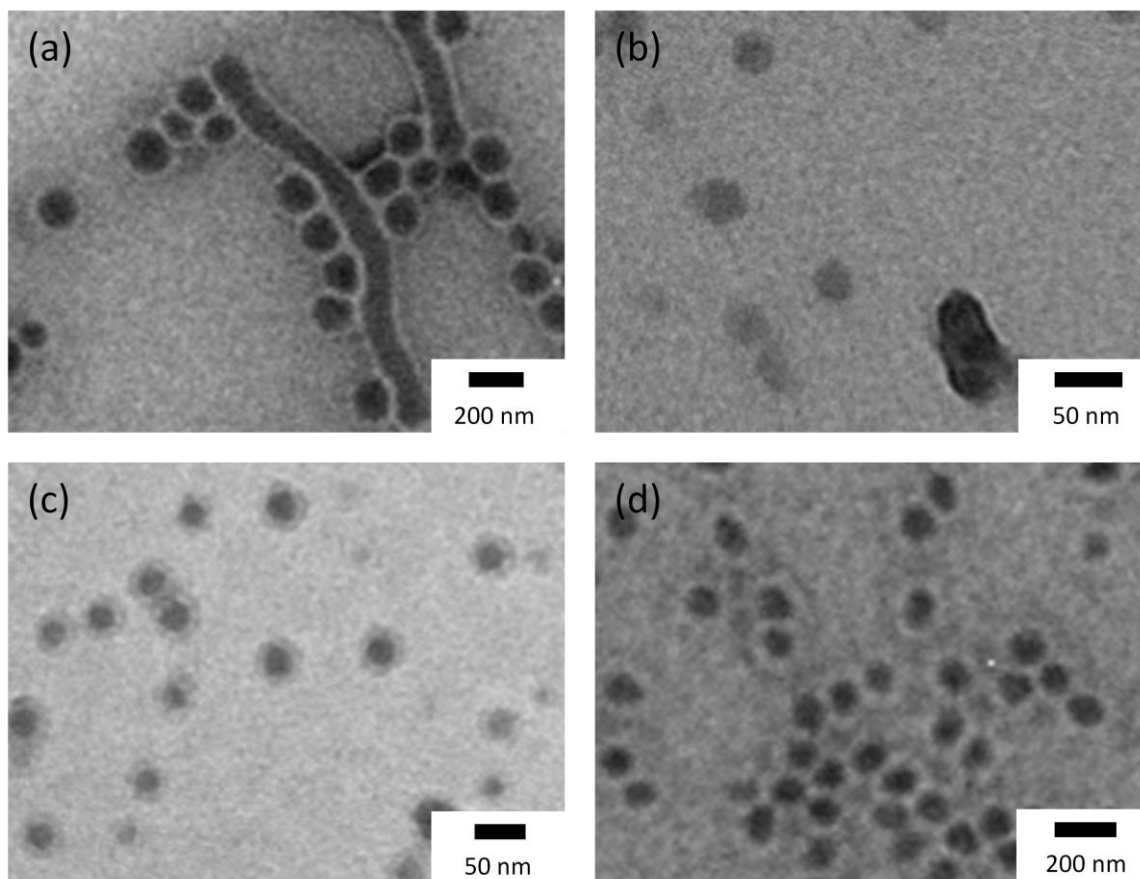
Figure 6. TEM micrographs of micellar solutions of B$_{555}$M$_{452}$[75] in (a) acetonitrile, (b) acetone, (c) DMF, (d) acetonitrile @ 60°C for 12h.
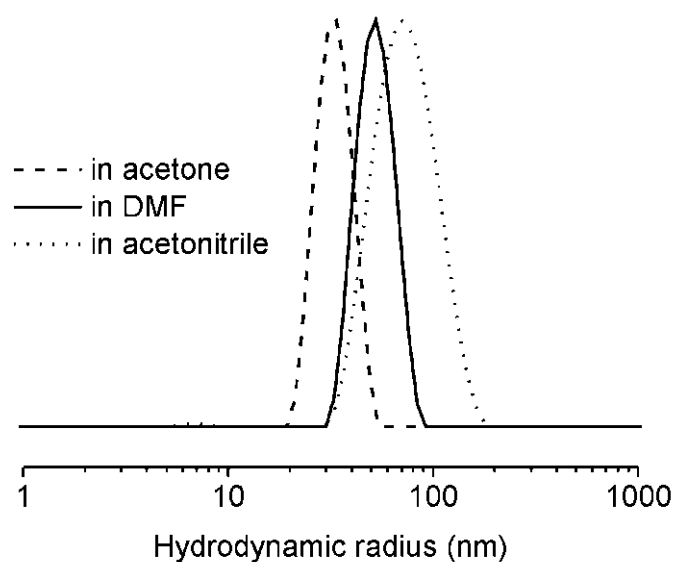

Figure 7. CONTIN analysis plots at 90° and 1 g/L for (a) B$_{540}$M$_{452}$[75] in acetone (dashed line), DMF (solid line) and acetonitrile (dotted line).

The aggregation number N_{agg} could be determined using static light scattering (SLS) for few micellar aggregates in acetonitrile by measuring their molecular weights from the Zimm plot (Figure 8). Results are reported in Table 3. The calculated values were obtained by the model established by Förster and Antonietti[50]: $N_{agg} \sim p_0 N_B^2 N_A^{-0.8}$, where N_B and N_A correspond to degrees of polymerization of the core and the corona blocks respectively and p_0 is a constant related to the interaction parameter χ and the monomer volume. The magnitude of order and the tendency described by the model seems in agreement with our experimental values and the constant can be estimated $p_0 = 1.6$. Such a scaling behavior is characteristic for micellization of strongly segregated block copolymers.
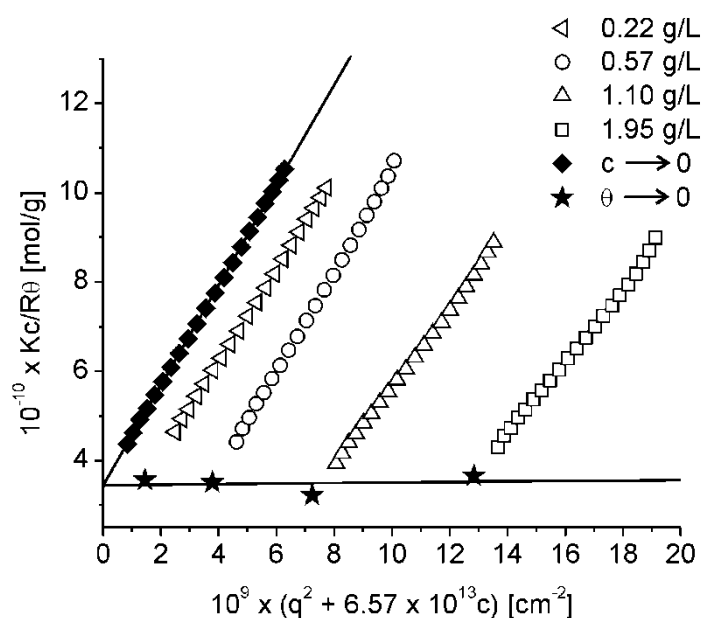

Figure 8. Zimm plot of $B_{540}M_{452}^{75}$ in acetonitrile.

The ratios $R_g/R_{h,z}$ were calculated from both static and dynamic light scattering. They are above the value expected for a hard sphere ($R_g/R_{h,z} = 0.775$)[50] and closer to values characteristic for star-like molecules[51] which seems reasonable considering our systems. Similar results have been found by Förster et al. for PS-P4VP in toluene[50]. Usually values of $R_g/R_{h,z}$ larger than 1.1 are measured for anisotropic particles. Polymers with large volume fractions of the core block are more likely to form such anistropic objects by undergoing transitions to rods or disks. $B_{68}M_{100}^{14}$ and $B_{540}M_{452}^{75}$ exhibit a volume fraction of 0.33 and 0.46 respectively and, therefore, would be prone to such a behavior. But, as shown in Figure 3b, no angular dependence of the micellar structure formed in acetonitrile was found and,

as we will see later, the corresponding cross-linked nanoparticles are perfectly spherical and very monodisperse. There is no hint that they would form anisotropic objects.

Table 3. Aggregation numbers of B-M micelles in acetonitrile.

	10^{-3} M_n (g/mol)	$R_{h,z}$ (nm)[a]	$R_{n, core\ TEM}$ (nm)	R_g (nm)[b]	$R_g/R_{h,z}$	N_{agg}[b]	$N_B^2\ N_A^{-0.8}$
$B_{68}M_{100}$[14]	13.7	14.3	aggr.	23 ± 5	1.6	190 ± 40	116
$B_{540}M_{452}$[75c]	73.2	68.8	42	99 ± 5	1.4	3760 ± 70	2239

[a] DLS; [b] SLS; [c] synthesized in THF

The solution behavior of B-M-H block copolymers is similar to that of B-M diblock copolymers in the same selective solvents. The PHEMA block does not have any influence on the micellization behavior due to its shortness. Micelles obtained are therefore functionalized with –OH groups on their external corona.

3.3.2.2 B-nBA and B-nBMA micelles

Molecular characteristics of B-nBA and B-nBMA block copolymers and radii of their micelles formed in DMF and DMAc respectively are listed in Table 4.

Table 4. Molecular parameters for B-nBA and B-nBMA block copolymers.

	M_n^{a+b} (kg/mol)	M_w/M_n[a]	%wt PnB(M)A[b]	% 1,4-PB[b]	$R_{h,z}$ (nm)	$R_{n, TEM}$ (nm)
$B_{119}n$BA$_{79}$[18]	16.5	1.13	61	57	13.2	3
$B_{91}n$BMA$_{58}$[15]	13.2	1.12	63	85	10.5[c]	6

[a] GPC with PB calibration, [b] 1H NMR; [c] measured at 10 g/L

$B_{119}n$BA$_{79}$[18] block copolymer forms micelles in DMF and CONTIN analysis plots obtained by DLS measurements exhibit sharp peak characteristic of very narrowly dispersed species. Hydrodynamic sizes are measured around 13 nm radius. In Figure 9a, the linear fit of the data passing through the origin suggests a spherical geometry of the micellar aggregates[49].
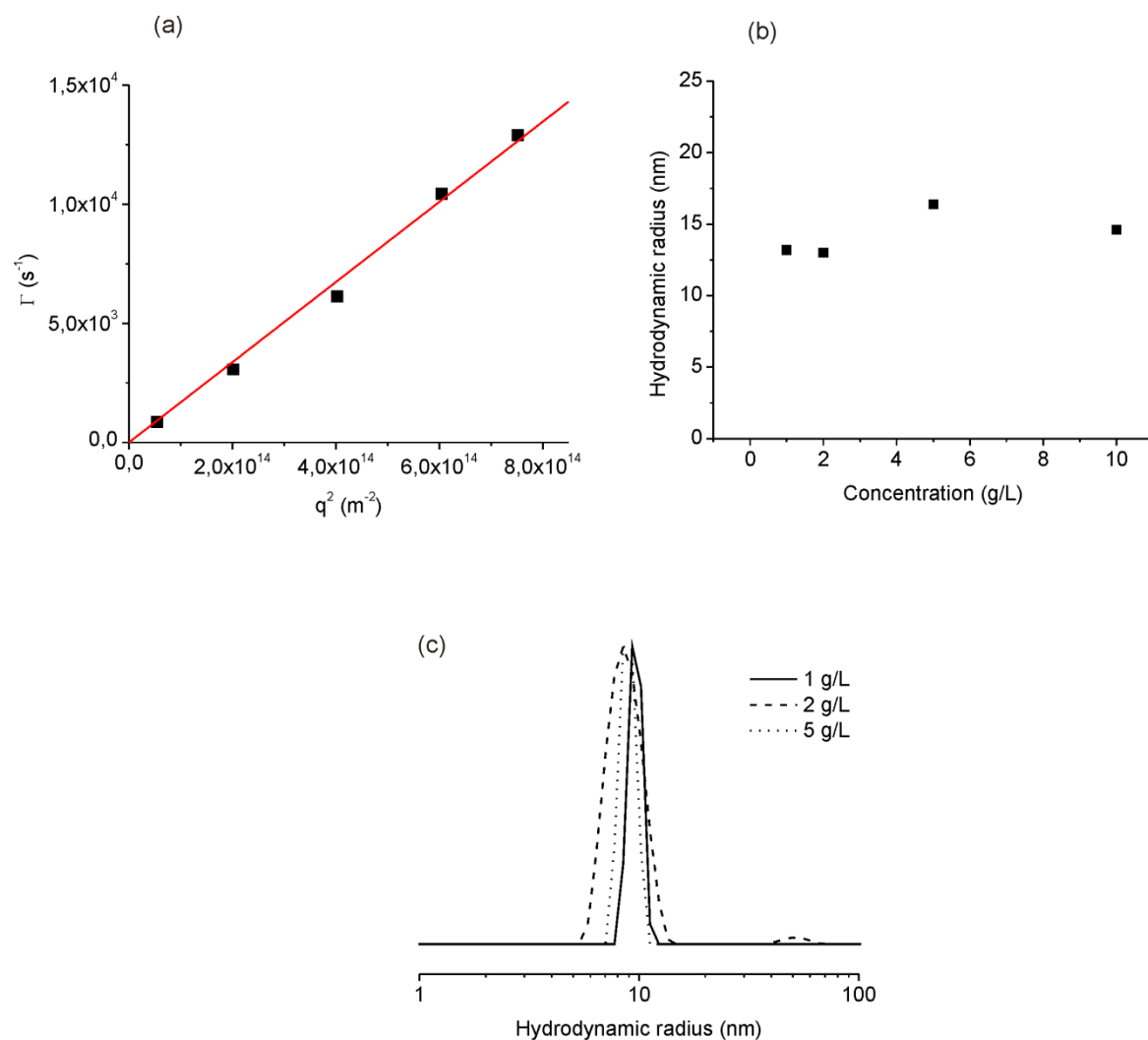
(a)

(b)

(c)

Figure 9. (a) Γ vs. q^2 for B$_{119}$$nBA_{79}$[18] in DMF (5 g/L), (b) concentration dependence of R$_h$, (c) CONTIN plot for B$_{91}$$nBMA_{58}$[15] at 90° at various concentration.
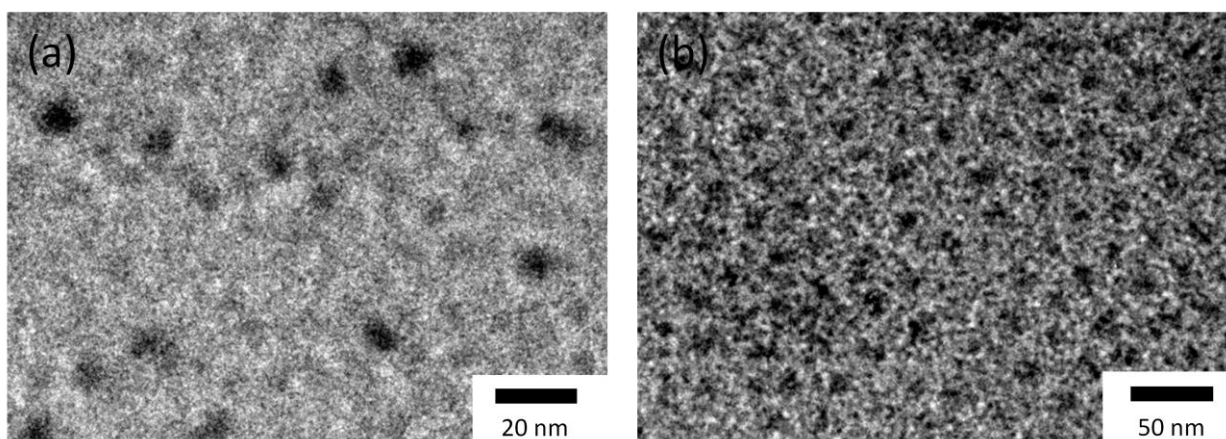

Figure 10. TEM images of (a) B$_{119}$$nBA_{79}$[18] in DMF, (b) B$_{91}$$nBMA_{58}$[15] in DMAc.

The concentration does not have any influence on the size of the micellar aggregates as observed in Figure 9b. TEM images show spherical micelles and the dark core is measured to

be about 3 to 4 nm radius (Figure 10a). This observation is consistent with our DLS measurement if we consider that only the core is measured and that it is shrunken due to drying on the grid.

$B_{91}nBMA_{58}$[15]block copolymers undergo micellization in DMAc and DLS measurements show very narrowly distributed objects with a radius of about 10 nm which is independent of the polymer concentration in solution (Figure 9c). TEM images (Figure 10b) display spherical aggregates with about 6 nm radius and are in good agreement with the previous result.

3.3.3   From self-assembly to nanoparticles through cross-linking

As we already discussed, observations using TEM of the obtained self-assembled aggregates in solution is often difficult for small dynamic structures. The preparation of the sample can induce, during the evaporation of the solvent, modifications in the initial structure. This is especially true in our case where the core block exhibits a very low T_g.
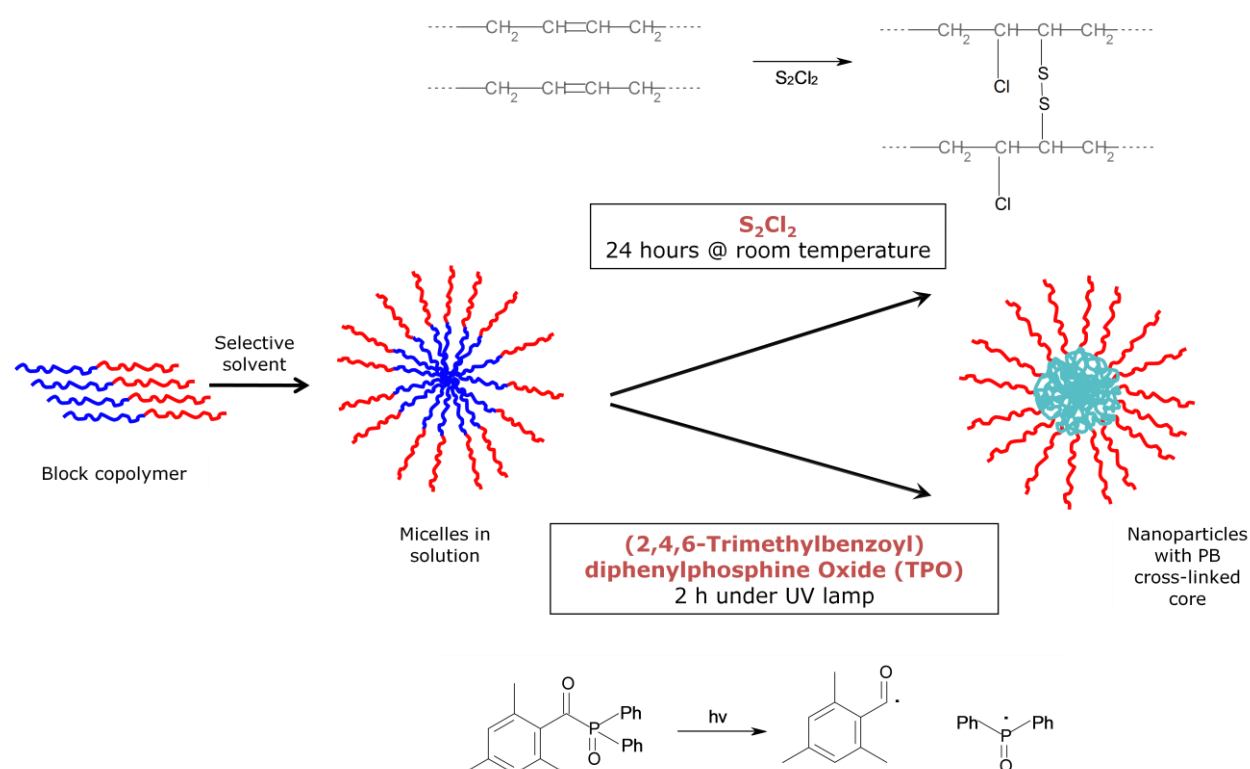
Scheme 3. Cross-linking strategies.

All samples were cross-linked in solution in the selective solvent using S_2Cl_2 or Lucirin TPO® as cross-linker. The different strategies are depicted in Scheme 3. After reaction, the

solutions were dialysed against THF which is a common solvent where both PB and the polymethacrylate blocks are soluble. Assessment of the efficiency of the cross-linking process was made through DLS measurements. Indeed, if no cross-linking occurred, during the purification dialysis, the micelles dissolve completely in THF and no characteristic scattering signal is detected. On the other hand, if the cross-linking took place, the micelles become insoluble in THF and swollen spherical micelles can still be detected in DLS.

3.3.3 B-M(-H) nanoparticles

We reported in Table 5, hydrodynamic radii, R_h, measured in THF solutions after cross-linking and purification by dialysis for B-M. In all cases, nanoparticles are detected. Their sizes are larger than those of the non cross-linked micelles in acetonitrile which can be due to the swelling of the PB cross-linked core by THF and/or to the further stretching of the PMMA corona in THF which is a better solvent for PMMA than acetonitrile (Figure 11a). Furthermore, the cross-linking does not affect the spherical structure of the micelles as seen on Figure 11b where no angular dependence of the hydrodynamic radius is noticed.

Table 5. Radii of cross-linked micelles measured by DLS and TEM.

	$10^{-3} M_n$ (g/mol)	%wt PMMA	$R_{h,z}{}^a$ / $R_{n, core}{}^c$ (nm)	$R_{h,z}{}^b$ / $R_{n, core\ TEM}{}^c$ (nm)			
				S_2Cl_2 1:0.5	S_2Cl_2 1:1	TPO 1:0.5	TPO 1:1
$B_{115}M_{122}$[19]	18.4	66	17.4	23.9	24.5/15	32.2	22.9
$B_{59}M_{63}$[10]	9.5	66	12.4	--	--	--	--
$B_{68}M_{100}$[14]	13.7	73	14.3	16.8/13	25.2	26.2/16	20.1/14
$B_{41}M_{152}$[17]	17.4	87	17.3/7	24.5/3	20.7/10	25.5/7	20.7/15
$B_{109}M_{98}$[16c]	15.7	61	17.5/14	21.9/15	22.4/17	21.4/21	19.8/18
$B_{540}M_{452}$[75c]	73.2	60	68.8/42	102.3/33	101.9/30	80.4/54	75.4/59

[a] in acetonitrile before cross-linking

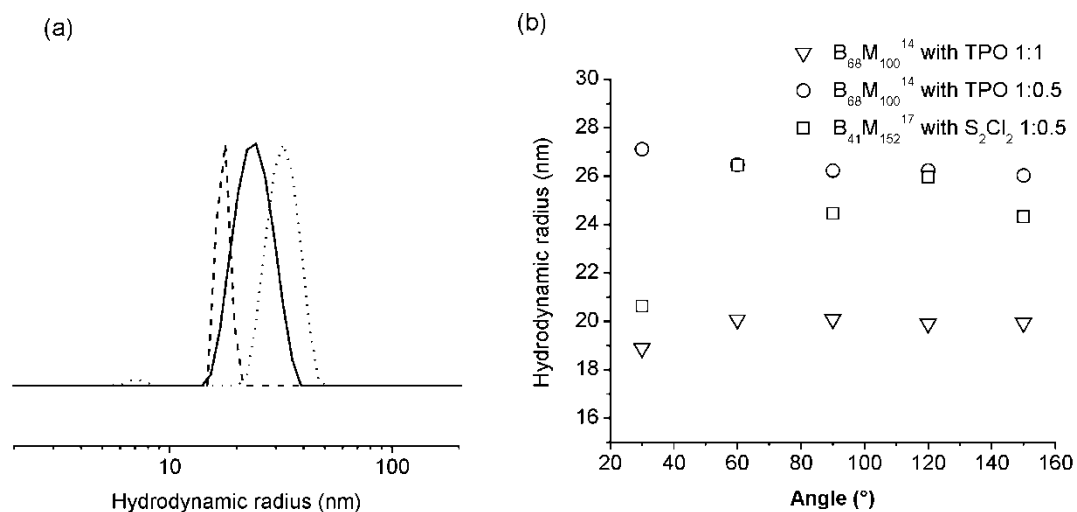[b] after cross-linking and dialysis against THF

[c] synthesized in THF.

Figure 11. (a) CONTIN analysis of $B_{115}M_{122}$[19] in acetonitrile (dashed line), after C-L with S_2Cl_2 (1:0.5) (solid line) and after C-L with TPO (1:0.5) (dotted line). (b) Angular dependence of R_h of the nanoparticles after cross-linking.

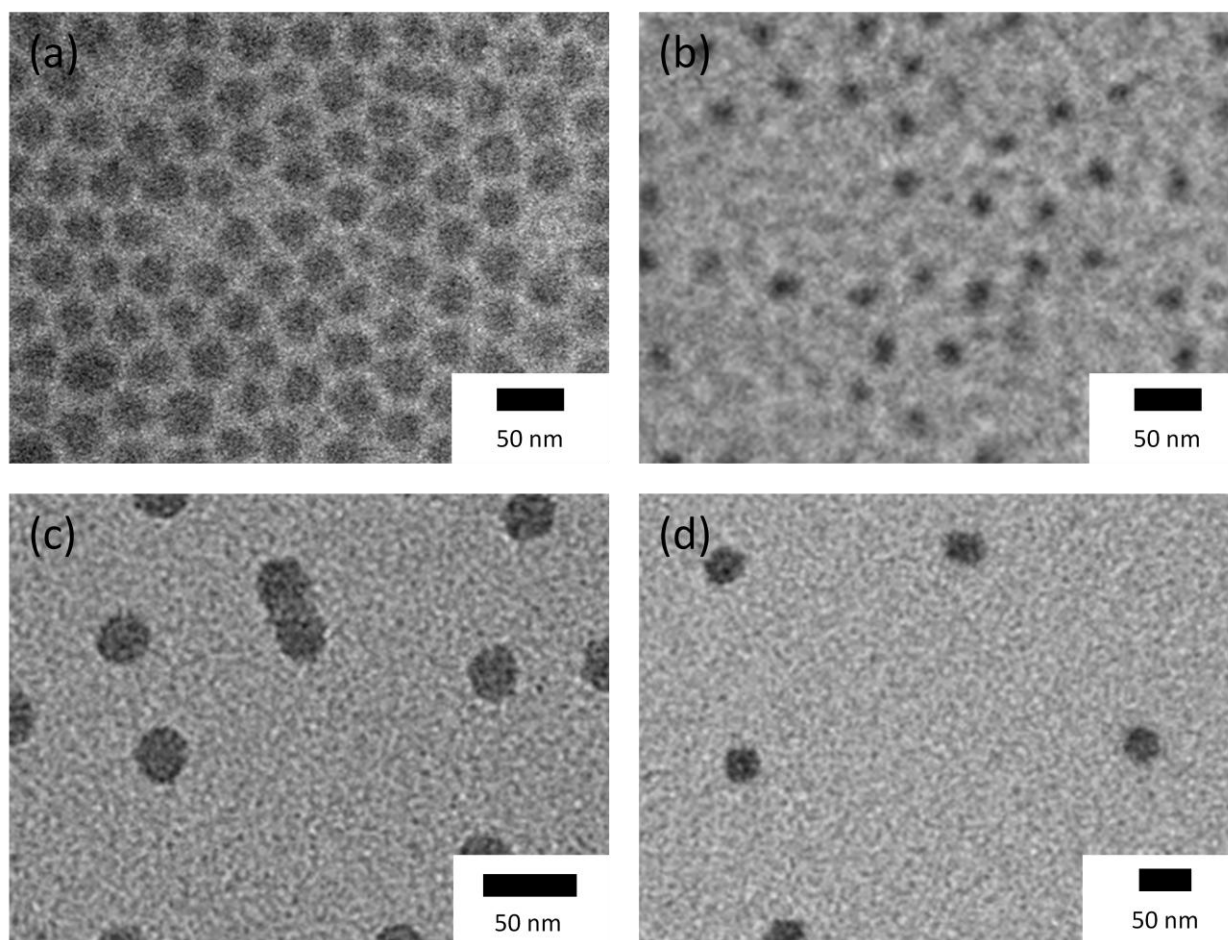Figure 12. TEM micrographs of cross-linked micellar solution of (a) $B_{115}M_{122}$(19) with S_2Cl_2 (1:1), (b) $B_{41}M_{152}$(17) : S_2Cl_2 (1:1), (c) $B_{109}M_{98}$(16) : S_2Cl_2 (1:1), (d) $B_{109}M_{98}$(16) : S_2Cl_2 (1:0.5).

The TEM micrographs obtained from THF solutions (Figure 12, Figure 13) reveal monodisperse nanospheres. Radii measured from the TEM images are reported in Table 5.

Sizes measured by TEM are, as mentioned for the non cross-linked micelles, significantly smaller than those measured by DLS. For example, $B_{68}M_{100}$[14] cross-linked with Lucirin TPO® (1:1) exhibit a radius of 15 nm on the TEM image but 20 nm when measured by DLS. Similarly, $B_{115}M_{122}$[19] cross-linked using S_2Cl_2, is 10 nm smaller on the TEM image than measured by DLS. Cold vulcanization with S_2Cl_2 of the PB core of the micelles leads to very monodisperse spherical nanoparticles which are even seen to pack hexagonally (Figure 12a). Using photo-cross-linking, the nanoparticles obtained do not seem to reach such a high degree of monodispersity. This phenomenon is still unclear to us but in both cases the cross-linking process is efficient and maintains the spherical shape of the micelles as they are in solution in selective solvent.
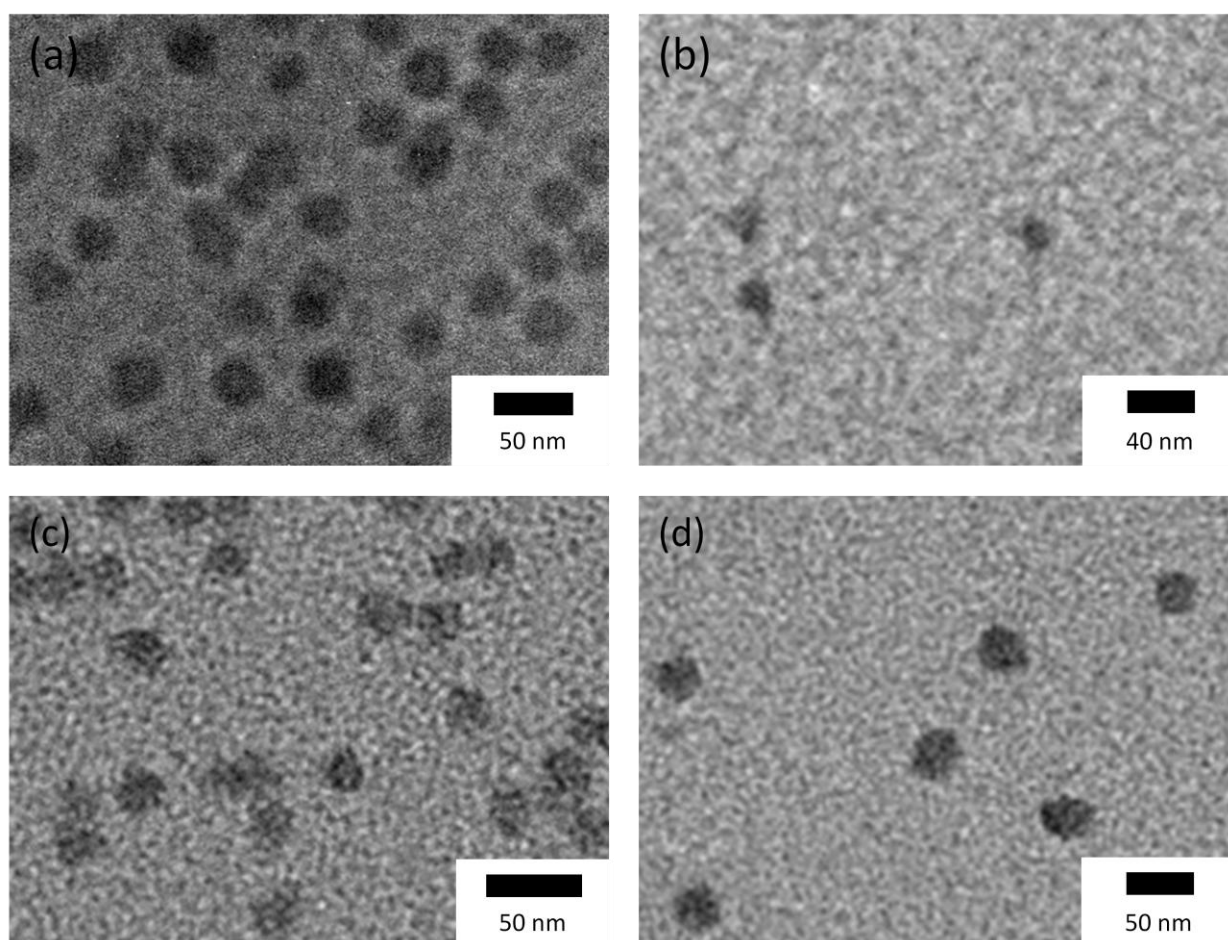

Figure 13. TEM micrographs of cross-linked micellar solution of (a) $B_{115}M_{122}$(19) with TPO (1:1), (b) $B_{41}M_{152}$(17) : TPO (1:1), (c) $B_{68}M_{100}$(14) : TPO (1:1), (d) $B_{109}M_{98}$(16) : TPO (1:1).

Degree of cross-linking

The degree of cross-linking can be measured by ^{1}H NMR where the residual double bonds are being quantified or when not possible by Elemental Analysis (see Table 6). For most of the vulcanized samples, the NMR measurements were not conclusive. The signals of the double bonds were non-existent at all. This phenomenon is ascribed to the loss of mobility within the core of the micelles, accentuated by the cross-linking reaction. Thus, only the PMMA corona was detected (Figure 15b). To overcome this, elemental analysis was carried out in order to quantify the amount of sulfur introduced into the core.

Photo-cross-linked samples do not exhibit such behavior and determination of the cross-linking degree is possible via ^{1}H NMR. The presence of the photo-intiator (phenyl rings at 8 and 7.5 ppm on Figure 14b) is also detected after dialysis which indicates it is integrated into the core. The presence of such a bulky component might induce more free volume and explain the higher mobility within the core compared to vulcanized ones. There is no significant dependence of the degree of cross-linking on the ratio [double bonds : cross-linker] used. A ratio of 1: 0.5 seems to be enough to yield a sufficient degree of cross-linking where between 55 and 75 % of the double bonds disappear.

Table 6. Degree of cross-linking of stabilized micelles.

	%wt PMMA	S_2Cl_2 1:0.5 [a]	S_2Cl_2 1:1 [a]	TPO 1:0.5 [b]	TPO 1:1 [b]
$B_{115}M_{122}$[19]	66	63%	51%	62%	44%
$B_{59}M_{63}$[10]	66	--	--	--	--
$B_{68}M_{100}$[14]	73	80%	54%	74%	69%
$B_{41}M_{152}$[17]	87	39%	58%	65%	56%
$B_{109}M_{98}$[16 c]	61	33%	75%	67%	64%
$B_{540}M_{452}$[75 c]	60	31%	39%	57%	60%

[a] Elemental analysis; [b] ^{1}H NMR; [c] synthesized in THF.

On the other hand, cold vulcanization seems to increase the degree of cross-linking with the amount of sulfur chloride used. Except for $B_{115}M_{122}$[19] and $B_{68}M_{100}$[14], where the highest degree of cross-linking is found for the lowest amount of S_2Cl_2. We speculate that the diffusion of the cross-linking agent into the core might explain the differences observed.
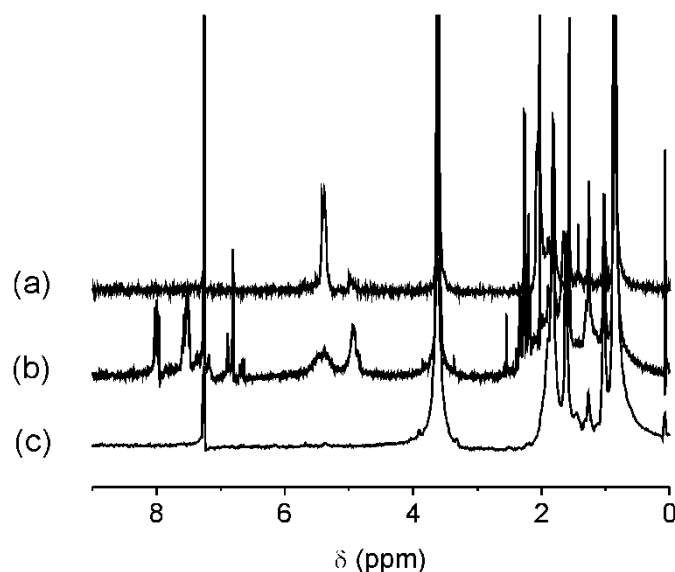
Figure 14. ^{1}H NMR spectra (300MHz) of (a) B-M, (b) B-M (1,2-PB) cross-linked with Lucirin TPO® and (c) B-M cross-linked with S_2Cl_2 in $CDCl_3$.

Differential Scanning Calorimetry

Polybutadiene presents interesting mechanical properties due to its low glass transition temperature. It is often used as an impact modifier when introduced in stiffer materials[52]. In order to verify if the synthesized nanoparticles retain their low glass transition temperature, DSC was performed before and after cross-linking.
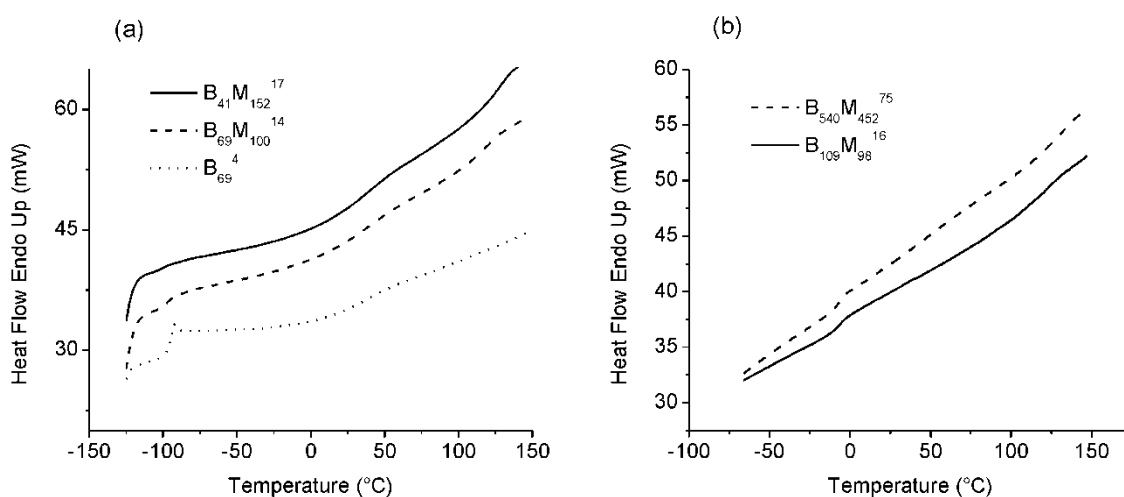

Figure 15. DSC curves for (a) B-M with high 1,4-PB content and (b) B-M with high 1,2-PB content.

The DSC measurements of the different neat diblock copolymers show all a glass transition temperature (T_g) between 110 and 120 °C which is attributed to the PMMA rich

phase and another low T_g around -95 °C corresponding to the 1,4-PB phase (Figure 15a). For $B_{109}M_{98}{}^{16}$ and $B_{540}M_{452}{}^{75}$, the lowest glass transition of the 1,2-PB phase is detected at -6 °C and -7 °C respectively (Figure 15b).
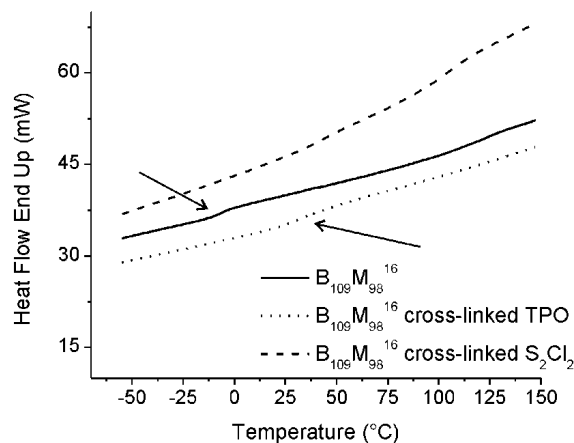

Figure 16. DSC curves of $B_{109}M_{98}{}^{16}$ before cross-linking (solid line) and after cross-linking with TPO (dashed line). The arrows indicate the transitions.

In Figure 17, DSC heating curves of $B_{109}M_{98}{}^{16}$ before and after cross-linking are reported and transitions indicated by arrows. In the case of photo-cross-linked nanoparticles, the glass transition temperature is seen shifting from -6 °C to 32 °C whereas cold vulcanized nanoparticles do not exhibit transitions at low temperature. For $B_{68}M_{100}{}^{14}$, independently of the cross-linking method, no glass transition is observed.

Cross-linking of the PB core of the nanoparticles shifts the initial T_g to higher temperatures. For samples where no transition could be observed, it might be too weak to be detected with our device or just non-existent. As a result, B-M nanospheres do not seem to retain their low glass transition upon cross-linking reaction.

3.3.3.2　B-nBA and B-nBMA nanoparticles

Cross-linking was performed in solution using Lucirin TPO® as photo-initiator and DLS and TEM data concerning the radii of the cross-linked nanoparticles are summarized in Table 7.

Spherical monodisperse nanoparticles were obtained as seen on TEM images (Figure 17a). CONTIN analysis (Figure 18b) shows non cross-linked spherical micelles of $B_{119}nBA_{79}{}^{18}$ in DMF with a radius of about 13 nm. After cross-linking (with Lucirin TPO® 1:0.5) and dialysis against THF, the radius is increased to 19 nm which is in good agreement with TEM images where the radius is measured to be around 14 nm. Similarly, $B_{91}nBMA_{58}{}^{15}$ shows

spherical micelles with 17 nm radius in DMAc which increase up to 23 nm after cross-linking and dialysis against THF. This last result is also in agreement with the TEM image in Figure 17b.

Table 7. Radii of B-*n*B(M)A cross-linked micelles measured by DLS and TEM.

	M_n^{a+b} (kg/mol)	PDI^a	%wt P*n*B(M)A^b	% 1,4-PB^b	$R_{h,z}$ (nm)^c	$R_{h,z}$ (nm)^d TPO 1:0.5	$R_{n,\text{core TEM}}$ (nm)
B$_{119}$*n*BA$_{79}$[18]	16.5	1.13	61	57	13.2	18.9	14
B$_{91}$*n*BMA$_{58}$[15]	13.2	1.12	63	85	17.5	23.1	15

[a] GPC with PB standards; [b] ^{1}H NMR; [c] DLS in respective selective solvents; [d] DLS after cross-linking and dialysis against THF.
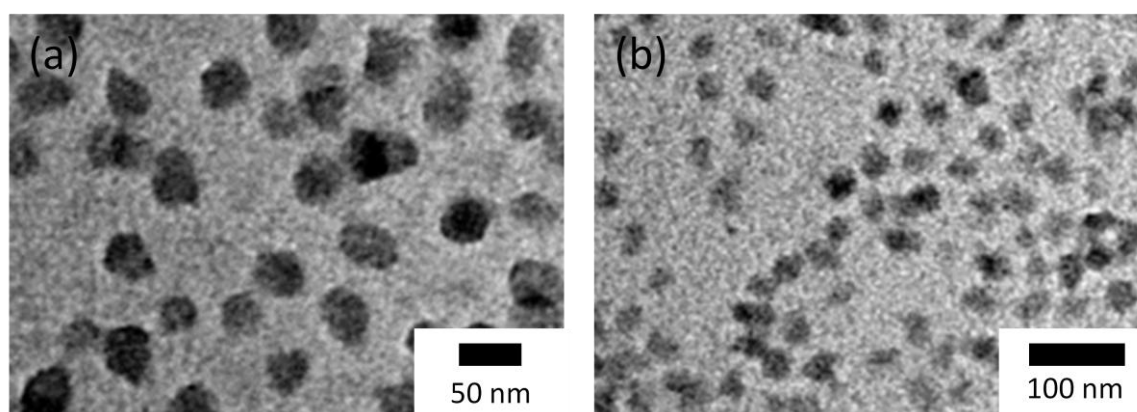
Figure 17. TEM images of (a) B$_{119}$-*n*BA$_{79}$[18] and (b) B$_{91}$-*n*BMA$_{58}$[15] cross-linked with TPO (1:0.5) (drop-casted from THF solution after dialysis).
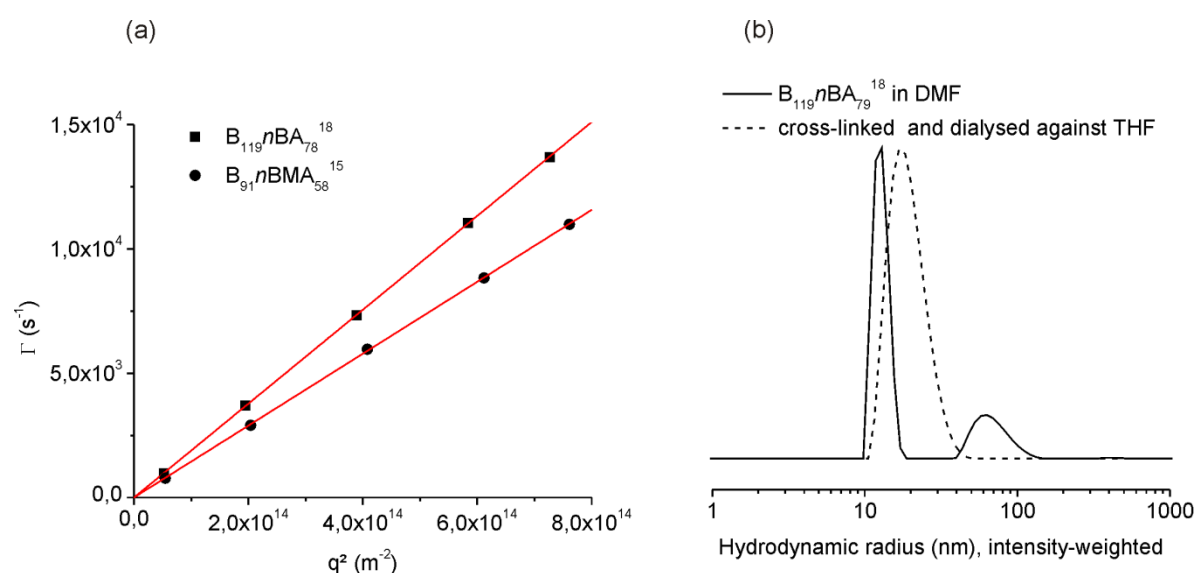
Figure 18. (a) Γ vs. q² for B$_{119}$*n*BA$_{79}$[18] and B$_{91}$*n*BMA$_{58}$[15] cross-linked with TPO (1:0.5) in DMF and DMAc respectively after dialysis against THF and (b) CONTIN plot analysis before (solid line) and after (dashed line) cross-linking for B$_{119}$*n*BA$_{79}$[18].

Degrees of cross-linking could be measured by ^{1}H NMR spectroscopy and seem, in this case, to increase with the amount of photo-initiator Lucirin TPO® introduced. From 1:0.5 to 1:1, the degree of cross-linking increases from 13 % to 28 % for $B_{119}nBA_{79}$[18] and from 33 % to 59 % for $B_{91}nBMA_{58}$[15]. These degrees of cross-linking are significantly lower than those obtained for B-M cross-linked micelles. This last observation is not fully understood.

DSC measurements were also performed and results are summarized in Table 8 and DSC curves are shown on Figure 19. For the uncross-linked polymer, one can distinguish two sharp glass transitions at -47 °C and -66 °C for $B_{119}nBA_{79}$[18]. The lowest is ascribed to the PB phase whereas the second one is characteristic of PnBA. After cross-linking, a unique and very broad transition is observed from -23 °C to -10 °C. The evaluation at half the ΔC_p indicates a T_g at ca. -14 °C. For $B_{91}nBMA_{58}$[15], the lowest transition appears at -85 °C and the highest around 25 °C which corresponds to the T_g of the PnBMA rich phase. After cross-linking reaction, similarly to the $B_{119}nBA_{79}$[18] case, a unique and broad transition is observed from -3 °C to 10 °C. T_g is evaluated to be at 2 °C. In both case, relatively low T_g are obtained after cross-linking reaction.

Table 8. Glass transition temperatures measured by DSC before and after cross-linking.

	T_{g1} (°C)	T_{g2} (°C)
$B_{119}nBA_{79}$[18]	-66,0	-46,7
$B_{119}nBA_{78}$[18] cross-linked	-14,1	--
$B_{91}nBMA_{58}$[15]	-86,5	24,9
$B_{91}nBMA_{58}$[15] cross-linked	2,4	--
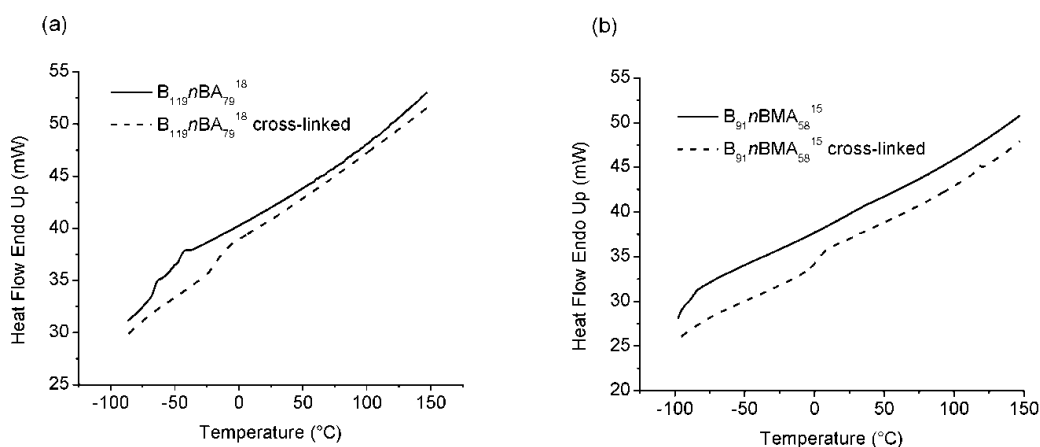
Figure 19. DSC heating curves of (a) $B_{119}nBA_{79}$[18] and (b) $B_{91}nBMA_{58}$[15] before (solid line) and after (dashed line) cross-linking.

3.3.4   Water-soluble nanoparticles

From the self-assembly of $B_{230}tBMA_{129}$[31] block copolymers into spherical micelles, water-soluble nanoparticles could be obtained after cross-linking of the PB core and subsequent hydrolysis of the poly(*t*-butyl methacrylate) (P*t*BMA) corona to yield a polymethacrylic acid (PMAA) corona. Polymer characteristics and data concerning the size of the micelles obtained in different selective solvents are summarized in Table 9.

Table 9. Molecular parameters of B-*t*BMA block copolymer and hydrodynamic sizes of B-*t*BMA micelles measured by DLS and TEM.

	M_n^{a+b} (kg/mol)	M_w/M_n^{a}	%P*t*BMA [b]	% 1,4-PB [b]	Selective solvent	$R_{h,z}$ (nm)	$R_{n, TEM}$ (nm)
$B_{230}tBMA_{129}$[31]	30.9	1.04	60	17	DMAc	10.5	9
					Acetone	aggr.	16

[a] MALDI-ToF; [b] ^{1}H NMR

3.3.4.1 Solution behavior

In acetone, over the whole range of concentrations, $B_{230}tBMA_{129}$[31] only seems to form large aggregates according to DLS measurements (Figure 21, solid line). However, TEM observations reveal well-defined spherical objects with radii varying between 15 to 25 nm (dark PB core measured only, Figure 20a).Their size distribution over the TEM grid is quite broad. Micellar aggregates could also be obtained in DMAc. The first TEM observations (Figure 20b) let appear a mixture of worm-like and spherical micelles where the PB domains are about 9 nm thick. These worm-like structures disappeared after annealing of the micellar solution at 60 °C for few hours and polydisperse aggregates with an average radius of 23 nm are finally measured on the TEM micrographs (Figure 20c).

3.3.4.2 Cross-linking

The cross-linking of B_{230}-$tBMA_{129}$[31] micelles in acetone was carried out by adding S_2Cl_2 to the micellar solution. The solution was then purified by dialysis and transfered to THF to verify the efficiency of the cross-linking process. According to the CONTIN analysis in Figure 21 (dashed line), cross-linked micelles with 147 nm radius in THF are obtained. This result is

in agreement with TEM measurements for which micellar aggregates with a cross-linked core of about 62 nm radius are observed (Figure 23a).
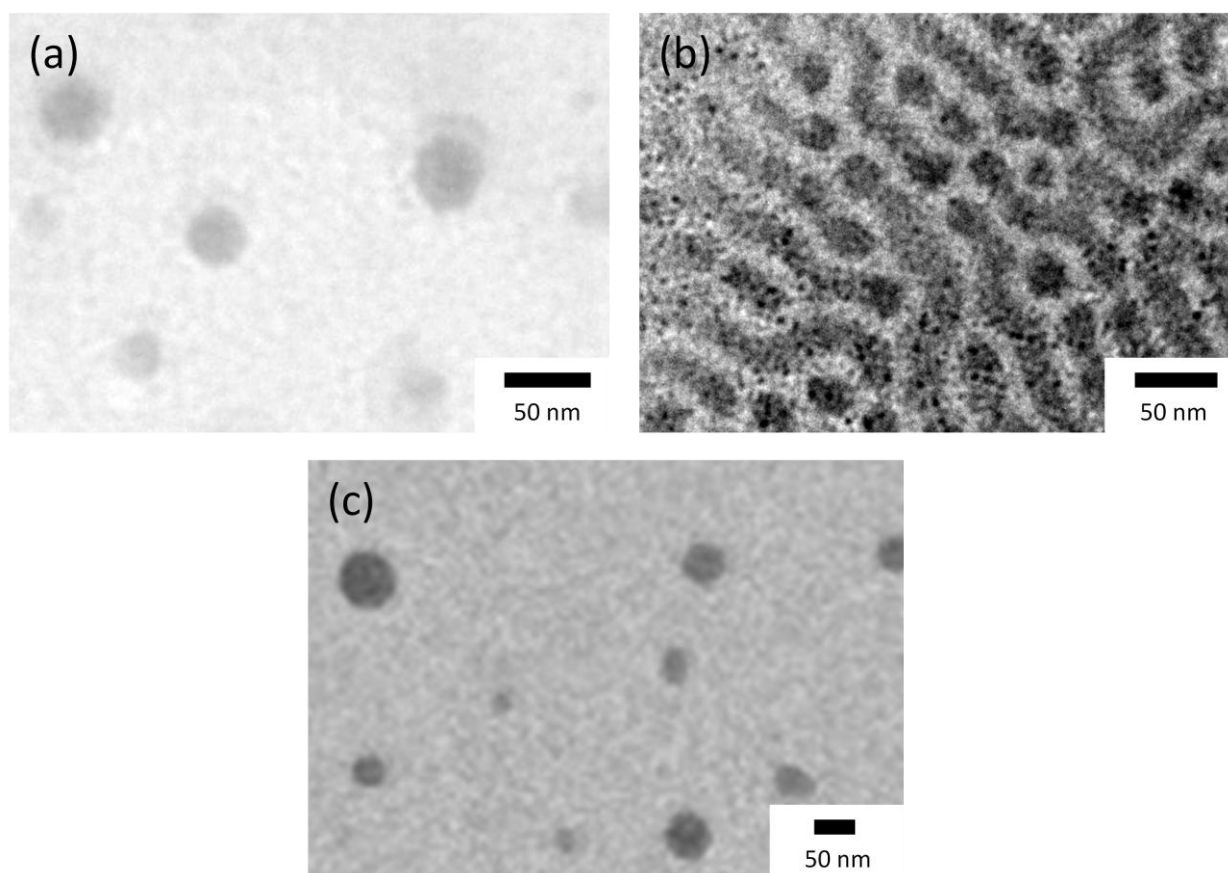

Figure 20. TEM images of B$_{230}$$tBMA_{129}$[31] in (a) acetone, (b) DMAc and (c) DMAc after annealing @ 60 °C for 12 hours.
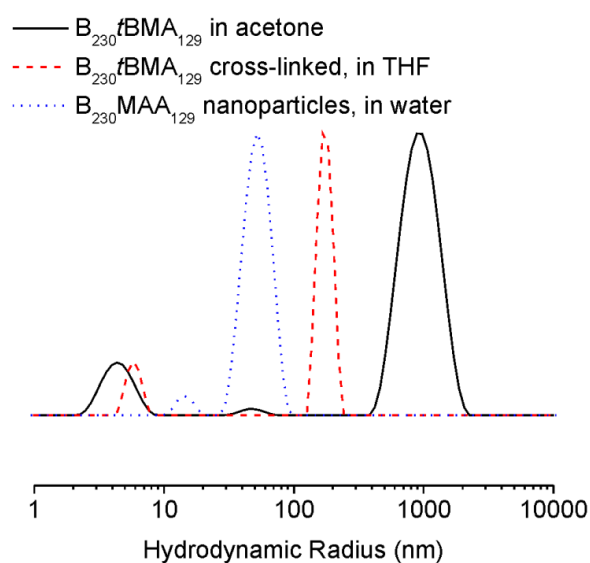

Figure 21. CONTIN analysis of B$_{230}$$tBMA_{129}$[31] block copolymer in acetone (solid line), its corresponding cross-linked micelles after dialysis against THF (dashed line) and after hydrolysis and dialysis against water (doted line).

3.3.4.3   Hydrolysis

The hydrolysis of the PtBMA corona of the nanoparticles was carried out as described earlier in the experimental part. The hydrolyzed product was not directly soluble in water and was dialysed from THF against water for three days. In water, the nanoparticles were stable and did not precipitate or aggregate even after few months. The DLS measurements of the hydrolyzed nanoparticles in water show spherical objects with ca. 52 nm radius (Figure 21, dotted line). These results were confirmed by TEM observations (Figure 22b) where the nanospheres exhibit similar polydispersity and radii of the core varying between 30 and 15 nm.
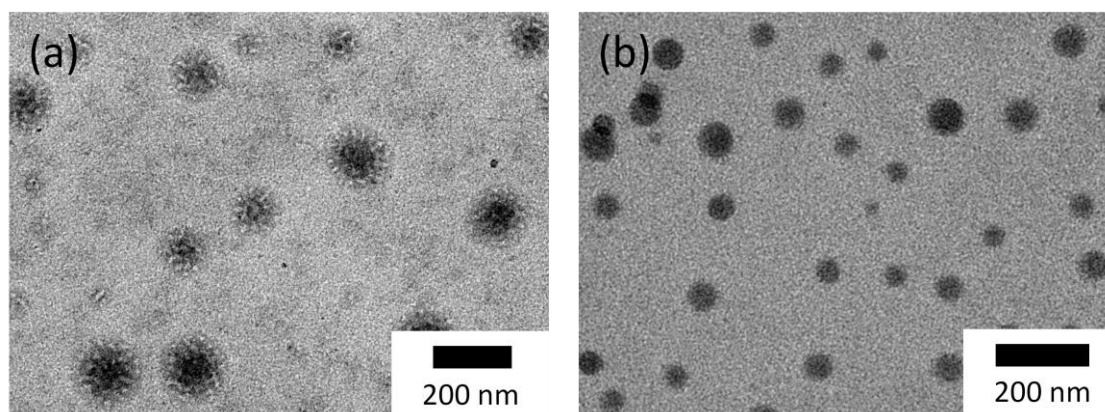
Figure 22. TEM images of B$_{230}$tBMA$_{129}$[31] (a) after cross-linking of micelles formed in acetone with S$_2$Cl$_2$ (drop-cast from THF solution) and (b) after hydrolysis of PtBMA corona of the cross-linked micelles (drop-cast from water solution)

3.3.4.4   Thermal behavior

The investigation of their thermal behavior by DSC after cross-linking with S$_2$Cl$_2$ was unsuccessful while when photo-cross-linked, the nanoparticles exhibit higher glass transition temperature than for the uncross-linked polymer. Before cross-linking, the lowest T$_g$, ascribed to the PB rich phase, was measured around -16 °C. After photo-cross-linking in DMAc, a broad transition was observed between 39 °C and 53 °C. The value calculated at half of the C$_p$ indicated 45 °C. Here again, the glass transition is shifted to higher temperature upon cross-linking reaction of the PB core.

3.5   Conclusions

The synthesis of polymeric nanoparticles was successfully achieved by cross-linking of PB-containing block copolymers self-assembled into spherical micelles. Cross-linking of the micelles in solution did not alter their spherical structure and narrowly distributed nanoparticles were obtained. The size of the nanoparticles can be tuned by the molecular weight of the block copolymer and depends also on the nature of the solvent used. Self-assembly of B-M block copolymer into micelles occurs in many different selective solvents but acetonitrile proved to be the best for spherical micelle formation, regardless of the composition and molecular weight of the block copolymers. Their micellar behavior is similar to those for strongly segregated block copolymers described by Förster and Antonietti. Upon cross-linking, the B-M nanoparticles loose their low glass transition temperature whereas B-*n*BMA and B-*n*BA nanoparticles still exhibit relatively low glass transition temperature after cross-linking reaction. Those latter might provide better impact toughness than B-M nanoparticles when introduced in a stiffer material, provided they are dispersed in a matrix which is compatible with the shell of the nanoparticles (PMMA, P*n*BA or P*n*BMA).

Water-soluble nanoparticles could also be successfully obtained from B-*t*BMA cross-linked micelles. The hydrolysis of the *t*BMA corona of the cross-linked nanoparticles led to water soluble B-MAA nanospheres. Their glass transition temperature was also strongly shifted to temperatures above room temperature. They can be used as nanomodifiers for waterborne PU coatings.

References

1.   Matsen, M. W.; Bates, F. S., *Macromolecules* **1996,** 29, (23), 7641-7644.

2.   Darling, S. B., *Progress in Polymer Science* **2007,** 32, (10), 1152-1204.

3.   Riess, G., *Progress in Polymer Science* **2003,** 28, (7), 1107-1170.

4.   Akagi, T.; Baba, M.; Akashi, M., *Polymer* **2007,** 48, (23), 6729-6747.

5.   Wang, X.; Hall, J. E.; Warren, S.; Krom, J.; Magistrelli, J. M.; Rackaitis, M.; Bohm, G. G. A., *Macromolecules* **2007,** 40, (3), 499-508.

6.   Christof M. Niemeyer, *Angewandte Chemie International Edition* **2001,** 40, (22), 4128-4158.

7.   H. Yabu; T. Higuchi; M. Shimomura, *Advanced Materials* **2005,** 17, (17), 2062-2065.

8.   Lei, L.; Gohy, J-F.; Willet, N.; Zhang, J-X.; Varshney, S.; Jérôme, R., *Macromolecules* **2004,** 37, 1089-1094.

9.   Shen, L.; Wang, H.; Guerin, G.; Wu, C.; Manners, I.; Winnik, M. A., *Macromolecules* **2008,** 41, (12), 4380-4389.

10.   Walther, A.; Goldmann, A. S.; Yelamanchili, R. S.; Drechsler, M.; Schmalz, H.; Eisenberg, A.; Müller, A. H. E., *Macromolecules* **2008,** 41, (9), 3254-3260.

11.   Park, S.-Y.; Park, M.-H., *Langmuir* **2007,** 23, (12), 6788-6795.

12.   Bhargava, P.; Zheng, J. X.; Li, P.; Quirk, R. P.; Harris, F. W.; Cheng, S. Z. D, *Macromolecules* **2006,** 39, 4880-4888.

13.   Zhang, L.; Eisenberg, A., *Journal of the American Chemical Society* **1996,** 118, (13), 3168-3181.

14.   Choucair, A.; Eisenberg, A., *Eur. Phys. J. E* **2003,** 10, (1), 37-44.

15.   Bang, J.; Jain, S.; Li, Z.; Lodge, T. P.; Pedersen, J. S.; Kesselman, E.; Talmon, Y., *Macromolecules* **2006,** 39, (3), 1199-1208.

16.   Tung, P.-H.; Kuo, S.-W.; Chen, S-C.; Lin, C.-L.; Chang, F.-C., *Polymer* **2007,** 48, 3192-3200.

17.   Qin, A.; Tian, M.; Ramireddy, C.; Webber, S. E.; Munk, P.; Tuzar, Z., *Macromolecules* **1994,** 27, (1), 120-126.

18.   Jada, A.; Hurtrez, G.; Siffert, B.; Riess, G., *Macromolecular Chemistry and Physics* **1996,** 197, (11), 3697-3710.

19.   Pispas, S.; Hadjichristidis, N., *Macromolecules* **2003,** 36, (23), 8732-8737.

20.   Wang, D.; Peng, Z.; Liu, X.; Tong, Z.; Wang, C.; Ren, B., *European Polymer Journal* **2007,** 43, 2799-2808.

21.   Rakhmatullina, E.; Braun, T.; Chami, M.; Malinova, V.; Meier, W., *Langmuir* **2007,** 23, (24), 12371-12379.

22.   Schacher, F.; Walther, A.; Müller, A. H. E., *Langmuir* **2009,** 25, (18), 10962-10969.

23.   Piogé, S.; Fontaine, L.; Gaillard, C.; Nicol, E.; Pascual, S., *Macromolecules* **2009,** 42, (12), 4262-4272.

24.   Yu, Y.; Zhang, L.; Eisenberg, A., *Langmuir* **1997,** 13, (9), 2578-2581.

25. Zhang, W.; Shi, L.; An, Y.; Gao, L.; Wu, K.; Ma, R.; Zhang, B., *Macromolecular Chemistry and Physics* **2004,** 205, (15), 2017-2025.

26. Schmidt, V.; Borsali, R.; Giacomelli, C., *Langmuir* **2009,** 25, (23), 13361-13367.

27. Ali, N.; Park, S.-Y., *Langmuir* **2008,** 24, (17), 9279-9285.

28. Khougaz, K.; Zhong, X. F.; Eisenberg, A., *Macromolecules* **1996,** 29, (11), 3937-3949.

29. Farinha, J. P. S.; Schillen, K.; Winnik, M. A., *The Journal of Physical Chemistry B* **1999,** 103, (13), 2487-2495.

30. Schillen, K.; Yekta, A.; Ni, S.; Farinha, J. P. S.; Winnik, M. A., *The Journal of Physical Chemistry B* **1999,** 103, 9090-9103.

31. Pitsikalis, M.; Siakali-Kioulafa, E.; Hadjichristidis, N., *Macromolecules* **2000,** 33, 5460-5469.

32. Imae, T.; Tabuchi, H.; Funayama, K.; Sato, A.; Nakamura, T.; Amaya, N., *Colloids and Surfaces A: Physicochemical and Engineering Aspects* **2000,** 167, 73-81.

33. Edelmann, K.; Janich, M.; Hoinkis, E.; Pyckhout-Hintzen, W.; Höring, S., *Macromolecular Chemistry and Physics* **2001,** 202, 1638-1644.

34. Fernyhough, C. M.; Pantazis, D.; Pispas, S.; Hadjichristidis, N., *European Polymer Journal* **2004,** 40, (237-244).

35. Korczagin, I.; Hempenius, M. A.; Fokkink, R. G.; Cohen-Stuart, M. A.; Al-Hussein, M.; Bomans, P. H. H.; Frederik, P. M.; Vancso, G. J., *Macromolecules* **2006,** 39, 2306-2315.

36. Schacher, F.; Walther, A.; Ruppel, M.; Drechsler, M.; Müller, A. H. E., *Macromolecules* **2009,** 42, (10), 3540-3548.

37. Lefèvre, N.; Fustin, C.-A.; Varshney, S. K.; Gohy, J.-F., *Polymer* **2007,** 48, 2306-2311.

38. Procházka, K.; Baloch, M. K., *Die Makromolekulare Chemie* **1979,** 180, (10), 2521-2523.

39. Wilson, D. J.; Riess, G., *European Polymer Journal* **1988,** 24, (7), 617-621.

40. Guo, A.; Liu, G.; Tao, J., *Macromolecules* **1996,** 29, (7), 2487-2493.

41. Yan, X.; Liu, G.; Li, H., *Langmuir* **2004,** 20, (11), 4677-4683.

42. Thurmond Ii, K. B.; Huang, H.; Clark Jr, C. G.; Kowalewski, T.; Wooley, K. L., *Colloids and Surfaces B: Biointerfaces* **1999,** 16, (1-4), 45-54.

43. Wooley, K. L., *Chemistry - A European Journal* **1997,** 3, (9), 1397-1399.

44. Ishizu, K.; Onen, A., *Journal of Polymer Science Part A: Polymer Chemistry* **1989,** 27, (11), 3721-3731.

45. Tuzar, Z.; Bedná, B.; Konák, C.; Kubín, M.; Svobodová, S.; Procházka, K., *Die Makromolekulare Chemie* **1982,** 183, (2), 399-408.

46. Ruckdäschel, H.; Sandler, J. K. W.; Altstädt, V.; Schmalz, H.; Abetz, V.; Müller, A. H. E., *Polymer* **2007,** 48, (9), 2700-2719.

47. Quirk, R.; Yoo, T.; Lee, Y.; Kim, J.; Lee, B., *Advances in Polymer Science* **2000**, 153, 67-162.

48. Auschra, C.; Stadler, R., *Polymer Bulletin* **1993,** 30, 257-264.

49. Stepanek, P., *The Journal of Chemical Physics* **1993,** 99, (9), 6384-6393.

50. Forster, S.; Zisenis, M.; Wenz, E.; Antonietti, M., *The Journal of Chemical Physics* **1996,** 104, (24), 9956-9970.

51. Burchard, W., *Advances in Polymer Science* **1983**, 143, 1-124.

52. Bucknall, C. B., *Journal of Elastomers and Plastics* **1982,** 14, (4), 204-221.

Chapter 4

Synthesis of hyperbranched block copolymers (Hyperstars) based on Polybutadiene

4.1   Introduction

Branched polymers have become a field of considerable scientific interests because of their particular properties differing from their linear analogs of similar molecular weights, in both solution and bulk. They generally present lower viscosities, are highly functionalizable and their solubility in solvents is higher where they usually behave as molecular micelles (globular structure)[1]. Hyperbranched polymers, in contrast to dendrimers, are complemented by an ease of synthesis which does not require tedious sequential step synthesis. Such simplification in synthesizing hyperbranched polymers allows them to be produced on a large scale and to be involved in application demanding significant amount of material.

Despite the numerous existing techniques to synthesize hyperbranched polymers including cationic, anionic, group transfer, controlled radical and ring-opening polymerization[2, 3], a straightforward methodology for branched polymers based on diene monomers has not been developed yet. Recently, Frey et al. demonstrated a two-step synthesis of branched polymers based on isoprene, so-called "Ugly-Stars"[4], by condensing preformed polymer segments with each other. As another alternative to classic AB_2 or A_2 + B_3 polycondensation, Fréchet et al. brought up the "self-condensing vinyl polymerization" (SCVP)[5] that later gave rise to its anionic equivalent (ASCVP) mainly investigated by Baskaran et al.[6, 7] on styrenic monomers like divinylbenzene (DVB) and 1,3-diisopropenylbenzene. The principle relies on the in-situ creation of a species bearing simultaneously an initiating site (B*) and a polymerizable group (A) so-called "inimer" (initiator-monomer) AB*. The asterisk indicates an active site.

Within our group, Nosov et al. reported a method for the synthesis of highly branched polybutadienes via anionic self-condensing vinyl copolymerization (ASCVCP) of a DVB based inimer and butadiene[8].

Herein we present a method for the synthesis of two-component highly branched polymers. The hyperbranched core is first synthesized using the method developed by Nosov et al., i.e. anionic self-condensing vinyl copolymerization (ASCVCP) of a DVB based inimer and butadiene. This reaction is followed by the subsequent anionic polymerization of a poly((meth)acrylate) corona. The resulting polymer is a hyperstar with a hyperbranched polybutadiene core protected by a poly((meth)acrylate) corona. Different isomers of DVB were used for this purpose.

4.2   Experimental part

4.2.1   Materials

Sec-butyl lithium (*sec*-BuLi) (Aldrich), dibutylmagnesium (Bu$_2$Mg), triethylaluminum (Et$_3$Al) (Aldrich), *iso*-butyl aluminum (2,6-di-tert-butyl-4-methylphenolate)$_2$ (*i*BuAl(BHT)$_2$) (0.45 mol/L in toluene, Kuraray Co. Ltd.) were used without further purification. 1,3-Butadiene (BD) (Messer Griesheim) was passed through columns filled with molecular sieves (4Å) and basic aluminum oxide and stored over Bu$_2$Mg. Methyl methacrylate (MMA), *n*-butyl (meth)acrylate (*n*-B(M)A) (BASF) were condensed from Et$_3$Al on a vacuum line and stored at liquid nitrogen temperature until use. Toluene (Merck) was distilled from CaH$_2$ and potassium. 1,2-Dimethoxyethane (DME) and *tert*-butylmethyl ether (TBME) were purified using a certain amount of *sec*-BuLi and condensed on a vacuum line.

4.2.2   Synthesis of Divinylbenzene (DVB) from its corresponding aldehyde

Para- and *meta*-DVB (*p*-DVB, *m*-DVB) were synthesized according to the literature[9] from their corresponding dialdehydes, terephtalic aldehyde and isophtalic aldehyde (Aldrich), by a Wittig olefination reaction. Typically, 0.16 mol (56 g) of triphenylmethyl phosphonium bromide, 0.2 mol (28 g) of K$_2$CO$_3$ in 120 ml of dioxane and 1.8 ml of distilled water were introduced into a round bottom flask equipped with a condenser and a magnetic stirrer. After dissolution of 0.08 mol (10.8 g) of the aldehyde in 40 ml of dioxane and 0.6 ml of

distilled water, it was successively introduced into the reaction vessel. The reaction mixture was refluxed for at least 12 hours. After reaction, the inorganic salts were first filtered off and the solvent evaporated under vacuum. The resulted product was re-heated until liquid and added in hexane under vigorous stirring. The triphenylphosphine oxide precipitated and was filtered off and washed with hexane. Hexane was then evaporated under vacuum and the resulting yellowish product subjected to flash chromatography on SiO_2 gel.

p-DVB, *m*-DVB and technical DVB (T-DVB) (Aldrich) were condensed on a vacuum line from Bu_2Mg and kept at liquid nitrogen temperature until use.

4.2.3   Anionic Self-Condensing Vinyl Copolymerization (ASCVCP) of (*p*-, *m*-, T-) DVB and butadiene (BD) yielding hyperbranched core precursor

All polymerizations were carried out under inert atmosphere in a thermostated glass reactor (Büchi, Switzerland). Typically, to 200 ml of toluene was added 0.15 mol (18.3 ml) of TBME as polar additive to control the microstructure. The reactor was cooled down to 0 °C. 3.8 mmol (2.74 ml) of *sec*-BuLi and 3.8 mmol (0.55 ml) of DVB were introduced, in this order, with a syringe into the reaction vessel and an immediate deep red color appeared, sign of the rapid formation of the inimer. 0.13 mol (10.1 ml) of butadiene were condensed from Bu_2Mg into an ampoule cooled down to -20 °C and then added to the reaction mixture. The ASCVCP of DVB and butadiene was left to proceed for 24 hours at 0 °C. The reaction was terminated with degassed methanol. The solvent was evaporated, the product dissolved in hexane and subjected to flash chromatography over SiO_2. The molecular weights and molecular weight distributions of the DVB-BD hyperbranched copolymer were measured by GPC.

4.2.4   Synthesis of (*p*-, *m*-, T-)DVB-BD-PMMA hyperstar

After the ASCVCP of DVB and butadiene (DVB-BD), an aliquot was withdrawn for characterization. A mixture of 0.11 mol (12.3 ml) DME and 0.02 mol (51.2 ml) *i*BuAl(BHT)$_2$ was introduced into the reactor to enable the subsequent polymerization of 0.1 mol (10.6 ml) methyl methacrylate (MMA), in a controllable manner at room temperature. After adding MMA, the reaction solution turned yellow. This color is characteristic of the complex formed between the aluminum compound and the (meth)acrylate monomer[10]. When the

reaction is complete, no complexes are formed anymore and the reaction medium is colorless. Thus, the end of the reaction was visually remarkable when the yellow color of the solution vanished. The reaction was terminated with degassed methanol and the reaction mixture was stirred for an hour with an aqueous solution of sulfuric acid (2 %wt) to remove the aluminum additive. The organic phase was extracted and washed with distilled water. The polymer was finally precipitated in methanol and dried under vacuum at room temperature. After dissolution in hexane, it was subjected to a silica gel column. The molecular weights and molecular weight distributions of the DVB-PB-PMMA branched block copolymers were measured using GPC.

4.2.5   Synthesis of *p*-DVB-BD-P*n*BA hyperstar

After the ASCVCP of *p*-DVB and BD, an aliquot of the polymer was withdrawn for characterization and the reactor was cooled down to -20 °C. The mixture of DME (0.11 mol, 12.3 ml) and *i*BuAl(BHT)$_2$ (0.02 mol, 51.2 ml) was added and 0.08 mol (11.1 ml) of the monomer *n*BA was introduced with a syringe drop-wisely. The reaction was terminated with degassed methanol and the reaction mixture was stirred for an hour with an aqueous solution of sulfuric acid (2 %wt). The organic phase was extracted and washed with distilled water. The polymer was finally precipitated in methanol and dried under vacuum at room temperature. After dissolution in hexane, it was subjected to a silica gel column. The molecular weights and molecular weight distributions of the *p*-DVB-PB-P*n*BA branched block copolymers were measured using GPC.

### 4.2.6   Synthesis of *p*-DVB-BD-P*n*BMA hyperstar

After the ASCVCP of *p*-DVB and BD, an aliquot of the polymer was withdrawn for characterization and a mixture of DME (0.11 mol, 12.3 ml) and *i*BuAl(BHT)$_2$ (0.02, 51.2 ml) was added. 0.07 mol (11.1 ml) of the monomer *n*BMA was introduced with an ampoule into the reactor which was warmed up to room temperature. The reaction was terminated with degassed methanol and the reaction mixture was stirred for an hour with an aqueous solution of sulfuric acid (2 %wt). The organic phase was extracted and washed with distilled water. The polymer was finally precipitated in methanol and dried under vacuum at room temperature. After dissolution in hexane, it was subjected to a silica gel column. The

molecular weights and molecular weight distributions of the *p*-DVB-PB-P*n*BMA branched block copolymers were measured using GPC.

4.3   Results and discussion

4.3.1   Anionic Self-Condensing Vinyl CoPolymerization (ASCVCP) of DVB-BD

The polymerization is depicted in Scheme 1. Three different isomers of the inimer were used: *p*-DVB, *m*-DVB and technical DVB (T-DVB), commercially available which is a mixture of *p*-DVB, *m*-DVB and 35 % of ethylstyrene. For all polymerizations, the following conditions were used: MTBE/Li = 40/1, BD/DVB = 32/1 at 0 °C for 24 hours. In the case of T-DVB, as it contains only 65 % of DVB, the ratio BD/DVB was recalculated to be 50/1.
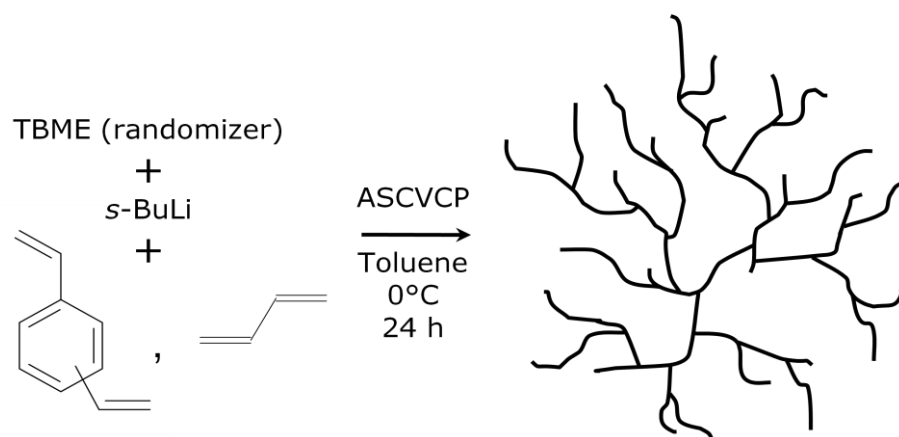
Scheme 1. Synthesis of hyperbranched DVB-BD via ASCVCP

The reactivity of DVB can be assimilated to the reactivity of styrene. It is known that in hydrocarbon solvents, the reactivity ratios of styrene and butadiene favor the formation of so-called "tapered" block copolymers. To avoid this, TBME was added as a "randomizer" so that the reactivity ratios of DVB and butadiene become closer to each other resulting in the formation of a random copolymer.

The hyperbranched samples are denoted *p*-DVB-BD, *m*-DVB-BD and T-DVB-BD according to the type of isomer used. ^{1}H NMR was measured for the three different isomers and spectra are displayed in Figure 1. For each of them, the presence of an aromatic signal at around 7 ppm, confirmed the presence of DVB in all polymers. The content of 1,4 units of PB was also calculated according to the vinyl signals at 4.9 and 5.4 ppm and was found to vary between 38 and 43% due to the presence of polar additive (TBME). Molecular weights and

molecular weight distributions are reported in Table 1. GPC using linear PB standards calibration and GPC using MALS detector were both measured.
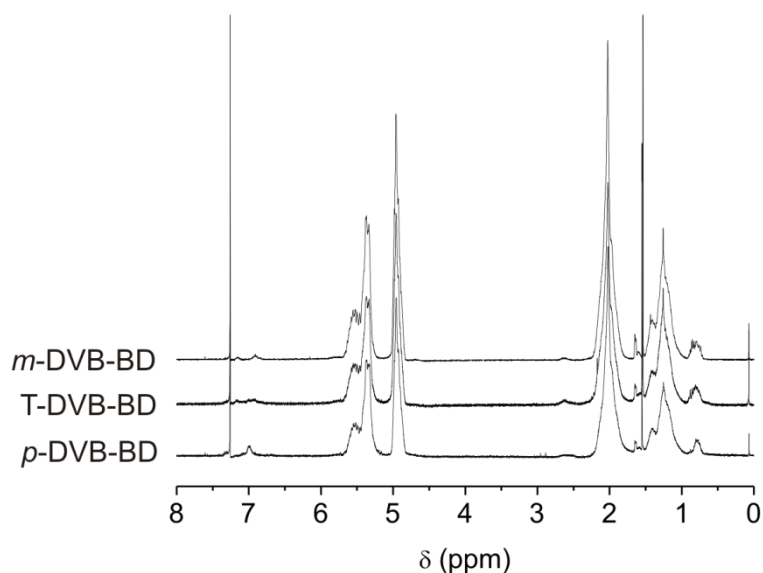

Figure 1. ^{1}H NMR spectra (300 MHz) of *p*-, *m*-, T-DVB-BD hyperbranched copolymers in CDCl$_3$.

Table 1. Molecular parameters for ASCVCP of different DVB isomers with 1,3-butadiene in toluene at 0 °C, MTBE/Li = 40, BD/DVB = 32 = γ.

	$10^{-3} M_n{}^a$ (g/mol)	PDI^a	$10^{-3} M_n{}^b$ (g/mol)	PDI^b	α^c
p-DVB-BD	5.2	3.2	8.2	3.1	0.45
m-DVB-BD	4.2	1.1	3.2	1.06	(0.33)
T-DVB-BD	5.3	1.6	4.8	1.2	0.59

^{a}GPC, PB linear standards, ^{b}GPC/MALS detection, ^{c}Mark-Houwink-Sakurada exponent, GPC/viscosity detection

The ASCVCP of BD and DVB was studied earlier in our group[8] and possible routes for the reaction were proposed (see Scheme 2). In the case of the *para*- isomer, the rate constant k_1 is significantly higher than the rate constant for the second addition, k_2. This is due to the fact that both vinyl groups are conjugated to each other. More specifically, the first addition of *sec*-BuLi induces an extensive charge delocalization stabilizing the formed carbanion and therefore, deactivates the second vinyl group. The addition of comonomer M, in our case butadiene, will favor the macroinimers mechanism as $k_{BM} > k_{BA}$. This reactivity promotes the formation of macroinimers and their subsequent self-condensation to yield hyperbranched polymers.
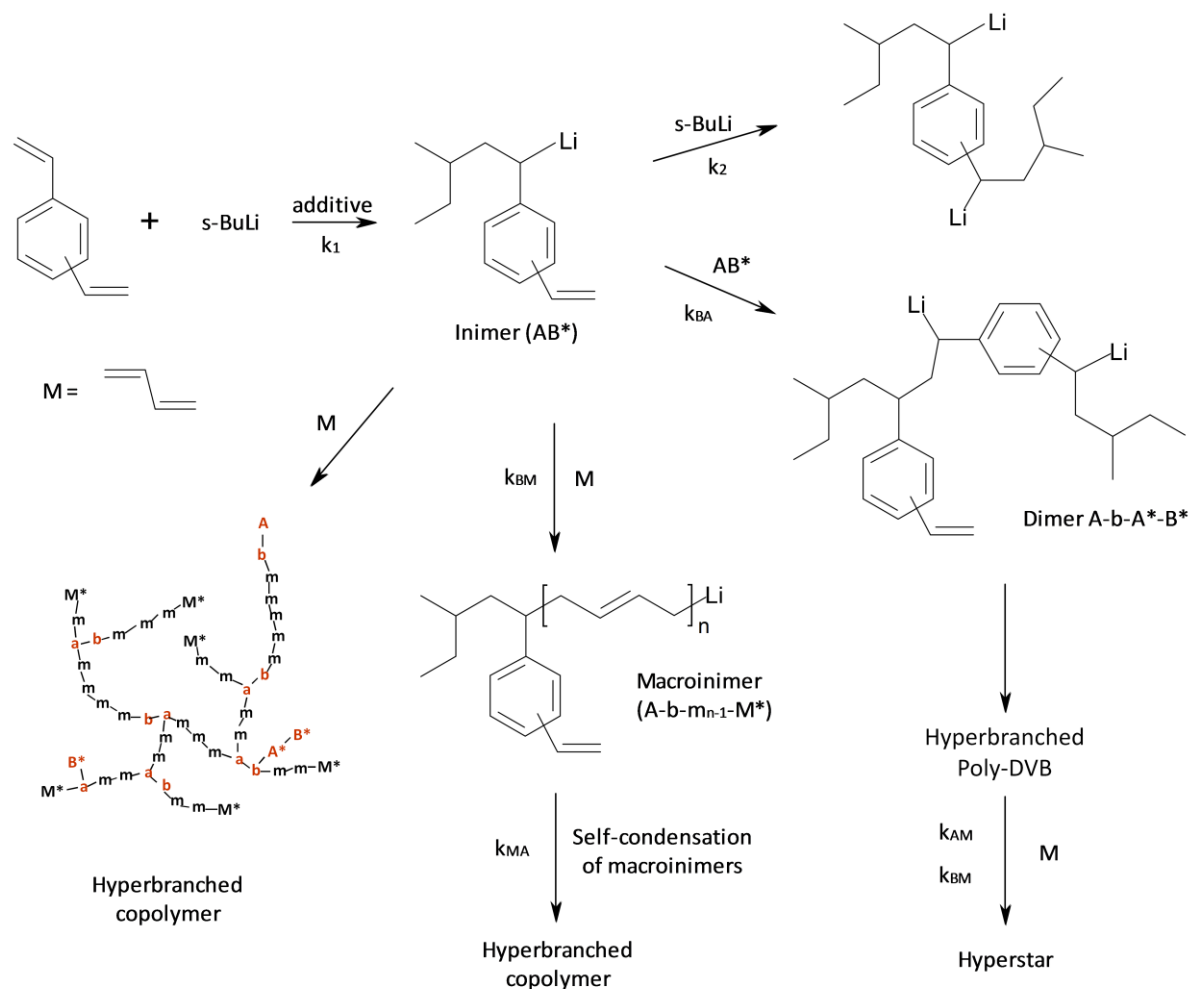
Scheme 2. Synthetic strategies towards branched polybutadienes[8]. A*, B*, M* denote active sites, a, b, m reacted ones.

The reaction of *p*-DVB and BD was followed by GPC and data are shown in Figure 2 and Table 2. In the early stage of the polymerization, macroinimers of linear polybutadiene (A-b-M*) are formed as $k_{BM} > k_{BA}$. After 12 hours of reaction, self-condensation of the macroinimers can already be assessed by the presence of a tiny shoulder at lower elution volume. As the polymerization proceeds, more shoulders are appearing at lower elution volume. The concentration of macroinimers decreases all along the polymerization as self-condensation occurs and the amount of the branched products increases. The final polymer is therefore a mixture of macroinimers and their self-condensation products in various concentrations.

More details about the mechanism of the ASCVCP of BD with *p*-DVB as well as the effect of solvent, temperature and comonomer ratios are discussed by Nosov et al.[8]
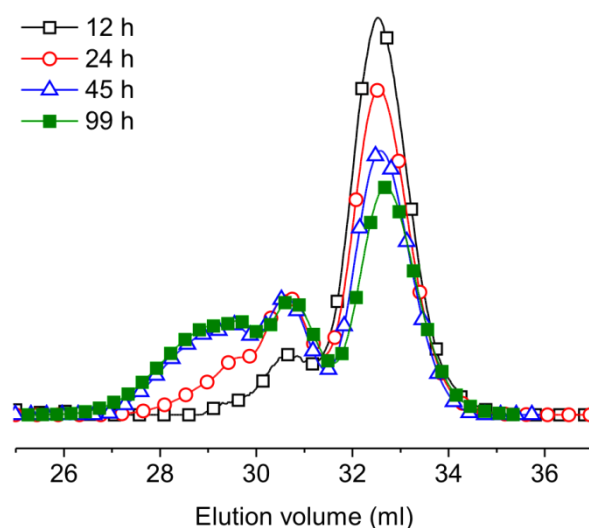
Figure 2. GPC traces (RI signal) of *p*-DVB-BD after different reaction times. PB calibration.

Table 2. Molecular parameters at various polymerization time for the ASCVCP of *p*-DVB with 1,3-butadiene in toluene at 0 °C, MTBE/Li = 40, BD/DVB = 32 = γ.

Reaction time (hours)	$10^{-3}M_n{}^a$ (g/mol)	PDI[a]
12	2.6	1.2
24	2.9	1.4
45	3.4	1.6
99	3.7	1.7

[a]GPC, PB linear standard

GPC traces are displayed in Figure 3 for *p*-DVB-BD, T-DVB-BD and *m*-DVB-BD synthesized under the same conditions. The latter exhibits a monomodal narrow molecular weight distribution, indicating that mostly linear polymers are produced. Indeed, in the case of *m*-DVB, the rate constants k_1 and k_2 are of comparable values and both vinyl groups can, therefore, add *sec*-BuLi simultaneously forming a difunctional initiator instead of an inimer. Molecular weights obtained from GPC with MALS detection confirmed this hypothesis. The theoretical length of a PB segment initiated from one site on the DVB is 32 repeating units. When calculated, one DVB unit initiated by two equivalents of *sec*-BuLi presents a theoretical molecular weight of 3700 g/mol, i.e. 64 butadiene units. GPC gives a value of 3200 g/mol which means 56 butadiene repeating units. This last result is consistent with our explanation within the experimental errors.

T-DVB is a mixture of *meta-* and *para-* isomers and some ethylstyrene. The hyperbranched copolymer T-DVB-BD shows a higher concentration in linear product than *p*-DVB-BD obtained from the para- isomer exclusively. This is probably due to the presence of ethylstyrene which cannot participate in the self-condensation reaction. The presence of *m*-DVB, as described earlier also mostly results in linear products.
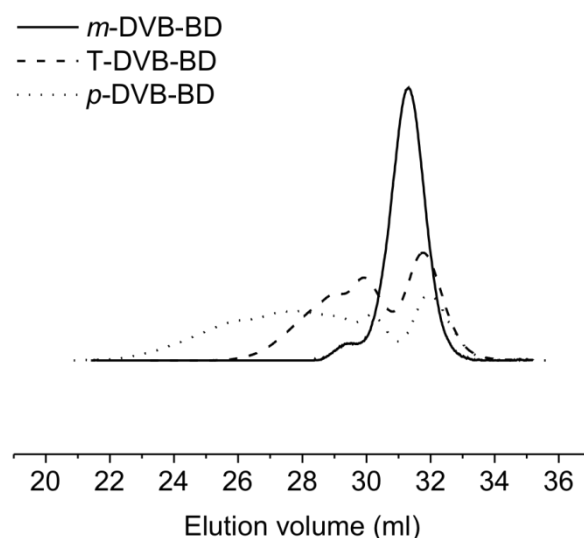

Figure 3. GPC traces (RI signal) of DVB-BD copolymers with different DVB isomers. PB calibration (see Table 1).

When comparing molecular weights of the different hyperbranched products synthesized under the same conditions, *p*-DVB-BD reaches higher molecular weights than T-DVB-BD and *m*-DVB-BD. This can be related to the different mechanisms described earlier. In the case of the copolymerization with *p*-DVB, self-condensation occurs to yield hyperbranched polymers while *m*-DVB produces linear PB which does not seem to self-condense later on. T-DVB-BD can be described as a mixture of these two plus a certain amount of linear PB initiated from ethylstyrene. Therefore, its molecular weight is lower than that of *p*-DVB-BD but higher than that of *m*-DVB-BD.

The difference observed in the case of *p*-DVB-BD where molecular weights measured in GPC are lower than those measured in GPC/MALS also confirms that most of the polymer is branched. Indeed, branched polymers exhibit smaller hydrodynamic volume than their linear analogues and therefore lead to lower apparent molecular weights values. Mark-Houwink-Sakurada (MHS) parameters were also measured with GPC/viscocity. For the *p*- and T- isomers, α values, displayed in Table 1, are 0.45 and 0.59 respectively which is lower

than 0.74, the value for linear PB. This observation confirms further, the dense topology of the different polymers and therefore their branched structures. In Figure 4, Mark-Houwink-Sakurada plots are established for linear PB and hyperbranched *p*-DVB-BD. The contraction factors g' = [η_{br}]/[η_{lin}] were calculated from the plots and show that the density of the hyperbranched polymer increases with molecular weight (solid line in Figure 4). The extremely low α value obtained for *m*-DVB-BD (α = 0.33) is not reliable due to the very narrow distribution of the polymer.
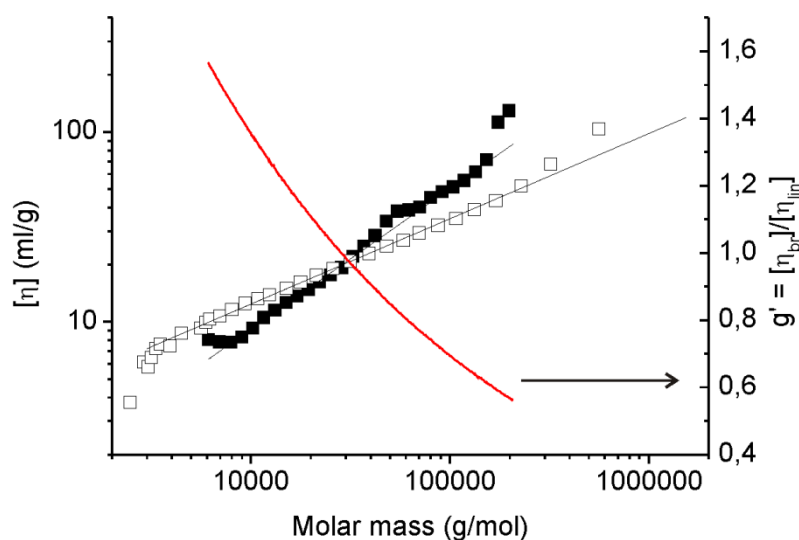

Figure 4. Mark-Houwink-Sakurada plots for linear PB (■) and *p*-DVB-BD (□), contraction factors g' of *p*-DVB-BD (solid line).

According to previous studies carried out by Nosov et al., higher molecular weights of the hyperbranched polymers can be obtained when increasing the comonomer ratio, γ, or the amount of polar additives (randomizer). Taking the exemple of *p*-DVB-BD, increasing the comonomer ratio strictly means increasing the amount of BD introduced into the reaction. Therefore, macroinimers increase in molecular weight and through self-condensation the overall molecular weight of the hyperbranched copolymer is also increased. When the amount of polar additive is increased, the formation of macroinimers will, in the first place, occur faster and yield a high content of 1,2-PB microstructure. More importantly, increasing the amount of randomizer should result in k_{BM} ~ k_{BA}. Thus, DVB is distributed more randomly over the PB macroinimers increasing the number of potential branching points subsequently leading to higher molecular weights of the final hyperbranched polymer. At the same time, TBME facilitates the access to styrenyl anions and therefore promote self-

condensation. GPC traces for *p*-DVB-BD synthesized with a high comonomer ratio, typically γ = 32, and two different TBME/Li ratios are shown in Figure 5 and data are summarized in Table 3. Higher molecular weights are reached with TBME/Li = 40, the concentration in branched products is higher.
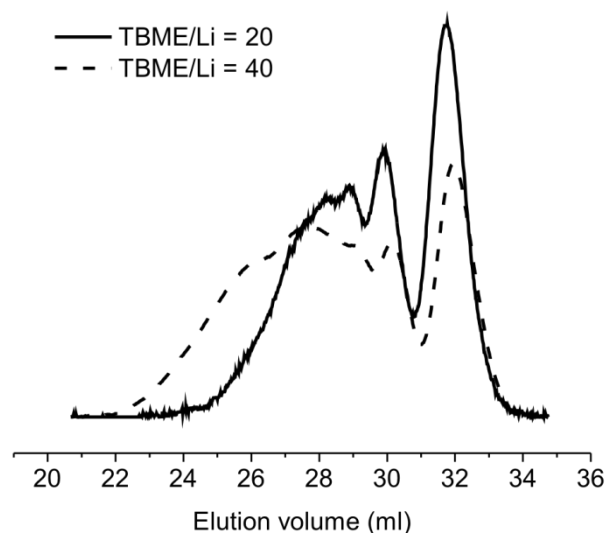

Figure 5. GPC traces RI signal) of *p*-DVB-BD with different TBME/Li ratios. PB calibration.

However, further increase in molecular weights is prevented by the intramolecular reaction occurring between B* (or M*) and A. This back-biting reaction consumes potential self-condensing sites limiting the degree of branching and subsequently the final molecular weight.

Table 3. Molecular parameters for *p*-DVB-BD hyperbranched copolymers synthesized with various TBME/Li ratios

TBME/Li	$10^{-3}M_n{}^a$ (g/mol)	PDI^a
20	2.7	1.5
40	7.3	3.1

^{a}GPC, PB linear standards

For this reason, another approach to increase the total molecular weight was elaborated. Additional DVB and butadiene were introduced to the reaction medium after 24 hours of reaction. In this way, the consumption of A sites due to back-biting reactions is compensated by the introduction of new DVB and back-biting reactions are themselves lowered. GPC traces are shown in Figure 6 and data are summarized in Table 4. In Figure 6, a

clear shift of the molecular weights distribution towards higher molar masses can be observed. This addition permits the introduction of more potential self-condensing sites but does not seem to increase in a significant way the amount of branched products.
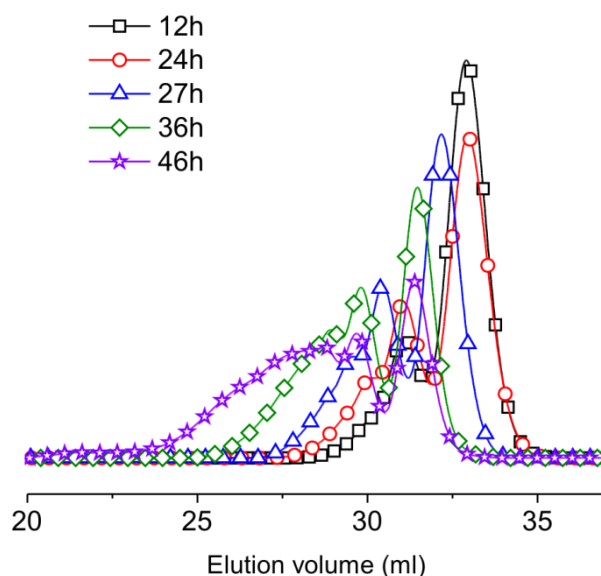

Figure 6. GPC traces (RI signal) over the course of the ASCVCP of butadiene and *p*-DVB, γ = 32, TBME/Li = 40. After 24 h, 0.3 ml of *p*-DVB and 3 ml of butadiene are added. At 27 h, i.e. 3 hours after the addition, molar masses shift to higher values. PB calibration.

Table 4. Molecular parameters for *p*-DVB-BD at various reaction times. After 24 hours, 0.3 ml of *p*-DVB and 3 ml of butadiene are added.

t (hours)	$10^{-3}M_n{}^a$ (g/mol)	$10^{-3}M_{peak}{}^a$ (g/mol)	PDI[a]
12	2.4	2.2	1.2
18	2.6	2.2	1.3
24	2.7	2.2	1.4
27	3.9	3.0	1.4
36	6.1	4.0	1.5
46	8.4	4.2	2.3

[a]GPC, PB linear standards

Another polymerization was carried out with additional DVB being introduced after 12 hours reaction time. For this experiment no additional butadiene was introduced. The data are summarized in Figure 7 and Table 5. The GPC trace obtained 13 hours after the addition of 0.1 ml of DVB (-□- in Figure 7) exhibits no significant shift towards higher molecular weights but is greatly broadened through an additional peak at lower elution volume. This

peak is related to the amount of branched products present in the polymer and is constantly increasing. At 64 hours reaction time (-Δ- in Figure 7), it becomes the predominant species with an apparent molecular weight of 13,500 g/mol.
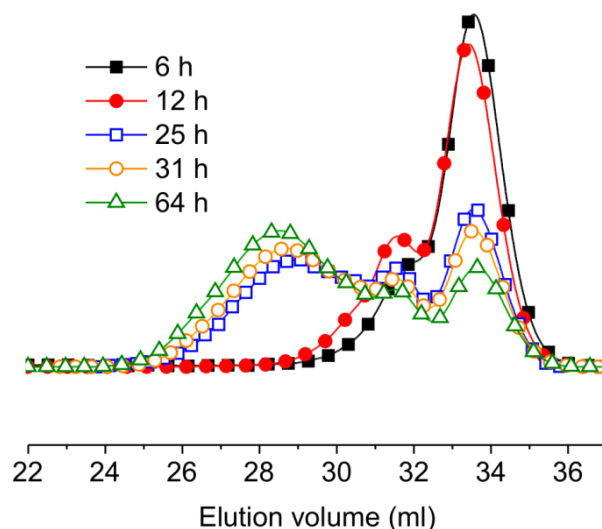

Figure 7. GPC traces (RI signal) over the course of the ASCVCP of butadiene and *p*-DVB, γ = 32, TBME/Li = 40. After 12 h, 0.1 ml of *p*-DVB are added. At 25 h, i.e. 13 hours after the addition, the amount of branched products is significantly increased. PB calibration.

Table 5. Molecular parameters for *p*-DVB-BD at various reaction times. After 12 hours, 0.1 ml of *p*-DVB are added.

t (hours)	$10^{-3}M_n{}^a$ (g/mol)	$10^{-3}M_{peak}{}^a$ (g/mol)	PDI[a]
6	1.8	1.7	1.3
12	2.0	1.8	1.3
25	3.2	1.7	2.6
31	3.5	1.7	2.7
64	4.2	13.5	2.7

[a]GPC, PB linear standards

In Figure 8, the GPC curve of *p*-DVB-BD obtained after 99 h reaction time is shown (solid line). Its M_{peak} lies at around 2500 g/mol. The same reaction after only 46 h with addition of 0.3 ml of *p*-DVB and about 3 ml of BD at t = 24 h, is seen strongly shifting towards higher molar masses (dashed line) but shows similar shape. The predominant product is the linear product with M_{peak} = 4200 g/mol. When *p*-DVB only is added to the reaction medium at t = 12 h, the GPC trace measured after 55 h reaction time (dotted line) is not much more shifted than previously but presents a completely different shape where its M_{peak} is now at

13,500 g/mol. The concentration in hyperbranched products seems to be significantly increased by the introduction of *p*-DVB during the polymerization which also increases the overall molecular weight.
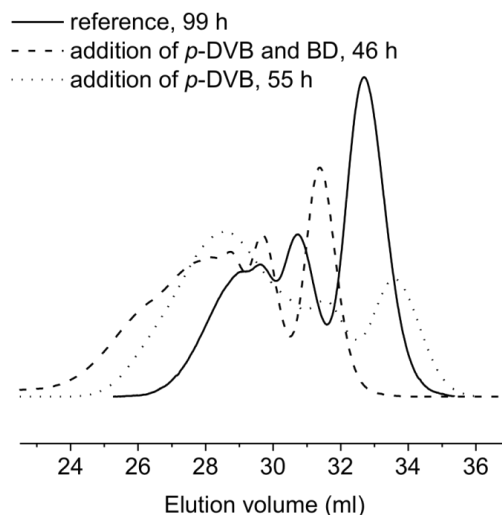

Figure 8. THF-GPC traces (RI signal) of *p*-DVB-BD after 99 h (solid line), after 46 h of reaction and addition of *p*-DVB and BD at t = 24 h (dashed line), after 55 h of reaction and addition of *p*-DVB at t = 12 h (dotted line). PB calibration.

4.3.2   Synthesis of hyperstars

The synthesis is described in Scheme 3. After the ASCVCP of DVB and BD, a mixture of DME and an aluminum compound is added to enable the polymerization of (meth)acrylate monomer in a controllable manner without the help of an end-capping agent. The resulting hyperstar consists of a hyperbranched core of DVB-BD copolymer and poly(meth)acrylates arms. The amount of (meth)acrylate monomers was adjusted in order to maintain 40 %wt of butadiene within the hyperstar (see Table 6). Polymerization of the methacrylate block proceeds faster than in the case of a linear polybutadiene-*b*-poly(methyl methacrylate) block copolymer. This phenomenon is clearly visible by the disappearance of the yellow color of the reaction medium[10]. In the case of linear block copolymer (Chapter 3), the yellow color persisted several hours while, for the hyperstar polymers, the yellow color vanished within one or two hours. Such a rapid reaction might be explained by the higher number of initiating sites but also by the presence of TBME. Added as a randomizer for the synthesis of the hyperbranched DVB-BD core, TBME can also act as a Lewis base additionally to DME and therefore increase the kinetics of reaction. Molecular parameters are listed in Table 6.

Neglecting the presence of DVB, compositions were calculated from the molar fraction determined by ^{1}H NMR.
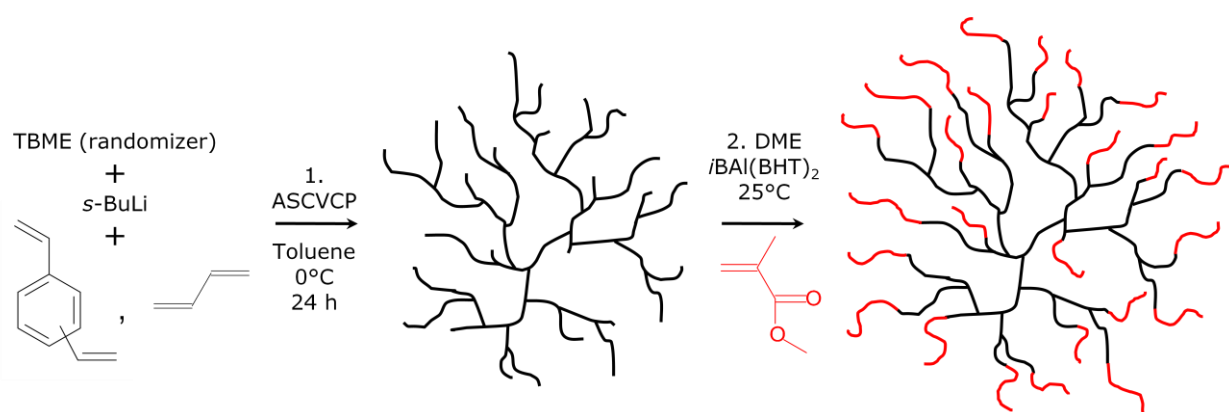
Scheme 3. Synthesis of DVB-BD-PMMA hyperstars via 1. ASCVCP of DVB and BD and 2. anionic polymerization of methyl methacrylate monomer.
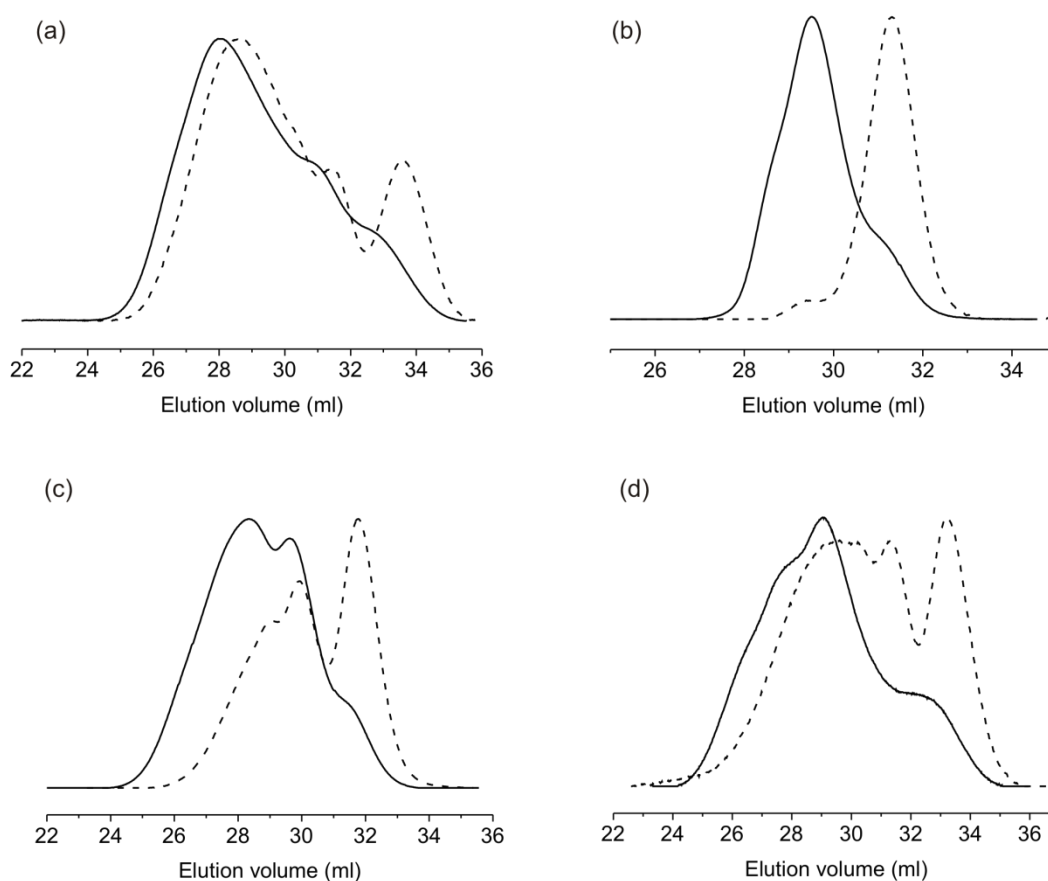

Figure 9. GPC traces (RI signal) for (a) *p*-DVB-BD-PMMA, (b) *m*-DVB-BD-PMMA, (c) T-DVB-BD-PMMA, (d) *p*-DVB-BD-P*n*BMA (solid lines) and their corresponding DVB-BD hyperbranched precursor (dashed line).

From hyperbranched polymers to hyperstars, molar mass distributions are shifted to higher molecular weights and can be observed in the GPC traces shown in Figure 9. The

successful initiation and introduction of the respective (meth)acrylate blocks are also assessed by ^{1}H NMR after purification of the hyperstars. In Figure 10, the example of *p*-DVB-BD-PMMA is shown where a peak appears at 3.58 ppm for PMMA (-OC$\underline{H}_3$). Additionally, signals related to the α-methyl protons of PMMA appear at 0.85 and 1.02 ppm corresponding to rr and rm triads respectively. The PMMA arms are predominantly syndiotactic, similar to polymers obtained in THF. For *p*-DVB-BD-P*n*BMA and *p*-DVB-DB-P*n*BA, characteristic peaks at 3.94 ppm and 4.04 ppm (-OC$\underline{H}_2$(CH$_2$)$_2$CH$_3$) respectively are also detected.

Table 6. Molecular parameters for the hyperstar polymers prepared by ASCVCP of DVB with BD and subsequent anionic polymerization of different (meth)acrylate monomers.

	10^{-3} M_n[a] (g/mol)	PDI[a]	10^{-3} M_n[b] (g/mol)	10^{-3} M_{peak}[b] (g/mol)	PDI[b]	%wt PB[c]	α[d]
m- DVB-BD	4.2	1.1	3.2	3.3	1.06	--	(0.33)
m-DVB-BD-PMMA	7.8	1.1	13.0	13.0	1.06	41	(0.59)
T-DVB-BD	5.3	1.6	4.8	3.4	1.2	--	0.59
T-DVB-BD-PMMA	9.8	1.6	15.4	21.6	1.7	46	0.45
p-DVB-BD	4.7	2.3	3.7	2.4	1.7	--	0.54
p-DVB-BD-PMMA	7.0	2.0	15.0	27.3	1.8	44	0.46
p-DVB-BD	3.8	2.1	3.2	2.0	1.5	--	0.43
p-DVB-BD-P*n*BMA	6.8	2.1	20.6	17.7	1.6	41	0.43
p-DVB-BD	5.2	3.2	8.2	21.2	3.1	--	0.45
p-DVB-BD-P*n*BA	10.4	3.1	19.2	40.7	3.4	42	0.42

[a] GPC, linear PB calibration, [b] GPC/MALS, [c] ^{1}H NMR, [d] MHS exponent, GPC/viscosity

Intrinsic viscosity and Mark-Houwink-Sakurada (MHS) parameters were measured and results are reported in Table 6 and Figure 11. All hyperstars exhibit low α values ranging from 0.42 to 0.46. These values are significantly lower than typical α values for linear polymer which are usually around 0.6-0.8 and, therefore, confirm the branched topology of those hyperstar polymers. As mentioned earlier, the case of *m*-DVB-BD-PMMA for which α = 0.59 has to be handled with care due to the very narrow distribution of the polymer. The assumption made previously, that the *meta*- isomer may lead to linear products is further reinforced.
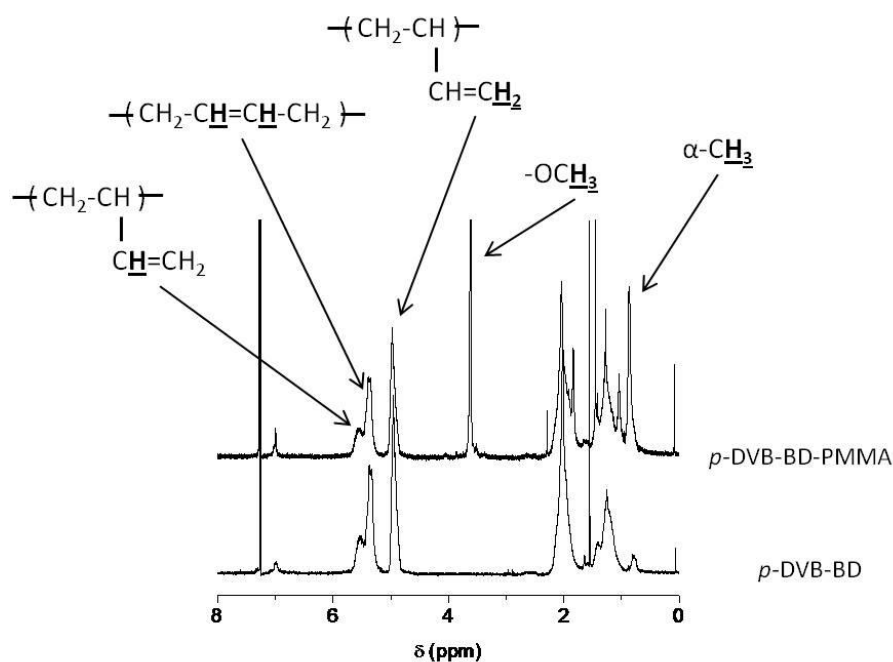
Figure 10. ^{1}H NMR spectra (300MHz) in CDCl$_3$ of the DVB-BD precursor and its corresponding DVB-BD-PMMA hyperstar, γ = 32.
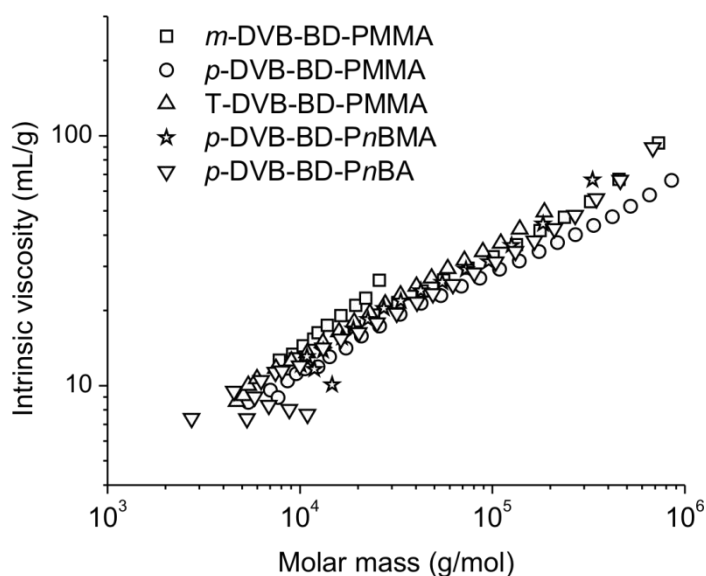
Figure 11. Mark-Houwink-Sakurada plots for the different hyperstars.

4.4   Conclusion

The synthesis of hyperbranched PB polymers was successfully performed following the procedure developed by Nosov et al. For all isomers of the inimer used, MHS parameters confirmed the branched topology of the polymers except when *m*-DVB was used. The introduction of additional DVB during the course of the polymerization seems to be an

efficient method to increase the molecular weight of the hyperbranched polymer and more precisely to increase the concentration of branched product in the final polymer. The subsequent polymerization of a (meth)acrylate block from the hyperbranched PB was also successfully achieved and low α values still confirmed the branched topology of the obtained hyperstars.

References

1.   Burchard, W., *Advances in Polymer Science* **1999,** 143, 113-194.

2.   Mori, H.; Müller, A. H. E., *Progress in Polymer Science* **2003,** 28, (10), 1403-1439.

3.   Mori, H.; Müller, A. H. E.; Simon, P. F. W., In *Macromolecular Engineering*, Wiley-VCH: 2007; Vol. 2, pp 973-1005.

4.   López-Villanueva, F.J.; Wurm, F.; Kilbinger, A. F. M.; Frey, H., *Macromolecular Rapid Communications* **2007,** 28, (6), 704-709.

5.   Fréchet, J. M. J.; Henmi, M.; Gitsov, I.; Aoshima, S.; Leduc, M. R.; Grubbs, R. B., *Science* **1995,** 269, (5227), 1080-1083.

6.   Baskaran, D., *Macromolecular Chemistry and Physics* **2001,** 202, (9), 1569-1575.

7.   Baskaran, D., *Polymer* **2003,** 44, (8), 2213-2220.

8.   Nosov, S.; Schmalz, H.; Müller, A. H. E., **in preparation**.

9.   Bigot, Y. L.; Delmas, M.; Gaset, A., *Synthetic Communications* **1983,** 13, (2), 177 - 182.

10.   Schlaad, H.; Schmitt, B.; Müller, A. H. E., *Angewandte Chemie International Edition* **1998,** 37, (10), 1389-1391.

Chapter 5

Incorporation of nanomodifiers in a two-component polyurethane (2K PUR) system for automotive clearcoats

5.1   Introduction

The modification of plastics (thermoplastics, thermosets, elastomers…) is a common way to create new materials with improved properties. The improvement of toughness or impact resistance in thermoplastics and thermosets, for example, was achieved by different methods which all included the introduction of a rubber phase as toughening agent[1]. For polymers traditionally modified with micron-sized rubbery inclusions to expand their toughness over a broad range of temperature, famous examples, like High Impact Polystyrene (HIPS)[2] or Polycarbonate/Acrylonitrile-Butadiene-Styrene (PC/ABS)[3, 4], can be cited. However, the introduction of such rubbery inclusions usually involves a change in the refractive index which results in opaque systems. Therefore, for specific applications where the major challenge is to retain the transparency while reaching such high impact resistance, this approach has to be optimized. For this, two ways are possible. Either one has to design the inclusions so that their refractive index matches that of the matrix or one has to be careful that the inclusions do not exceed a certain size, typically the wavelength of the visible light. In this case, inclusions below 100 nm size are recommended.

Experiments have demonstrated that the particles size plays a major role in toughening as for a given volume fraction of rubber particles, the smaller the particles the higher the toughness achieved in the composite[5]. The necessary loading of nanoparticles is usually lower than for their microfiller counterparts which is an non-negligible advantage, industrially and economically speaking. After nanomodification, the transparency of the unmodified polymer is preserved as well as its light weight and good processability is also provided.

In the domain of thermoset polymers, block copolymers have been extensively used for this purpose[6-9]. In the ideal case, if the block copolymer is wisely chosen (chemical nature, composition…) and introduced in a sufficient amount, self-assembly occurs within the polymer blend and nano-size domains such as micelles are formed which further improve mechanical properties. Like in solution, the shape and size of the inclusions formed in a polymer matrix by block copolymers are variable and sensitive to many parameters (solubility in the matrix, temperature, concentration). Therefore, macrophase separation can also occur leading to micron-size domains and therefore no optimal mechanical improvement can be reached and transparency of the material is lost. The introduction of already size-defined and stabilized nanoparticles, such as cross-linked micelles, would hinder such a risk provided they disperse well.

Here, we apply these concepts of toughness to PU coatings. Two types of nanomodifiers are tested: nanoparticles obtained by cross-linking of core-shell micelles (presented in Chapter 3) and hyperstar polymers consisting of a hyperbranched rubber core and a protective (meth)acrylate shell (presented in Chapter 4). Their miscibility and dispersibility into the coating before and after curing reaction are detailed by TEM. Furthermore, their influence on impact resistance, hardness, adhesion and chemical resistance of the obtained nanocomposite coatings are also investigated at different modification rate into the coating.

5.2   Experimental part

5.2.1   Materials

A typical 2K PUR formulation for automotive clearcoats is shown in Table 1. Desmophen® A870 (Bayer AG) is a hydroxyl functional polyacrylate polymer based on *n*-butyl acrylate, 2-hydroxyethyl acrylate and possesses some units of styrene. Desmodur® N3300 and Desmodur® Z4470 (Bayer AG) are both aliphatic oligoisocyanate. The first is made of hexamethylene diisocyanate (HDI) trimers and the second consists of isophorone diisocyanate (IPDI) trimers.

Table 1. Solventborne 2K PUR clear coating formulation

1. Polyol	Desmophen® A870	100.0 g	
2. Leveling agent	Baysilone® OL 17 (10 % in MPA)	1.0 g	
3. Anti-foamer	BYK 070	1.0 g	"Component 1"
4. Catalyst	Dibutyltin dilaurate (DBTL) (1 % in butyl acetate)	1.0 g	
5. Nanoparticles	10 % in butyl acetate	20.7 g	
6. Polyisocyanate	Desmodur® N3300 or Z4470	33.4 g	"Component 2"

Two different types of nanomodifiers are tested:

1. TYPE A: Nanoparticles based on self-assembly of block copolymers (preparation described in Chapter 3).

2. TYPE B: Hyperstars (preparation described in Chapter 4)

The exact nature of the nanomodifiers tested is described in Table 2. B-M-H refers to nanoparticles carrying hydroxyl functions on their surface.

Table 2. List of the different nanomodifiers tested.

Cross-linked micelles (Type A)	Hyperstars (Type B)
B-M	*p*-DVB-BD-PMMA
B-*n*BMA	T-DVB-BD-PMMA
B-M-H	*p*-DVB-BD-P*n*BMA
--	*p*-DVB-BD-P*n*BA

5.2.2   Preparation of the lacquer and tests substrates

We will refer to the compounds of the coating formulation according to the numbered list in Table 1. To polyol 1 are added the compounds 2, 3 and 4 subsequently in this order. The nanomodifiers 5 are added at last as a 10 %wt solution in butyl acetate. Additional solvent (2-methoxypropyl acetate, MPA) is introduced in order to adjust the viscosity of the mixture ("component 1") for an optimal application later on. "Component 1" is stored over night at room temperature. The following day, after making sure that neither sedimentation nor flocculation occurred, the hardener ("component 2") is added to "component 1". The

final mixture is shaken and immediately applied. The application is made by manual spray gun on different supports:

        -Support 1: steel panel ST 1405 (DC 04B) or ST 1203 (DC 01A)

        -Support 2: aluminum coated with a cationic lacquer

        -Support 3: OEM panels with black basecoat

        -Support 4: glass

The panels were all dried at room temperature for 30 minutes, then at 140 °C for 25 minutes and finally at 60 °C for 16 hours.

The final film thicknesses were measured to be between 39 and 45 µm.

All the nanomodifiers were introduced as a dilute solution in butyl acetate and typical modification contents were 1, 2, 5 or 10 %wt of the solid content of the formulation.

5.2.3   Tests

For more details about the different tests performed on the coatings, see Chapter 2 – Methods.

On Support 1, formulations using the system A870/Z4470 were applied and the following tests were carried out:

    - Multi-impact

    - Single-impact

    - Ball shot

    - Cross-cut adhesion

    - Hardness

On Support 2, formulations using the system A870/N3300 were applied and the following tests were carried out:

    - Scratch resistance (steel wool and Scotch Brite ®)

    - Chemical resistance

On Support 3, formulations using the system A870/N3300 were applied and the following tests were carried out:

    - Scratch resistance (car-wash)

    - Scratch resistance (steel wool and polishing paper)

- Gradient-oven

On Support 4, formulations using the system A870/N3300 were applied and the following
tests were carried out:

- Pendulum hardness

- Micro-hardness

- Gloss/Haze

5.3   Results and discussion

5.3.1   Miscibility and dispersibility of the nanomodifiers

To be efficient as a nanomodifier and to increase the chances to maintain the
transparency of the coating, our particles have to be correctly dispersed into the matrix.
Dispersing nanoparticles to obtain a nanocomposite material is a challenging issue,
especially when the matrix has a different chemical structure than the nanoparticles. For
example, the introduction of polar nanoparticles into a non polar matrix will lead to poor
dispersion because of the weak interaction of the particles with the matrix[10]. However,
according to Mackay et al.[11], such dispersion should be possible if the size of the
nanoparticles does not exceed the radius of gyration of the polymer matrix. But usually, in
the absence of any kind of stabilizer, the surface energy of the dispersed nanoparticles will
be so high that it will favor the formation of larger aggregates[12, 13]. To improve dispersion,
efforts have been put into experimental procedures to obtain nanocomposites like multi-
mixing[14] or in-situ polymerization[15, 16]. Depending on the method used for a same
composite, properties found were differing. The chemical modification of the surface of the
nanoparticles turned out to be another efficient way to improve their dispersion by
increasing their interfacial interaction with the matrix[17].

In our case, Desmophen A870 is a hydroxyl functional polyacrylate polymer based on *n*-
butyl acrylate, 2-hydroxyethyl acrylate and which also possesses some units of styrene. This
polyol is the major component of the coating formulation which is why we based our
miscibility tests on it. It is provided as a 70 %wt solution in butyl acetate and exhibits the
consistency of a resin. Poly(meth)acrylates were synthesized as coronas for the
nanoparticles because of their miscibility with Desmophan A870. However, preliminary tests

were performed in order to verify the solubility of the nanoparticles in butyl acetate which is the solvent used in the coating formulation. All nanomodifiers of type A and type B were soluble in butyl acetate. To further decrease the chances of aggregation of the nanomodifiers and facilitate their dispersion, it was decided to solubilize the particles in butyl acetate prior to introducing them into the formulation.

5.3.1.1 Nanoparticles based on self-assembly of block copolymers (Type A)

A schematic representation of the nanoparticles type A is shown in Figure 1. These nanoparticles were added to the polyol as a dilute solution in butyl acetate. Even after few months no flocculation or sedimentation seemed to occur in "component 1". The characterization by dynamic light scattering (DLS) of the mixture polyol + nanomodifiers indicated the presence of narrow dispersed nanoparticles with radii similar to those of the original micelles in selective solvent, with no angular dependence (see Figure 2). No larger aggregates were detected giving a hint that the nanomodifiers were well dispersed and free of aggregation.
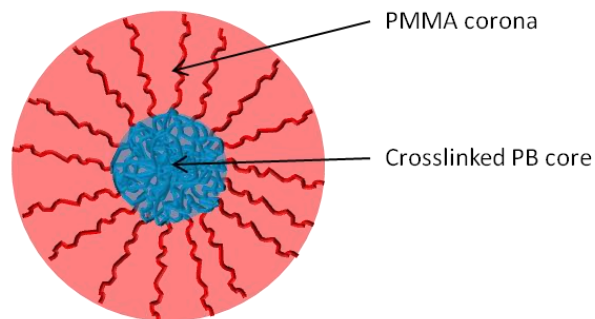

Figure 1. Schematic representation of nanoparticles type A. Here, the example of a B-M nanoparticle.

TEM images taken from the final modified coating (after curing reaction of the polyol with its cross-linker) are shown on Figure 3. The TEM measurements are made on a 10 %wt modified coating for ease in localizing the nanoparticles. It can clearly be seen that the nanoparticles are properly dispersed and do not form big aggregates even at 10 %wt modification. As a counter example, on Figure 4, the same nanoparticles are dispersed in a PS matrix (M_n = 1.6*10^6 g/mol) at 5 %wt. PS exhibit a completely different chemical structure than the corona of our nanoparticles (here PMMA) and therefore dispersion should not be favored. Indeed, aggregates as large as 500 nm in diameter are observed. Single nanoparticles can also be identified within the aggregates. This observation

demonstrates the importance of the compatibility of the corona of the nanoparticles with the matrix for an optimal dispersion.
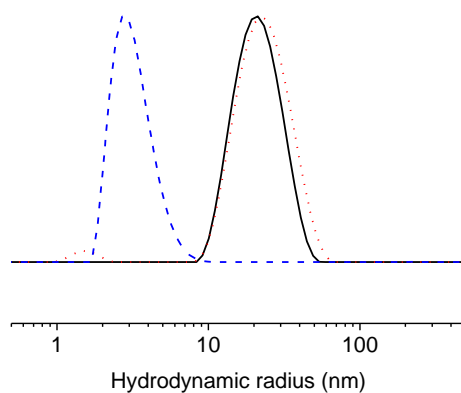
Figure 2. CONTIN plots at 90° for B-M nanoparticles in Desmophan A870/butyl acetate (solid line, intensity-weighted), B-M block copolymer in acetone forming micelles (dotted line, intensity-weighted) and B-M block copolymer in Desmophan A870/butyl acetate (dashed line, mass-weighted).

Figure 3. TEM images of B-M nanoparticles in PU coating film (A870/Z4470) stained with OsO₄.
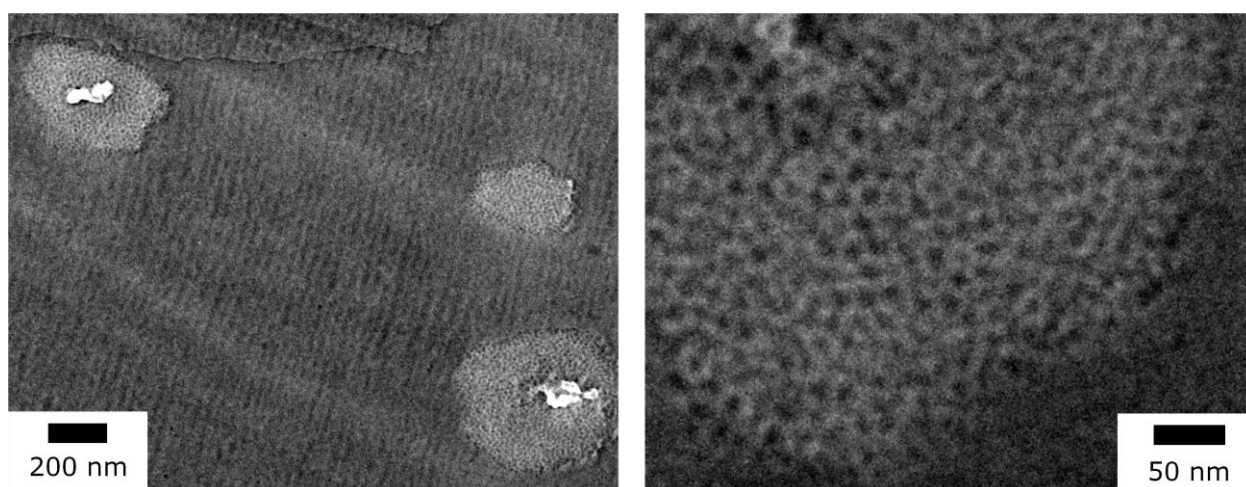
Figure 4. TEM images of B-M nanoparticles in PS matrix stained with OsO₄.

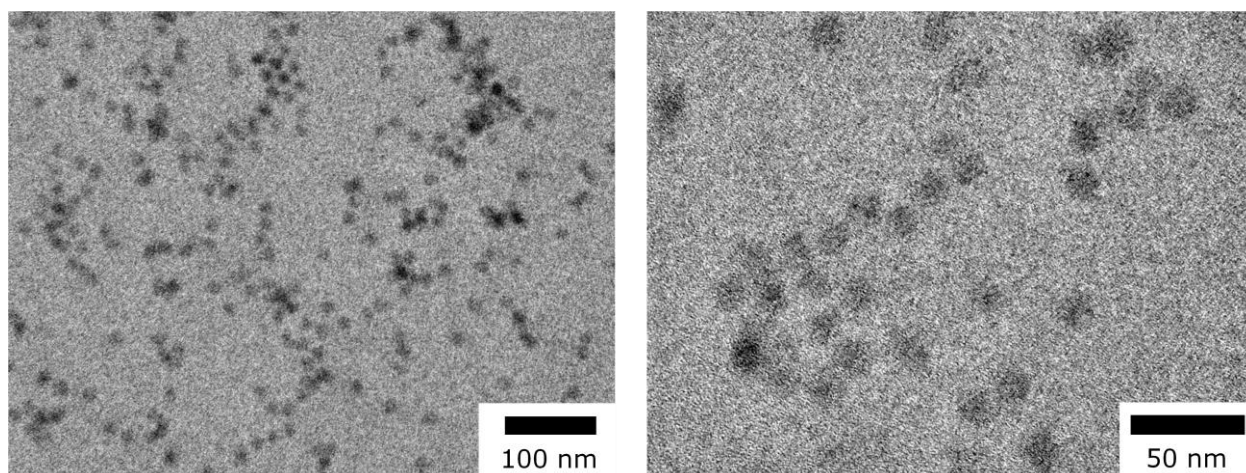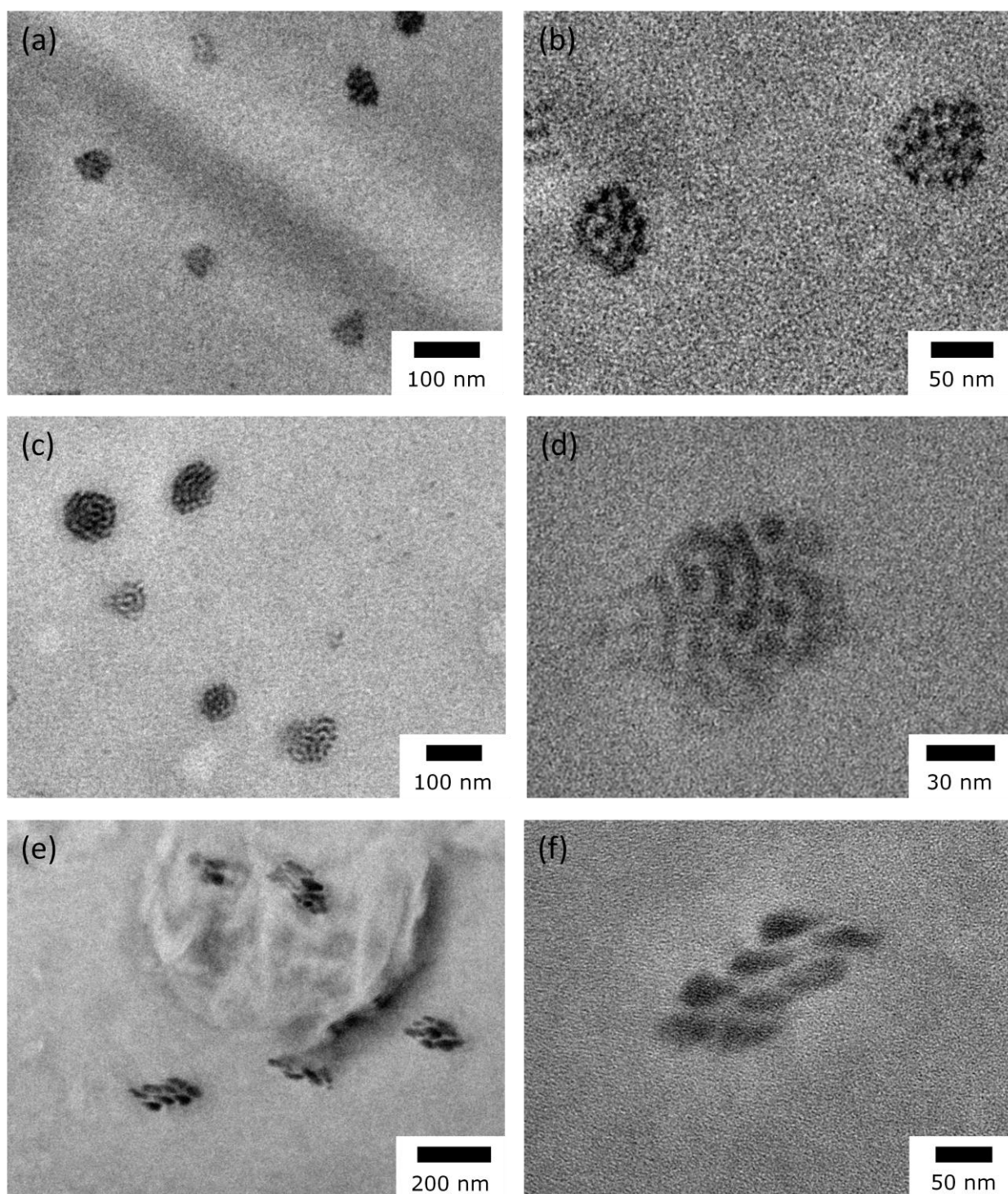**Figure 5. TEM images of PU coating (A870/N3300) modified with 2 %wt of block copolymers (a), (b) $B_{41}M_{152}{}^{17}$, (c), (d) $B_{68}M_{100}{}^{14}$ and (e), (f) $B_{540}M_{452}{}^{75}$ (stained with OsO_4 after curing reaction).**

Non-cross-linked block copolymers could also be introduced into the polyol resin and dispersed without any problem. Neither micelles nor vesicles were detected through DLS measurements. The block copolymers seemed to be dispersed as unimers (dashed line in Figure 2). However, after reaction of the resin with the oligoisocyanate cross-linker, TEM images taken suggest the formation of well-dispersed structures (Figure 5). In the case of

$B_{41}M_{152}$[17] (Figure 5a, b), which possesses the longest PMMA block, aggregates formed are 50 nm in diameter and seem to be composed of single micelles. The (dark) core of the single micelles is measured to be 8 to 9 nm. For $B_{68}M_{100}$[14] (Figure 5c,d), the presence of spherical and worm-like objects is seen within the formed aggregates. The aggregates are between 50 and 100 nm in diameter and the domains of PB within those aggregates are measured to be around 10 nm thick. For the high molecular weight polymer $B_{540}M_{452}$[75] (Figure 5e, f), the distribution of the aggregates obtained is not as uniform as for the two previous coatings. However, one can distinguish within these aggregates smaller PB domains with sizes varying between 20 and 35 nm.

When the polyol resin reacts with the cross-linker, changes in miscibility of the block copolymer with the formulation seem to occur leading to specific phase separation between the block copolymer and the coating.

The cross-linking of self-assembled block copolymer micelles, obtained in a selective solvent, prior to the introduction in the coating, prevents such discrepancies and allows us to keep perfectly monodisperse spherical particles with sizes not bigger than 50 nm in diameter all along the curing process.

To summarize, the nanoparticles of type A, based on block copolymer self-assembly, are well dispersed in the coating system of our interest. Flocculation and sedimentation are not observed in the polyol, even after months of storage. The dispersion appears to be very stable. After reaction of the polyol with its hardener, the nanoparticles are still well-dispersed and free of aggregation in the final coating film. The neat B-M block copolymer does not undergo self-assembly in the polyol and leads to large aggregates after curing reaction.

5.3.1.2 Nanoparticles Type B

Hyperstar nanoparticles are introduced without further cross-linking reaction of the polymer. The synthesis method of these nanomodifiers already provides them with a "core-shell" architecture as depicted in Figure 6.
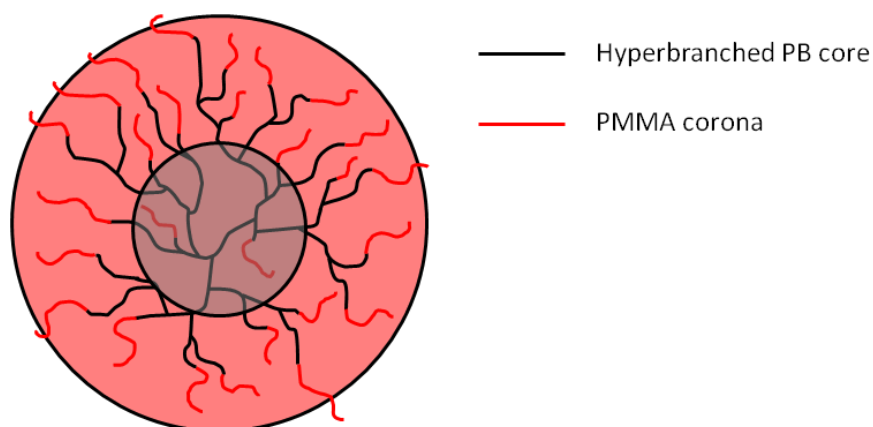
Figure 6. Schematic representation of the hyperstars architecture. Here, the example of DVB-BD-PMMA hyperstar.

Hyperstar nanoparticles are more difficult to characterize using DLS or TEM measurements due to their very low radius of gyration. In solution, the detection of individual species was only possible for p-DVB-BD-PMMA with a molecular weight of M_w = 110 kg/mol and shows a hydrodynamic radius of about 17 nm in THF.

Figure 7 shows TEM images of coatings modified with hyperstar nanoparticles. The introduction of p-DVB-BD-PMMA leads to the formation, after curing reaction, of aggregates, in which lamellae can be distinguished. The aggregates exhibit an "onion-like" structure and are evenly dispersed into the coating. Their sizes vary between 80 and 120 nm in diameter while the rubbery lamellae domains are 8 to 9 nm thick. In the case of T-DVB-BD-PMMA, similar aggregates are observed with slightly larger sizes compared to those formed by p-DBVB-BD-PMMA. They are measured being close to 200 nm while their PB lamellae seem, on the other hand, thinner with 6 to 8 nm thick. The size of the rubbery domains are in agreement with the respective PB content in T-DVB-BD-PMMA (46 %wt) and in p-DVB-BD-PMMA (50 %wt).

Whereas before curing reaction, the hyperstars are well dispersed in the polyol resin and do not form defined structures, after reaction of the polyol resin with polyisocyanate, hyperstars are self-assembled into onion-like structured aggregates. This behavior confirms that changes in interaction parameters seem to occur during the curing of the coating.
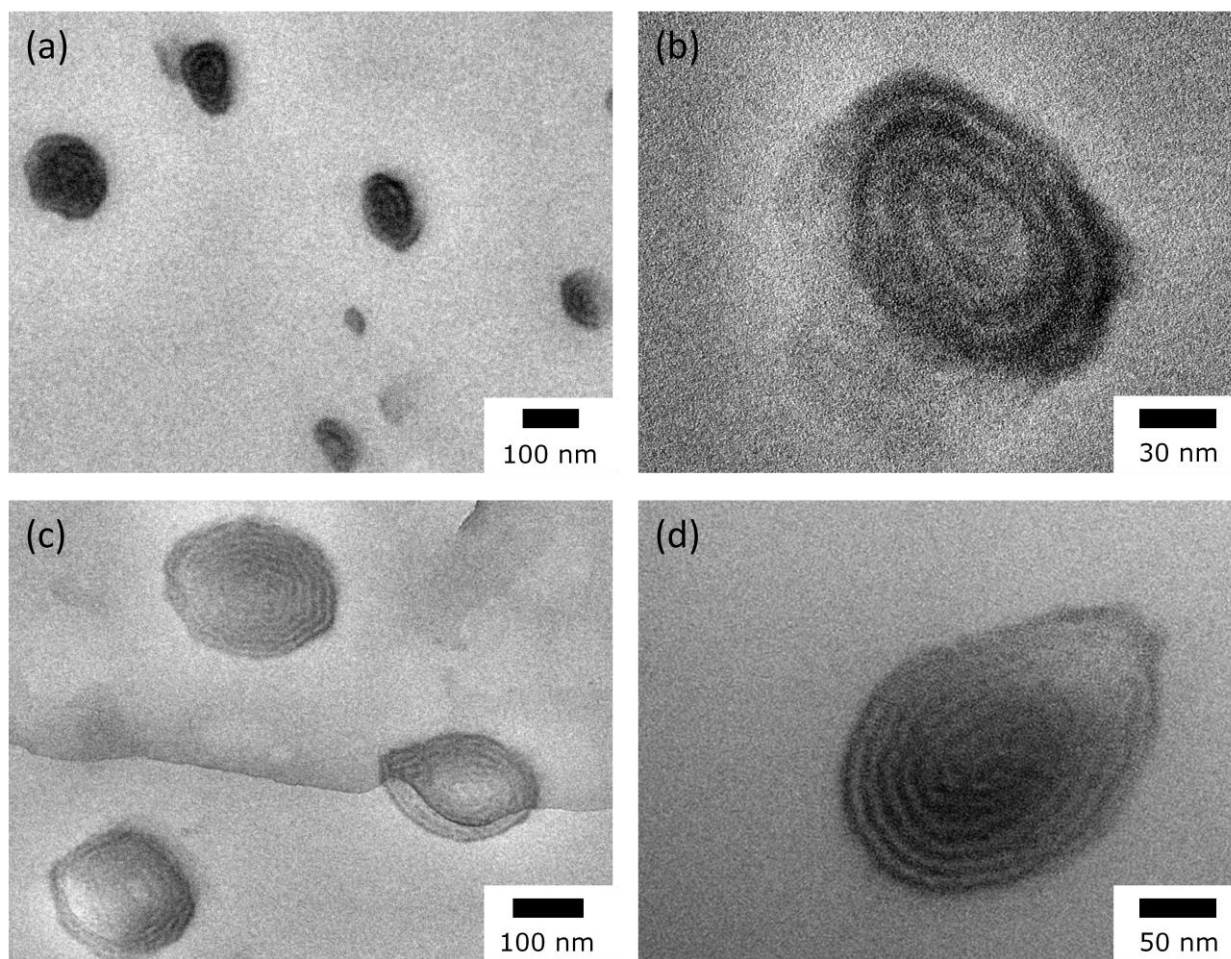
Figure 7. TEM images of modified PU coating (A870/N3300) with 2 %wt of (a), (b) *p*-DVB-BD-PMMA and (c), (d) T-DVB-BD-PMMA (stained with OsO$_4$ after curing reaction).

5.3.2 Appearance

The introduction of nanoparticles into the coating should not disturb in any way the appearance of the final clearcoat. As its name indicates, the main appearance property to be kept is the transparency of the coating. Both types of nanomodifiers were designed to fulfill such conditions, i.e. their radii are about 10 to 20 nm. Once the nanomodifiers are mixed with the resin, the transparency can be roughly judged by naked eyes, and does not seem to be affected by their addition.

After curing reaction, gloss/haze measurements (see Table 3) made on Support 4 (glass substrate) show that all gloss 20° values are measured to be 92.4 ± 0.1. This confirms that the addition of nanoparticles A does not have any influence on the gloss of the coating

On the other hand, the haze values seem to slightly decrease within the modification. At 2 % modification only, the haze decreases from 6.3 to 5.2 for B-*n*BMA nanoparticles.

Table 3. Gloss and haze measured for different modified coatings on support 4 (glass) and support 3 (OEM panel)

Support 4	Standard	+ 2 % B-M	+ 2 % B-M-H	+ 2 % B-*n*BMA
Gloss 20°	92.3	92.4	92.5	92.4
Haze	6.3	6.1	5.5	5.2
Support 3				
Gloss 20°	90.7	90.8	90.8	91.2
Haze	14.4	15.4	15.4	12.3

On the OEM panels, the gloss values are lower (and the haze values higher). In comparison with the glass substrate, this difference can be ascribed to the black basecoat. This coat can already possess some imperfections affecting the gloss/haze of the support contrary to the glass substrate which has not been treated prior to the application of the transparent coating. Apart of this, the results reflect the same trend as previously measured on the glass substrate. The coating modified with B-*n*BMA nanoparticles presents on both substrate slightly improved gloss and haze.

The sizes of the hyperstars are smaller than the B-M nanoparticles and are therefore believed not to affect the transparency of the coating. But, as observed on the TEM images previously, hyperstars assemble to form larger aggregates of 100 to 200 nm diameter which are more likely to affect the appearance of the coating. No gloss/haze measurements were made in this case, the defects were perfectly visible with naked eyes.

5.3.3 Mechanical/physical properties

5.3.3.1 Adhesion

Tape (or cross-cut) test and/or pull-off test were carried out in order to test the adhesion of the unmodified and modified coatings on support 1. Nanomodifiers A and B were tested at 1, 5 and 10 % modification and results are listed in Table 4 and Table 5 where "Std." refers to the standard coating without modification. The results are expressed according to a scale from 0 (no damage) to 5 (> 65 % of the area is damaged). For more details, refer to Chapter 2.

The addition of B-M nanoparticles seems to have a positive influence on the adhesion of the coating as the tape test values show improvement of the adhesion from 5.0 up to 2.0 for 10 % modification (see Figure 8). The pull-off test exhibits a similar trend with a debonding force of 2.19 MPa at 10 % modification against 0.45 MPa for the neat coating.

Table 4. Tape test and pull-off test results for coatings modified with B-M nanoparticles (support 1, ST 1203)

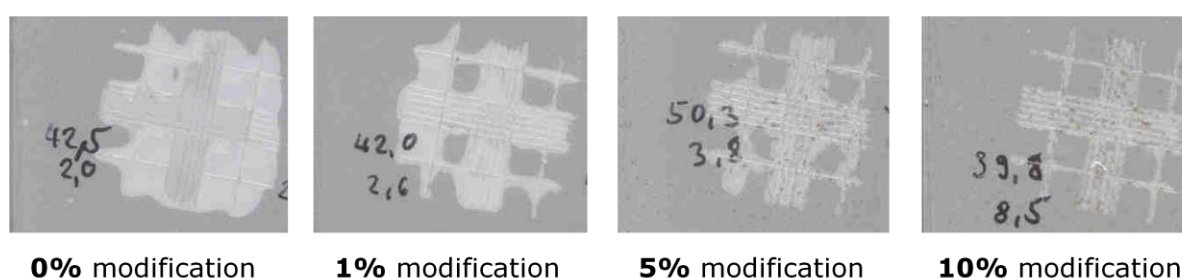|	Std.	+ 1 % B-M	+ 5 % B-M	+ 10 % B-M
Cross-cut test	5.0	4.0	3.0	2.0
Pull-off test (MPa)	0.45	1.05	1.84	2.19

0% modification   **1% modification**   **5% modification**   **10% modification**

Figure 8. Film coatings modified with B-M nanoparticles at different modification rate after cross-cut testing (support 1, ST 1203).

Concerning the effects of the hyperstar nanomodifiers, the behavior is more complex. While improvement in adhesion can already be noticed at 1 % modification with B-M nanoparticles, the addition of hyperstars does not show improvement below 5 % modification. The addition of 1 % hyperstars even exhibits negative effects on the adhesive behavior in the case of T-DVB-BD-PMMA and *p*-DVB-BD-P*n*BA nanomodifiers. At 5 % and 10 % modification, T-DVB-BD-PMMA seems to improve the adhesion at best.

Table 5. Tape test results for coatings modified with hyperstar nanoparticles (support 1, ST 1405)

	Std.	+ 1 %	+ 5 %	+ 10 %
p-DVB-BD-PMMA	4.5	4.0	2.3	2.3
T-DVB-BD-PMMA	4.5	4.7	1.0	1.0
p-DVB-BD-P*n*BA	4.3	4.7	3.7	3.3
p-DVB-BD-P*n*BMA	4.3	4.3	4.3	3.7

5.3.3.2 Scratch resistance

Scratch tests can be divided into two categories: "dry scratch resistance" and "wet scratch resistance" tests. For the dry scratch resistance, different scratching materials are used like steel wool, polishing paper or Scotch Brite®. Further details about the tests are given in Chapter 2.

5.3.3.2.1 Dry scratch resistance

In Table 6, the results of the scratch test using Steel wool as stress agent are reported.

On support 2, the gloss of modified and non modified films is initially the same. The addition of nanoparticles A does not alter the gloss. The standard film, without modification, exhibits the lowest gloss values after stress and after reflow. The introduction of 2 % nanoparticles A seems to improve the gloss after stress as 51.1 % of the initial gloss is retained after stress against 43.1 % for the standard formulation. After reflow, the residual gloss is improved from 84.4 % up to 93.3 %. The best results are obtained for B-nBMA nanoparticles.

Table 6. Results for "dry" scratch resistance tests using steel wool. "Std." refers to the standard coating without modification.

Steel wool	Std.	+ 2 % B-M	+ 2 % B-M-H	+ 2 % B-nBMA
Support 2				
Gloss 20°	92.3	92.4	92.5	92.4
After stress	39.8	42.9	46.8	47.2
After reflow 2 h at 60 °C	77.9	83.1	85.1	86.2
Residual gloss after stress (%)	43.1	46.4	50.6	51.1
Residual gloss after reflow 2 h at 60 °C (%)	84.4	89.9	92.0	93.3
Support 3				
Gloss 20°	91.0	90.5	90.7	91.0
After stress	23.5	24.1	25.6	25.4
After reflow 2 h at 60 °C	73.3	70.9	79.1	79.4
Residual gloss after stress (%)	25.8	26.6	28.2	27.9
Residual gloss after reflow 2 h at 60 °C (%)	80.5	78.3	87.2	87.3

On support 3, the addition of nanoparticles A does not affect the gloss as on support 2. Here again, the gloss after stress is improved by the introduction of nanoparticles A. For the standard formulation the percent residual gloss is 25.8 % while the modified ones exhibit values from 26.6 % to 28.2 %. After reflow, the residual gloss is also improved by the addition f nanomodifiers except with B-M modifiers which recover only 78.3 % of its initial gloss against 80.3 % for the standard formulation.

In Table 7, Scotch Brite ® is used as stressing agent and causes greater damages than steel wool. For this reason, gloss is preferably measured at 60°. When measured at 20°, the results do not allow a proper interpretation of the results. The standard formulation exhibits the best residual gloss after stress with 43.2 %. The coating modified with B-nBMA retains only 39.1 % of its initial gloss but, after reflow, possesses the highest residual gloss value with 65 % against 63.9 % for the standard formulation. Apart of this improvement, after such heavy stress and deformation, the addition of nanoparticles A is inefficient.

Table 7. Results for "dry" scratch resistance tests using Scotch Brite®."Std." refers to the standard coating without modification.

Scotch Brite® - Support 2	Std.	+ 2 % B-M	+ 2 % B-M-H	+ 2 % B-nBMA
Gloss 60°	97.2	96.4	96.8	97.1
After stress	42.0	41.6	38.9	38.0
After reflow 2 h at 60 °C	62.1	57.6	50.3	63.1
Residual gloss after stress (%)	43.2	43.2	40.2	39.1
Residual gloss after reflow 2 h at 60 °C (%)	63.9	59.8	52.0	65.0

Table 8. Results for "dry" scratch resistance tests using polishing paper. "Std." refers to the standard coating without modification.

Polishing paper - Support 3	Std.	+ 2 % B-M	+ 2 % B-M-H	+ 2 % B-nBMA
Gloss 20°	91.0	90.5	90.7	91.0
After stress	19.6	17.3	17.3	19.6
After reflow 2 h at 60 °C	85.4	81.4	82.6	82.3
Residual gloss after stress (%)	21.5	19.1	19.1	21.5
Residual gloss after reflow 2 h at 60 °C (%)	93.8	89.9	91.1	90.4

In Table 8, polishing paper is used as stressing agent on OEM panels. This test shows no improvement with modification of the coatings by addition of the nanoparticles A. The

residual gloss after stress and after reflow are equal or below the values for the standard formulation.

5.3.3.2.2   Wet scratch resistance

Concerning the "wet" scratch resistance, the only system which seems to be affected is modified with B-nBMA nanoparticles. The residual gloss after stress and after reflow for such a system are increased up to 68.9 % and 90.6 % respectively. For comparison, a standard formulation recovers the gloss after stress and after reflow only up to 65.5 % and 89.2 % respectively. The improvements stay, however, relatively weak.

Table 9. Results for "wet" scratch resistance tests on the mini car-wash plant. "Std." refers to the standard coating without modification.

Scratch resistance "wet" (car-wash plant)	Std.	+ 2 % B-M	+ 2 % B-M-H	+ 2 % B-nBMA
Gloss 20°	90.7	90.8	90.8	91.2
After stress	59.4	59.6	58.9	62.8
After reflow 2 h at 60 °C	80.9	81.1	79.7	82.6
Residual gloss after stress (%)	65.5	65.6	64.9	68.9

Against damages caused by relatively weak stressing agents (steel wool and polishing paper), the addition of nanoparticles A seems efficient in reducing their impact on the gloss of the surface. B-nBMA is particularly interesting as it improves the gloss after reflow. This is probably due to the fact that nBMA has a low T_g (20 °C) compared to PMMA (100 °C). During the reflow, more mobility will be induced in a coating modified with B-nBMA than with B-M.

5.3.3.3 Chip resistance

Chipping tests were all performed on Support 1 and details about the tests are found in Chapter 2.

5.3.3.3.1   Multi-impact

Results for the multi-impact tests are given in Figure 9 and expressed in terms of affected area from 0.5 (0.2 % affected area) to 5.0 (81.3 % affected area or more) for each modifiers at different rate modification. "Std." indicates the standard formulation without modifiers. Examples of tested samples are shown in Figure 10.
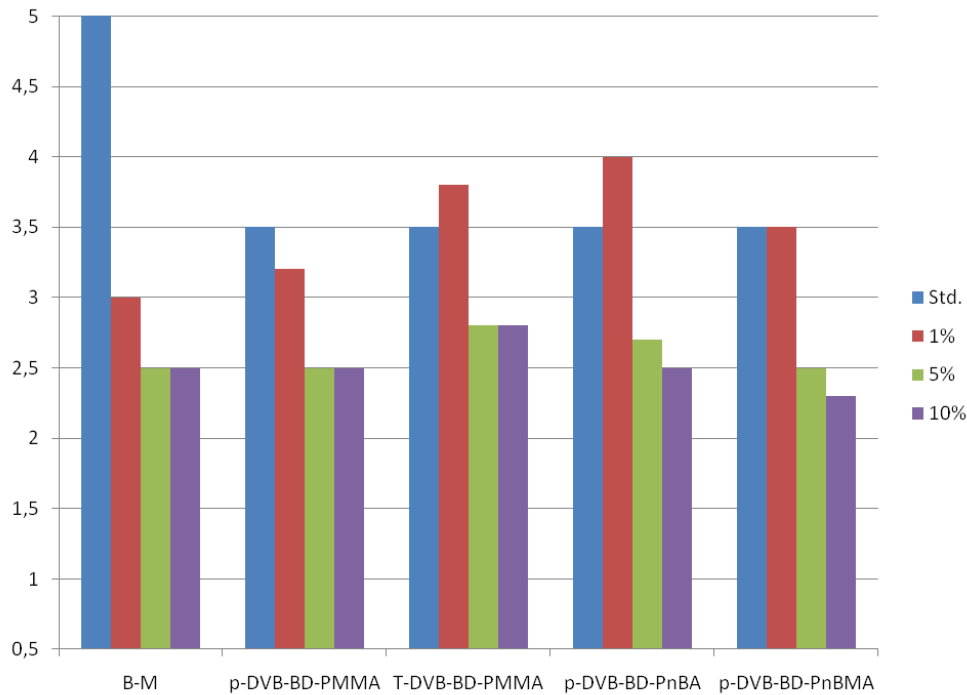
Figure 9. Multi-impact tests results at different modification rate.

The addition of B-M nanoparticles already significantly improved the chip resistance at 1% modification by lowering the affected area from 5.0 to 3.0 and down to 2.5 for 10 % modification. In the case of hyperstar modified coatings, the addition of 1 % of nanoparticles seems to have negative effects on the chip resistance. For all types of hyperstars, the optimum modification rate seems to lay at 5 % where a positive effect on the chip resistance can significantly be noticed. 10 % of nanoparticles do not bring further improvements compared to the 5 % modified paints.
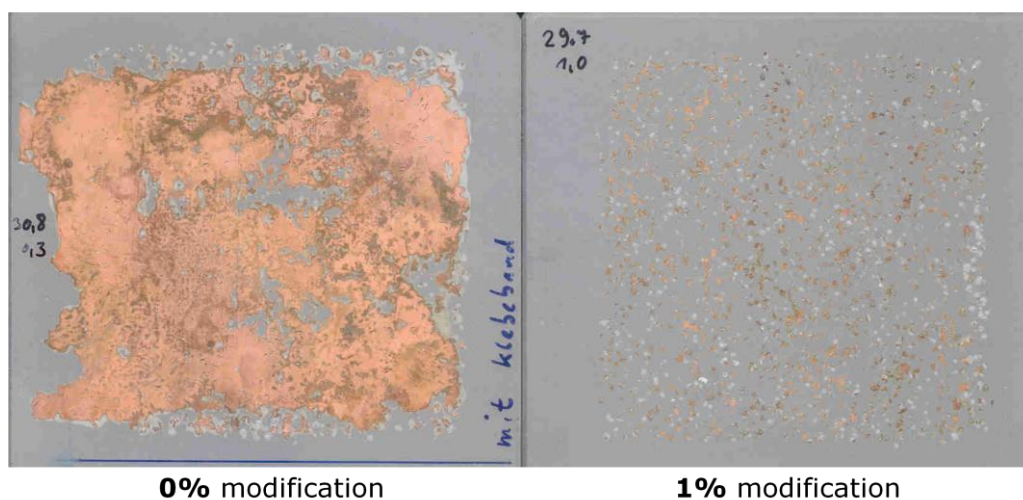

0% modification   **1%** modification

Figure 10. Coated surfaces modified with 0 % and 1 % B-M nanoparticles after the multi-impact test.

5.3.3.3.2   Single-impact

Results are reported in Figure 11 and expressed as the width of damage in millimeters for each modifier at different rate modification. "Std." indicates the standard formulation without modifiers and pictures of tested surfaces are shown in Figure 12.

As observed previously for the multi-impact tests, the addition of B-M nanoparticles improved single-impact resistance from 1 % modification while, the addition of hyperstars exhibit worsened effects. In the case of hyperstars, improvements in chip resistance occur at 5 % modification of the coating.
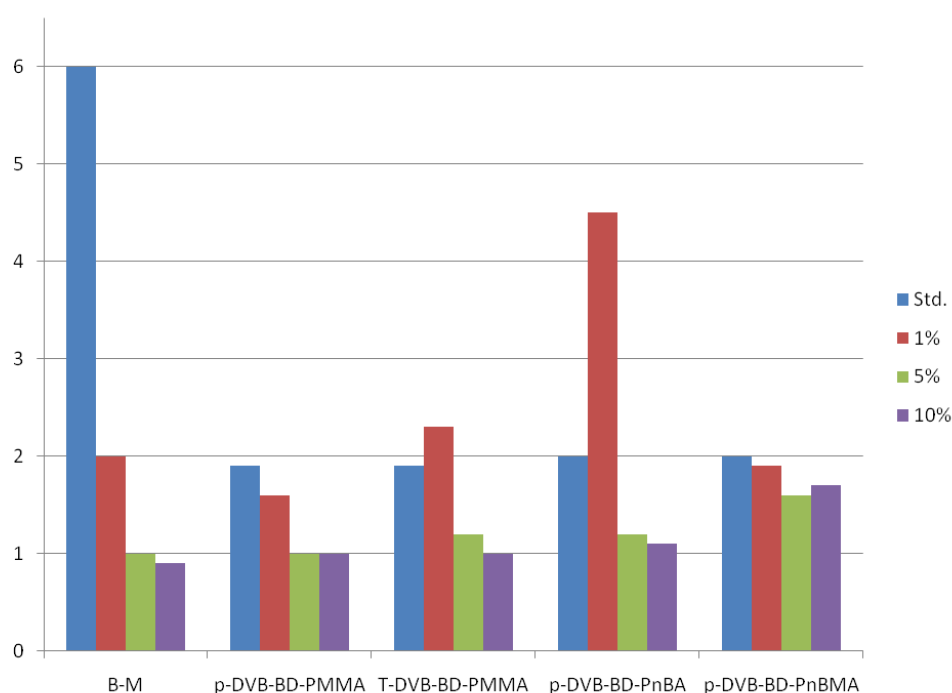
Figure 11. Single-impact tests results in mm at different modification rate.
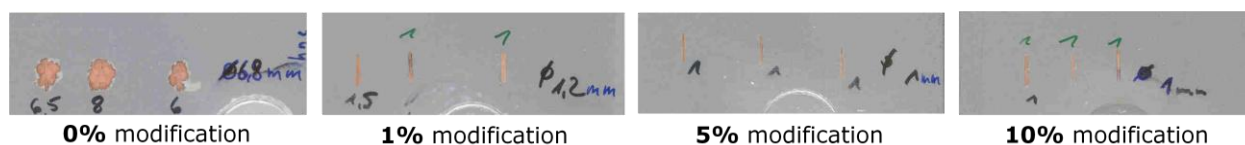
Figure 12. Coated surfaces modified with B-M nanoparticles after the single-impact test.

5.3.3.3.3   Ball-shot

Ball-shot test results are summarized in Figure 13 and expressed in square millimeters of damaged area for each modifier at different rate modification. "Std." indicates the standard formulation without modifiers and examples of tested surfaces are shown in Figure 14.

B-M nanoparticles decrease the size of the affected area of the ball-shot impact from 19.0 to 6.0 mm² at 1 % modification. Further addition of these nanoparticles reinforces this ball-shot resistance down to 2.0 mm² affected area for 10 % modification.

Within this test, the chip resistance behavior of nanomodified coatings with hyperstars confirms the trend already observed in multi- and single-impact tests. The affected area is greatly increased compared to the standard paint when 1 % of hyperstars nanomodifiers are added to the formulation. But this negative effect vanishes when 5 % or 10 % of nanoparticles are used and even lead to smaller affected area.
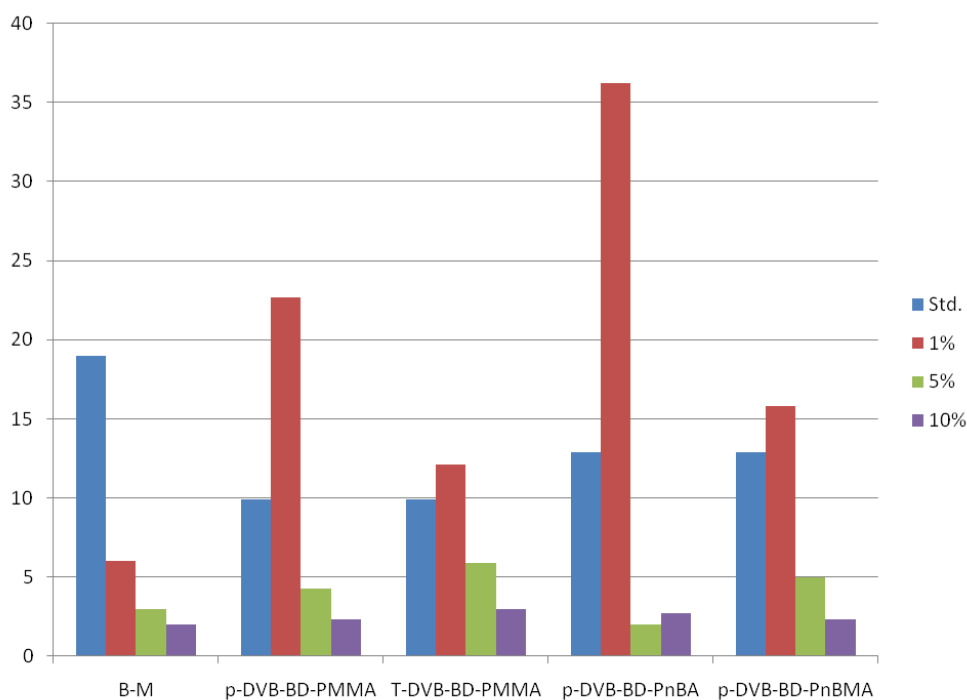
Figure 13. Ball-shot tests results in mm² at different modification rate.

0% modification   **1%** modification   **10%** modification

Figure 14. Coated surfaces modified with B-M nanoparticles after ball-shot test.

In all impact tests, B-M nanoparticles show positive effects and improvement in the chip resistance of the coating. The particular behavior observed for the hyperstar nanomodifiers at 1 % modification is not clearly understood but above 5 % modification, improvements in the chip resistance are observed.

5.3.3.4 Hardness

Two types of hardness are measured for 2 % modification of the coating on support 4. Results are given in Table 10.

Table 10. Hardness measured on Support 4. "Std." indicates the standard formulation without modifiers.

	Std.	+ 2 % B-M	+ 2 % B-M-H	+ 2 % B-*n*BMA
Micro-hardness (N/mm²)	156	154	153	153
Pendulum Hardness (s)	189	188	187	189

The addition of nanoparticles type A does not seem to influence the hardness of the final coating whatever the nature of the corona of the particle. In Figure 15, various modification rates are tested for B-M nanoparticles where no influence on the hardness of the coating is observed even with 10 % nanoparticles. This confirms the previous trend observed for this type of nanoparticles.

In the case of hyperstars nanoparticles, at 1 % modification, the hardness is slightly higher than for a non modified coating. When the amount of nanoparticles B introduced is increased, the hardness drops significantly of at least 10 N/mm² for 10 %wt nanoparticles. The lowest hardness is recorded for *p*-DVB-BD-PMMA which also possesses the highest rubber content (50 %wt).

It is interesting to note, concerning the hyperstars modifiers, that where the chip resistance is the lowest (at 1 %wt modification), the hardness is the highest. In this context, the chip resistance and the hardness can then be related to each other. The hardness reflects the elasticity of the coating. Therefore, its inability to absorb the energy of an impacting stone results in damages in the coating. The harder is the coating, the more damaged it will be.
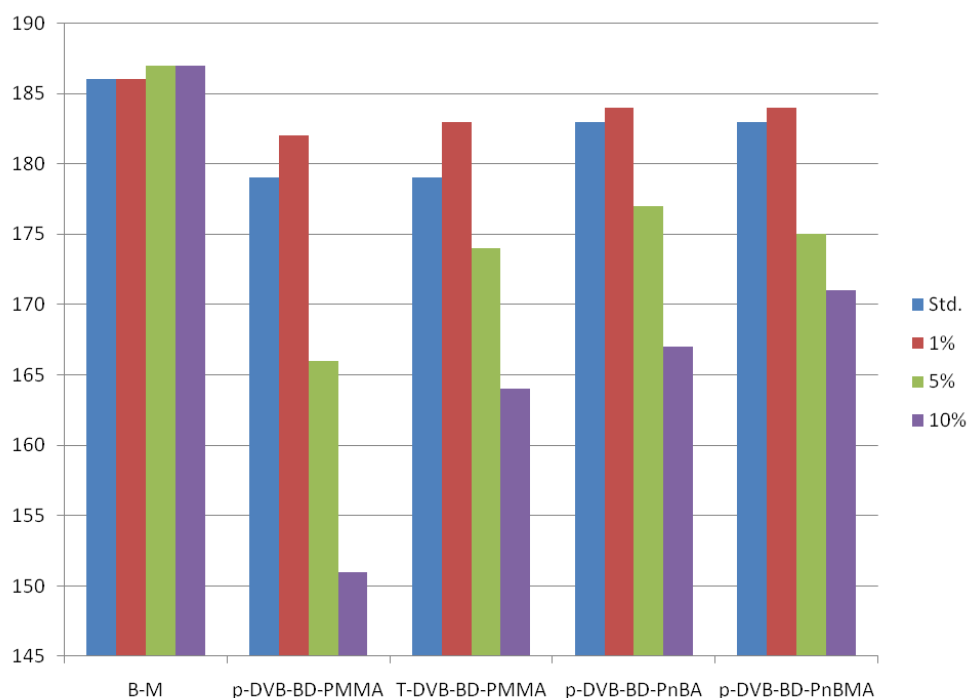
Figure 15. Micro-Hardness in N/mm² measured on Support 1. "Std." indicates the standard formulation without modifiers.

5.3.4   Chemical resistance

The chemical resistance of the modified coatings was tested with two different methods described more in details in Chapter 2.

5.3.4.1   10 minutes stress

This test was carried out on Support 2 and results are expressed in Table 11 according to a specific scale from 0 (no damage) to 5 (destroyed coating). The negative effects of the nanoparticles were highlighted in bold.

The neat coating exhibits already very good resistance against water, FAM-mixture, gasoline MPA and xylene. Ethyl acetate and acetone cause the worst damage with an evaluation at 3. Unfortunately, the addition of nanoparticles A does not improve the chemical resistance against these two solvents and even worsened it when B-M is added. The chemical resistance to xylene is also worsened whatever nanoparticles is added. B-*n*BMA nanoparticles weaken particularly the coating against FAM-mixture and gasoline.

Table 11. Evaluation of damage after chemical stress 10 minutes. "Std." indicates the standard formulation without modifiers.

	Std.	**+ 2 % B-M**	**+ 2 % B-M-H**	**+ 2 % B-*n*BMA**
Distilled water	0	0	0	0
FAM-mixture	0	0	0	**0-1**
Gasoline	0	**0-1**	0	**1**
MPA	0-1	1	1	1
Xylene	0	**2**	**1**	**0-1**
Ethyl acetate	3	3	3	3
Acetone	3	**4**	3	3

In general, such thermoset coatings exhibit very good chemical resistance essentially because of the presence of many cross-linking points. The presence of nanoparticles might disturb the cross-linking process during the curing reaction of the coating which results in poor chemical resistance.

5.3.4.2 Gradient-oven

This test is carried out on Support 3 and simulates the increase in temperature of a car body under the sun. The influence of the temperature on the resistance of the coating against substances such as tree-gum, bird's excrement or acid rain is examined. The results are expressed as the lowest temperature at which the first damage appears. The panel is heated 30 minutes into the gradient-oven and the evaluation is done after 1 and 24 hours of storage at room temperature. Naturally, the higher the temperature is, the better is the chemical resistance.

The addition of nanoparticles A does not seem to have an effect on the chemical resistance of the coating against tree-gum and pancreatin.

A slight negative effect can be noticed in the case of B-*n*BMA nanoparticles concerning tree-gum for which the temperature is brought down to 38 °C instead of 40 °C. For this same nanoparticle, negative effects of similar amplitudes are observed for the resistance against basic and acidic solutions. The resistance against distilled water remains unchanged.

For the addition of B-M and B-M-H nanoparticles, the resistance against distilled water is worsened even though they do not have a significant effect on the acid and base resistance.

Table 12. Chemical resistance in gradient-oven after 1h / 24h (at room temperature). "Std." indicates the standard formulation without modifiers.

	Std.	**+ 2 % B-M**	**+ 2 % B-M-H**	**+ 2 % B-*n*BMA**
Tree-gum	40/40	40/40	40/40	38/38
Pancreatin	36/36	36/36	36/36	36/36
Distilled water	>68/>68	43/43	44/44	>68/>68
NaOH, 1 %	48/48	51/51	49/49	45/45
H$_2$SO$_4$, 1 %	49/49	48/48	50/50	47/47

5.3.5   Stability of B-M nanoparticles

The hardness of coating samples modified with B-M nanoparticles was measured again after 2 years of storage and results are displayed in Figure 16.
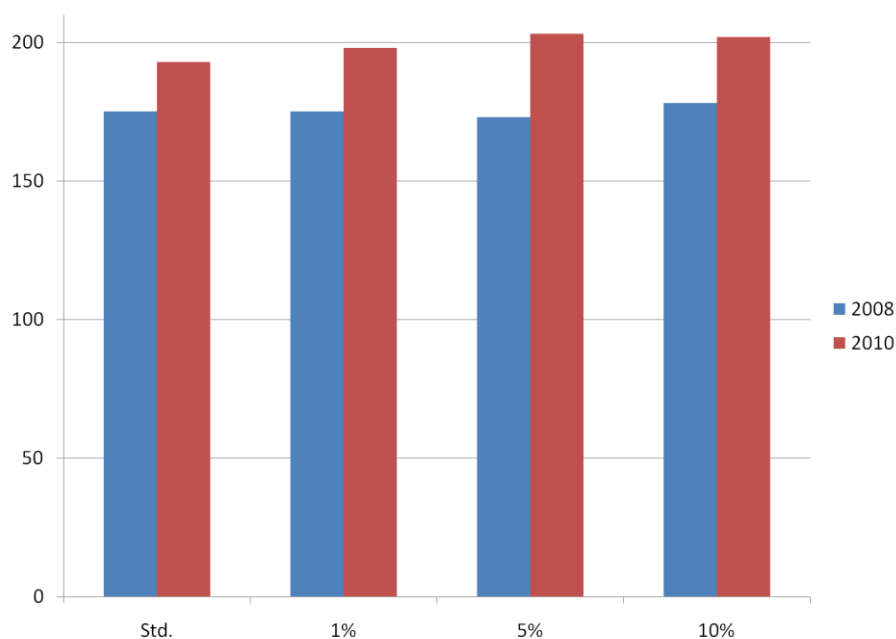
Figure 16. Micro-hardness in N/mm² of the B-M modified coatings at different modification rate right after obtaining the film (2008) and after 2 years of storage at room temperature (2010). "Std." indicates the standard formulation without modifiers.

After ageing for two years, the unmodified coating exhibits an increase in hardness from 175 to 193 N/mm². This gain in hardness seems to be a normal ageing effect which is also noticed in the modified coatings. The highest value is recorded at 5 % modification with 203 N/mm². Hardness values are slightly higher for modified coatings but not significantly enough.

New coating samples were prepared with the two years old B-M nanoparticles and adhesion, chip resistance as well as hardness tests were performed again. The results of the different tests are given in Table 13. The results for coating films prepared with "fresh" B-M nanoparticles are indicated between brackets.

Table 13. Different tests results for modified coatings prepared with 2-years-stored B-M nanoparticles.*

	Std.	+ 1 %	+ 5 %	+ 10 %
Cross-cut	5.0 (5.0)	5.0 (4.0)	5.0 (3.0)	5.0 (2.0)
Multi-impact	3.5 (5.0)	3.7 (3.0)	3.5 (2.5)	3.5 (2.5)
Single-impact	3.4 (6.0)	3.4 (2.0)	3.7 (1.0)	4.3 (0.9)
Ball-shot	12.7 (19.0)	13.3 (6.0)	9.8 (3.0)	18.0 (2.0)
Hardness	186 (175)	186 (175)	187 (173)	187 (178)

*data obtained with fresh samples in brackets.

The previous improvements obtained for samples prepared with "fresh" B-M nanoparticles are no longer observed. The hardness is still not affected by the addition of nanoparticles but the adhesion and the impact resistance are significantly worsened.

The stability of the hyperstar nanomodifiers will also have to be tested. The structure of these nanomodifiers also exhibits polybutadiene vinyl groups as well as aromatic groups (divinylbenzene). The presence of the latter might accentuate a yellowing effect within the coating with time.

5.4   Conclusion

The introduction of nanomodifiers into PU coating formulations was successfully achieved. The nanoparticles were first dissolved in butyl acetate before being added to the polyol resin. At this stage, dispersion of the nanoparticles is good enough not to disturb optical appearance of the coating. After curing reaction, depending on the type of nanoparticles two behaviors emerged.

Cross-linked nanoparticles B-M (type A), independent of the amount introduced, are well-dispersed into the cured coating and retain its transparency and its hardness while improving its chip resistance. The chip resistance is even better when the amount of nanoparticles A introduced is increased. Concerning the scratch resistance, slight

improvements were only obtained for B-*n*BMA after reflow. The chemical resistance against distilled water is usually worsened by the addition of these modifiers.

Hyperstar nanomodifers (type B) are not stable over the curing reaction of the coating and self-assemble in larger aggregates disturbing the transparency of the coating. Onion-like structures are formed in the case of PMMA corona but no defined structures could be seen in the case of P*n*BMA and P*n*BA coronas. The hardness of the coating decreases when the modification rate increases but exhibits a maximum at 1 % where the hardness is higher than for the non modified coating. This maximum is also observed in chipping tests and poorer chip resistance is obtained compared to the non modified coating. 5 % to 10 % hyperstars modifers improve, however, the chipping resistance of the coating.

On the long term, nanoparticles type A do not seem to retain their impact modifier properties while hyperstar modifiers still have to be tested after ageing. If this instability is due to the further reaction of vinyl bonds contained in the PB, the use of another rubbery polymer free of double bonds might be considered such as polyisobutylene. One could also hydrogenate the residual double bonds contained in the nanomodifiers.

For both types of nanoparticles, improvements in the chipping resistance of the coating are obtained, but parallel problems need to be solved. Nanoparticles A need to be optimized to improve their stability over time. Nanoparticles B need to be optimized to avoid their aggregation during curing of the coating and therefore retain the transparency of the final material.

References

1. Bucknall, C. B., *Journal of Elastomers and Plastics* **1982,** 14, (4), 204-221.

2. Molau, G. E.; Keskkula, H., *Journal of Polymer Science Part A-1: Polymer Chemistry* **1966,** 4, (6), 1595-1607.

3. Greco, R.; Astarita, M. F.; Dong, L.; Sorrentino, A., *Advances in Polymer Technology* **1994,** 13, (4), 259-274.

4. Greco, R.; Sorrentino, A., *Advances in Polymer Technology* **1994,** 13, (4), 249-258.

5. Bagheri, R.; Pearson, R. A., *Polymer* **1996,** 37, (20), 4529-4538.

6. Dean, J. M.; Lipic, P. M.; Grubbs, R. B.; Cook, R. F.; Bates, F. S, *Journal of Polymer Science: Part B: Polymer Physics* **2001,** 39, 2996-3010.

7. Dean, J. M.; Grubbs, R. B.; Saad, W.; Cook, R. F.; Bates, F. S., *Journal of Polymer Science: Part B: Polymer Physics* **2003,** 41, 2444-2456.

8. Dean, J. M.; Verghese, N. E.; Pham, H. Q.; Bates, F. S., *Macromolecules* **2003,** 36, (25), 9267-9270.

9. Liu, J.; Thompson, Z. J.; Sue, H.-J.; Bates, F. S.; Hillmyer, M. A.; Dettloff, M.; Jacob, G.; Verghese, N.; Pham, H., *Macromolecules* **2010,** 43, (17), 7238-7243.

10. Vollenberg, P. H. T.; Heikens, D., *Polymer* **1989,** 30, (9), 1656-1662.

11. Mackay, M. E.; Tuteja, A.; Duxbury, P. M.; Hawker, C. J.; Van Horn, B.; Guan, Z.; Chen, G.; Krishnan, R. S., *Science* **2006,** 311, (5768), 1740-1743.

12. Reynaud, E.; Jouen, T.; Gauthier, C.; Vigier, G.; Varlet, J., *Polymer* **2001,** 42, (21), 8759-8768.

13. Petrović, Z. S.; Javni, I.; Waddon, A.; Bánhegyi, G., *Journal of Applied Polymer Science* **2000,** 76, (2), 133-151.

14. Li, J.-X.; Wu, J.; Chan, C.-M., *Polymer* **2000,** 41, (18), 6935-6937.

15. Yang, F.; Ou, Y.; Yu, Z., *Journal of Applied Polymer Science* **1998,** 69, (2), 355-361.

16. Ou, Y.; Yang, F.; Yu, Z., *Journal of Polymer Science Part B: Polymer Physics* **1998,** 36, (5), 789-795.

17. Rong, M. Z.; Zhang, M. Q.; Zheng, Y. X.; Zeng, H. M.; Walter, R.; Friedrich, K., *Polymer* **2001,** 42, (1), 167-183.

Chapter 6

Summary / Zusammenfassung

Summary

Rubber-based nanomodifiers were successfully synthesized following two different strategies and were used as impact modifiers in polyurethane (PU) automotive clearcoats to improve chip resistance.

Various narrowly distributed polybutadiene-*b*-poly(methyl methacrylate) (B-M) block copolymers differing in composition and molecular weights were synthesized and studied with respect to their self-assembly in organic selective solvents. Dynamic light scattering and transmission electron microscopy measurements revealed that spherical micelles were obtained in acetonitrile for all block copolymers, independently of the polymer concentration. Their radii varied from 11 to 69 nm depending on the molecular weight of the initial linear block copolymer and their aggregation behavior in acetonitrile followed the model established by Förster and Antonietti for strongly segregated block copolymers. In DMF and acetone, block copolymers with 85 %wt PMMA were dissolved as unimers. For lower methacrylate contents, the sizes of the obtained spherical micelles were decreasing from DMF to acetone independently of the polymer concentration. The calculated interaction parameters confirmed acetonitrile as the best solvent for PMMA followed by DMF and acetone as the poorest one. The size of the spherical aggregates could be tuned by the molecular weight and/or by the nature of the selective solvent. Polybutadiene-*b*-poly(*n*-butly acrylate) (B-*n*BA), polybutadiene-*b*-poly(*n*-butyl methacrylate) (B-*n*BMA) and polybutadiene-*b*-poly(*t*-butyl methacrylate) (B-*t*BMA) did not show such a large choice in selective solvents and spherical micelles were obtained in DMF, DMAc and acetone respectively.

Cross-linking of the polybutadiene core of the obtained micelles was performed in solution using two different methods: cold vulcanization and radical reaction upon the decomposition of a photo-initiator under UV radiation. Both methods allow retaining the spherical shape of the micelles leading to narrowly distributed non fusible nanospheres. In

the case of B-M nanoparticles, the degree of cross-linking seemed independent of the amount of cross-linker used. Unlikely, B-*n*BMA and B-*n*BA nanoparticles exhibited increasing degrees of cross-linking with the amount of photo-initiator introduced. Their degrees of cross-linking were particularly lower than those of B-M nanoparticles.

The hydrolysis of the *t*-BMA corona of the nanoparticles obtained from B-*t*BMA linear block copolymers self-assembly in selective solvent resulted in water soluble nanoparticles carrying acid functions and thus potentially exhibiting pH-responsive behavior.

Various hyperstars consisting of a hyperbranched PB core and (meth)acrylate arms were synthesized by anionic self-condensing vinyl copolymerization (SCVCP) of divinylbenzene and butadiene followed by the anionic polymerization of the linear (meth)acrylate arms. The amount of hyperbranched products resulting from SCVCP could be enhanced by introducing additional DVB to the reaction while polymerizing. The topology of the hyperbranched PB cores was confirmed by viscosity measurements. All Mark-Houwink-Sakurada exponents were significantly below the value for linear PB. The initiation of (meth)acrylate arms was confirmed by ^{1}H NMR spectroscopy. Upon the arm-growth reaction, the branched topology was retained as witnessed by further viscosity measurements.

The introduction of cross-linked nanoparticles based on linear block copolymers did not disturb the transparency of PU coatings. Even after curing reaction, the nanoparticles were well-dispersed into the coating. TEM observations confirmed this last result where neither aggregation nor flocculation of the cross-linked nanoparticles was observed.

Hyperstar polymers were found to undergo self-assembly upon the curing reaction leading to "onion-like" structured aggregates, in the case of PMMA hyperstars, with sizes as large as 200 nm. Aggregates of the same size order were observed for the other hyperstars but no defined structures were found. For all hyperstar modified coatings, the transparency of the films was altered.

In both cases, cross-linked nanoparticles and hyperstar modified coatings, improvements of chip resistance were observed. The improvements were even better with increasing amount of cross-linked nanoparticles but no effect was noticed on the hardness of the coatings. Similar trends were observed for the hyperstar modified coatings. However, on the long term ageing for two years, cross-linked nanoparticles do not seem to retain their impact modifiers properties while hyperstar modifiers still have to be tested after ageing.

Zusammenfassung

Gummi-basierende Nanomodifikatoren konnten mittels zweier verschiedener Strategien erfolgreich synthetisiert werden und wurden zur Verbesserung der Steinschlagfestigkeit als Elastifikator in Polyurethan(PU)-Fahrzeugbeschichtungen verwendet.

Verschiedene eng verteilte Polybutadien-*b*-polymethylmethacrylat-Blockcopolymere (B-M) mit unterschiedlichen Zusammensetzungen und Molekulargewichten wurden synthetisiert und hinsichtlich ihrer Selbstorganisation in organischen selektiven Lösungsmitteln untersucht. Dynamische Lichtstreu- und transmissionselektronen-mikroskopische Messungen zeigten, dass sich bei allen Blockcopolymeren in Acetonitril sphärische Mizellen bilden, unabhängig von der jeweiligen Polymerkonzentration. Ihre Radien liegen im Bereich von 11 bis 69 nm, abhängig vom Molekulargewicht des linearen Ausgangsblockcopolymers und ihr Aggregationsverhalten folgt dem von Förster und Antonietti eingeführten Modell führ stark segregierte Blockcopolymere. In DMF und Aceton lagen Blockcopolymere mit 85 Gewichtsprozent PMMA als Unimere gelöst vor. Bei geringerem Methacrylatgehalt nahm die Größe der erhaltenen sphärischen Mizellen in Aceton gegenüber DMF unabhängig von der Polymerkonzentration ab. Die berechneten Wechselwirkungsparameter bestätigen, dass Acetonitril das beste Lösungsmittel für PMMA ist, gefolgt von DMF und dem schlechtesten Lösungsmittel, Aceton. Die Größe der sphärischen Aggregate konnte über das Molekulargewicht und/oder die Art des selektiven Lösungsmittels eingestellt werden. Polybutadien-*b*-poly(*n*-butylacrylat) (B-*n*BA), Polybutadien-*b*-poly(n-butylmethacrylat) (B-*n*BMA) und Polybutadien-*b*-poly(*t*-butylmethacrylat) (B-*t*BMA) boten keine derartige Auswahl an selektiven Lösungsmitteln, so dass sphärische Mizellen sowohl in DMF, DMAc als auch Aceton erhalten wurden.

Das Vernetzen des Polybutadienkerns der erhaltenen Mizellen wurde in Lösung über zwei verschiedene Methoden durchgeführt: Kaltvulkanisation und eine radikalische Reaktion aufgrund des Zerfalls eines Photoinitiators unter UV-Bestrahlung. Beide Methoden erlauben die Erhaltung der sphärischen Form der Mizellen und führen so zu eng verteilten nicht-schmelzbaren Nanosphären. Im Fall der B-M-Nanopartikel schien der Vernetzungsgrad unabhängig von der Menge an verwendetem Vernetzer zu sein. Dagegen zeigten die B-*n*BMA- und B-*n*BA-Nanopartikel steigende Vernetzungsgrade abhängig von der Menge an

eingebrachtem Photovernetzer. Insbesondere waren ihre Vernetzungsgrade niedriger als die der B-M-Nanopartikel.

Die Hydrolyse der *t*-BMA-Korona der Nanopartikel die über die Selbstorganisation linearer B-*t*BMA-Blockcopolymere erhalten wurden, führte zu wasserlöslichen Nanopartikeln, die eine Säurefunktion besitzen und somit potentiell pH-responsives Verhalten zeigen könnten.

Verschiedene Hypersterne bestehend aus einem hyperverzweigten PB-Kern und (Meth)acrylat-Armen wurden durch die anionische selbst-kondensierende Vinylcopolymerisation (SCVCP) von Divinylbenzol (DVB) und Butadien gefolgt von der anionischen Polymerisation der linearen (Meth)acrylat-Arme hergestellt. Die Menge an hyperverzweigten Produkten die auf diese Weise erhalten wurden, konnte durch das Einbringen zusätzlichen DVBs in die Reaktion während des Polymerisationsprozesses vergrößert werden. Die Topologie der hyperverzweigten PB-Kerne wurde durch Viskositätsmessungen bestätigt. Alle Mark-Houwink-Sakurada-Exponenten lagen deutlich unter dem Wert für lineares PB. Die Initiierung der (Meth)acrylat-Arme wurde durch ^{1}H-NMR-Spektroskopie bestätigt. Während der Armwachstums-Reaktion konnte die verzweigte Topologie erhalten werden wie mit Hilfe von weiteren Viskositätsmessungen beobachtet wurde.

Das Einbringen vernetzter Nanopartikel basierend auf linearen Blockcopolymeren beeinflusste die Transparenz von PU-Beschichtungen nicht. Auch nach dem Aushärtungsvorgang waren die Nanopartikel in der Beschichtung feinstverteilt. TEM-Aufnahmen bei denen weder eine Aggregation noch eine Ausflockung der vernetzten Nanopartikel beobachtet wurde bestätigten dieses Ergebnis.

Es wurde festgestellt, dass Hypersternpolymere sich während des Aushärtungsvorganges selbst anordnen. Im Fall von PMMA-Hypersternen führt dies zu zwiebelähnlich strukturierten Aggregaten mit einer Größe von bis zu 200 nm. Aggregate in der gleichen Größenordnung wurden auch bei den anderen Hypersternen beobachtet; definierte Strukturen wurden jedoch nicht gefunden. Bei allen mit Hypersternen modifizierten Beschichtungen veränderte sich die Transparenz der Filme.

Sowohl bei den mit vernetzten Nanopartikeln als auch bei den mit Hypersternen modifizierten Beschichtungen wurden Verbesserungen der Steinschlagfestigkeit beobachtet.

Dieser Effekt wurde mit zunehmender Menge an vernetzten Nanopartikeln verstärkt; ein Effekt auf die Härte der Beschichtung wurde aber nicht festgestellt. Ähnliche Tendenzen wurden bei den Hyperstern-modifizierten Beschichtungen beobachtet. Nach einer Langzeitalterung von zwei Jahren scheinen vernetzte Nanopartikel jedoch ihre schlagzähigkeitsverbessernden Eigenschaften nicht beizubehalten während die Hyperstern-Modifikatoren erst noch nach einer Alterung untersucht werden müssen.

Acknowledgments

First of all, my gratefulness goes to my supervisor Prof. Dr. Axel Müller who welcomed me already on two occasions to MC² in Bayreuth. The first occasion coincided with my very first experience abroad during a summer seven years ago already. There, I kind of left a piece of my heart and already knew I would be back to Pile High and Deep! I would like to thank him for giving me the opportunity to accomplish my PhD degree within his chair and therefore for trusting me along those four and a half years. I grandly appreciate the precious time he granted me with, his help, his advices and also his implicite support by sending me to several and various conferences all over the world where I had the chance to present my work and to meet always more people from the "polymer family". I think I will always be impressed and almost intimidated by the passionate and devoted scientist, very keen on marzipan and good whisky, I have discovered in him. Thank you for the great experience, Chef.

Of course, I would like to thank the MC² group for never making one day look like the other. Since I got in touch with MC², I have seen quite a number of people coming and leaving and I hope the forgotten ones will forgive me.

Directly related to my work, I would like to thank Dr. Holger Schmalz for introducing me to the difficult duty of anionic polymerization, Sergey Nosov, Dr. Felix Schacher and Dr. Andreas Walther for their precious advices as anionic experts. I will never forget the first time I cut potassium with Dr. Anuj Mittal. The anionic team, namely, Karina Möller, Dr. Andrew Ah Toy, Susanne Edinger, Dr. Stefan Reinicke, Andreas Hanisch and Joachim Schmelz is acknowledged for keeping it running and clean and for hearing my complains when things went just wrong. Who never broke an ampoule at the end of the day…? Thank you to the GPC team, especially Marietta Böhm for her devoted help in GPC/MALS/viscosity but also Sabine Wunder, Dr. Youyong Xu, Andreas Hanisch and André Gröschel for measuring countless of my samples. Thank you to all the people who contributed to promote the DLS to the "please book me three months in advance" status: Markus Ruppel, Dr. Markus Burkhardt and the successors: Dr. Felix Schacher and Joachim Schmelz. I am also grateful for their help in getting me familiar with the SLS-piranha routine. I have to thank quite a few TEM performers, Dr. Jiayin Yuan, Dr. Felix Schacher, André Gröschel, Jeanine Rockser, Annika Pfaffenberger, Melanie Förtsch and Kerstin Küspert either for preparing

and/or measuring my samples during endless hours in the dark TEM room. Dr. Manuela Schumacher, Dr. Anja Goldmann, Jeanine Rockser and Susanne Edinger are acknowledged for their help in MALDI-ToF measurements. Thank you to Annette Krökel and Dr. André Pfaff for taking good care of our NMR and freeze-dryer.

Thank you to Dr. Felix Plamper, Dr. Pierre-Eric Millard, Alexander Schmalz and Markus Müllner for fixing my computer problems and for the great administrator job that has been accomplished.

I can never thank enough Gaby Rösner-Oliver for the all the energy she puts into "paper work" and organization duties but also for her kindness and for being always ready to help and to answer my questions.

I would like to thank my "lab 769 partners", Dr. Evis Penott-Chang and Dr. Petar Petrov for their diverse and precious help as well as their everyday good mood. I also thank Dr. Francesca Bennett, Dr. Tony Granville, Dr. Raymond Joso, Dr. Shohei Ida, Prof. Dr. Hülya Arslan, Dr. Matthew Hunley, Dr. Darkeyah Reuven, Dr. Karim Aissou, Sylvain Catrouillet, Meirav Ben-Lulu, Dima, Sascha, the "Ivans", Dr. Ramon Novoa-Carballal, Dr. Girish Behera, Dr. Saikat Mandal, Dr. Bing Fang, Dr. Jie Kong Dr. Yong Zhang and Dr. Weian Zhang for bringing an international touch to the group especially when it turned alarmingly german. I also would like to make use of the occasion to thank all the other colleagues, Eva Betthausen, Dr. Markus Dreschler, Dr. Marina Krehkova, Alexander Majewski, Thomas Ruhland, Christopher Synatschke, Stephan Weiss, Dr. Michael Witt and Zhicheng Zheng for the teamwork and also all the other people I had the occasion to meet during my stay in MC². A special thank you goes to Andrea Wolf for her translation of my summary and her very entertaining literature seminars. I have to thank my master student David Heinrich for his work on the watersoluble nanoparticles and for challenging me with my supervisor skills.

Finally, I want to thank all MC² but also all the other chemistry departments at the university of Bayreuth for being such a united team and for all the good times spent at work but also outside work. I don't forget those who gave me company during my late polymerization nights, those who tried to improve my german or, better said, franconian language skills by introducing thursday as "Deutsch Tag", the spontaneous "Feierabend Bier" that ends in a nasty hangover the day after, all those cake sessions, barbecues under

the rain or the snow and other coffee breaks that definitely help and makes the PhD life a little easier in a way…

I want to thank my family for their unconditional support, especially my brother Eric who understood my "PhD"-joys and -pains more than anyone else, all my friends, in particular back in Paris, who always believed I would make it. I am very thankful to André Pfaff for keeping faith in me when I did not myself, for his wholehearted support, his patience and his love. I am glad I met you on the way.

Erklärung

Ich bestätige hiermit, dass ich die Arbeit selbstständig verfasst und keine anderen, als die von mir angegebenen Hilfsmittel und Quellen benutzt habe.

Zudem bestätige ich hiermit, dass ich nicht anderweitig mit oder ohne Erfolg versucht habe, eine Dissertation einzureichen oder mich einer Doktorprüfung zu unterziehen.

Bayreuth, 5. August 2011

_____

Sandrine Tea